

UNIVERSITY OF OKLAHOMA

GRADUATE COLLEGE

INTEGRATED GEOPHYSICAL AND GEOLOGICAL STUDIES OF SELECTED
MAJOR TECTONIC FEATURES IN SOUTH-CENTRAL U.S.

A DISSERTATION

SUBMITTED TO THE GRADUATE FACULTY

in partial fulfillment of the requirements for the

Degree of

DOCTOR OF PHILOSOPHY

By

HAMED ABDELHAMID ALREFAEE

Norman, Oklahoma

2013

INTEGRATED GEOPHYSICAL AND GEOLOGICAL STUDIES OF SELECTED
MAJOR TECTONIC FEATURES IN SOUTH-CENTRAL U.S.

A DISSERTATION APPROVED FOR THE
CONOCOPHILIPS SCHOOL OF GEOLOGY AND GEOPHYSICS

BY

Dr. G. Randy Keller, Chair

Dr. Kurt J. Marfurt

Dr. May Yuan

Dr. Michael J. Soreghan

Dr. Jamie Rich

ACKNOWLEDGEMENTS

First and foremost, I would like to express my sincere gratitude to my advisor Dr. G. Randy Keller for the continuous support of my PhD study and research, for his patience, motivation, enthusiasm, and immense knowledge. I would like to thank Dr. Kurt J. Marfurt for suggesting me the point of the research for the Arkoma basin. Great thanks to my committee members for their kind suggestions and prolific discussions.

Great thanks to Dr. Charles Gilbert and Dr Luza for their guidance during the scouting fieldtrips to the Meers fault area. My sincere thanks also go to Dr. Kevin Crain for his help and guiding during acquiring and processing of the gravity data in the Meers fault area. Special thanks also to Stephen Holloway for his kind tutoring to use the gravimeter and the GPS for collecting the gravity data and his continuous supporting for the laboratory instruments and maintenance. I would like also to thank Mr. Richard Andrew for providing us with the basement and Arbuckle well datasets in Oklahoma State.

Special thanks also to all my graduate friend Murari Khatiwada for sharing his knowledge and valuable assistance in using the software. Many thanks also should go to the Egyptian Management Mission and the High Education Ministry for providing the great opportunity to get this scholarship and for the financial aids.

Last but not the least, I wish to express my love and gratitude to my beloved family; for their understanding and endless love, through the duration of my studies. Especially, I would like to give my special thanks to my wife whose patient and continuous support enabled me to complete this work.

TABLE OF CONTENTS

ACKNOWLEDGEMENTS	iv
TABLE OF CONTENTS	v
LIST OF TABLES	vi
LIST OF FIGURES	vii
ABSTRACTS.....	xi
INTRODUCTION	1
CHAPTER I: INTEGRATED GEOPHYSICAL STUDIES OF THE BASEMENT STRUCTURE OF THE ARKOMA BASIN, OKLAHOMA AND ARKANSAS	2
CHAPTER II: UPPER CRUSTAL STRUCTURE OF THE LLANO UPLIFT: AN INTEGRATED GEOPHYSICAL INVESTIGATION	50
CHAPTER III: MAPPING THE EXTENSION OF THE MEERS FAULT IN SOUTHWESTERN OKLAHOMA, USING INTEGRATED GEOPHYSICAL AND GEOLOGICAL DATA	103
CONCLUSIONS	154

LIST OF TABLES

CHAPTER I: INTEGRATED GEOPHYSICAL STUDIES OF THE BASEMENT
STRUCTURE OF THE ARKOMA BASIN, OKLAHOMA AND
ARKANSAS

Table I.1. Wells penetrate to the top of Arbuckle Group	22
Table I.2. Wells penetrate to the top of the Arbuckle	23

LIST OF FIGURES

Chapter I: Integrated geophysical studies of the basement structure of the Arkoma basin, Oklahoma and Arkansas

Figure I.1. Index map of the Arkoma basin-Ouachita orogenic belt province.....	24
Figure I.2. Stratigraphic section of Arkoma basin-Ouachita orogenic belt province.....	25
Figure I.3. Tectonic evolution of the Arkoma basin-Ouachita orogenic belt province...26	
Figure I.4. Structural cross section OK4 across Ouachita Orogenic belt	27
Figure I.5. 3D view of the basement surface	28
Figure I.6. Vertical seismic section AA'	29
Figure I.7. Vertical seismic section BB'	30
Figure I.8. Vertical seismic section CC'	31
Figure I.9. Vertical seismic section DD'	32
Figure I.10. Vertical seismic section EE'	33
Figure I.11. Vertical seismic section FF'	34
Figure I.12. Zoomed in view of the vertical seismic section FF'	35
Figure I.13. Bouguer gravity map of the Arkoma basin	36
Figure I.14. The reduced-to-pole total magnetic intensity map	37
Figure I.15. The total horizontal derivative and tilt derivative	38
Figure I.16. Euler solution plot using structural index $SI = 0.0$	39
Figure I.17. Euler solution plot superimposed on the total horizontal derivative and the tilt derivative of the magnetic data.....	40

Figure I.18. Integrated seismic and magnetic data	41
Figure I.19. Residual gravity map showing the location of the wells and two selected profiles for the density models	42
Figure I.20. Gravity model along the profile AB	43
Figure I.21. Gravity model along the profile CD	44
Chapter II: Upper Crustal Structure of the Llano Uplift: An Integrated Geophysical Investigation	
Figure II.1. Index map of the Llano uplift and tectonic features in Texas	75
Figure II.2. Geologic map of the Llano uplift area.	76
Figure II.3. The stratigraphy of the Llano uplift area	77
Figure II.4. Tectonic model for the western Grenville orogeny.	78
Figure II.5. Regional complete Bouguer gravity map of the Llano uplift.....	79
Figure II.6. Regional upward continuation and residual gravity maps	80
Figure II.7. The complete Bouguer gravity map of Llano uplift	81
Figure II.8. The RTP map of Llano uplift	82
Figure II.9. Upward continuation of gravity and its residual gravity	83
Figure II.10. Rejection band-pass filter maps with different cutoffs.....	84
Figure II.11. Rejection rejection directional cosine filter	85
Figure II.12. Gravity model AB of the Llano uplift area	86
Figure II.13. Density model CD of the Llano uplift area	87
Figure II.14. Tectonic model for the current Llano uplift	88

APPENDIX	95
Figure A.1. Regional RTP map of Llano uplift area	96
Figure A.2. Upward continuation to heights of 10, 12, 15, 20, 30 and 40 km	97
Figure A.3. Upward continuation to heights of 50, 60, 70, 80, 90 and 100 km	98
Figure A.4. Residual gravity after upward continuation to heights of 10, 12, 15, 20, 30 and 40 km	99
Figure A.5. Residual gravity after upward continuation to heights of 50, 60, 70, 80, 90 and 100 km	100
Figure A.6. Band-pass filter maps of the gravity and magnetic data	101
Figure A.7. Rejection band-pass filter maps of the gravity and magnetic data	102
Chapter III: Mapping the extension of the Meers fault in Southwestern Oklahoma, using integrated geophysical and geological data	
Figure III.1. Index map of southwestern Oklahoma	123
Figure III.2A) Geologic map of the Meers fault area	124
B) Geologic map of Lawton	125
Figure III.3. Aerial photograph of southwestern Oklahoma	126
Figure III.4. Complete Bouguer anomaly map of the study area	127
Figure III.5. RTP anomaly map of the study area	128
Figure III.6. Residual gravity and residual magnetic maps of the study area	129
Figure III.7. Total horizontal derivative of gravity and magnetic data	130
Figure III.8. Tilt derivative of the gravity data	131
Figure III.9. Tilt derivative of the magnetic data	132
Figure III.10. Ground gravity profile AA'	133

Figure III.11. Ground gravity profile BB'	134
Figure III.12. Ground gravity profile CC'	135
Figure III.13. Ground gravity profile DD'	136
Figure III.14. Ground gravity profile EE'	137
Figure III.15. Ground gravity profile FF'	138
Figure III.16. Ground gravity profile GG'	139
Figure III.17. Ground gravity profile HH'	140
Figure III.18. Ground gravity profile II'	141
Figure III.19. Index map of seismic reflection lines	142
Figure III.20. Seismic reflection line A	143
Figure III.21. Seismic reflection line B	144
Figure III.22. Seismic reflection line C	145
Figure III.23. COCORP seismic line 2-2A	146
Figure 4.24. RTP map with gravity profiles and seismic lines	147

ABSTRACT

The current dissertation includes three separate chapters, each utilizing the power of the integration of different geophysical datasets with geology to investigate tectonic and structural processes responsible for the geological evolution of selected major tectonic features in south-central U. S. These tectonic features are; the Arkoma basin of Oklahoma and Arkansas, the Llano uplift of central Texas, and the Meers fault of the southwestern Oklahoma. Although, the study covers three different tectonic features, these features share a similar tectonic history and evolution. These tectonic features are located along the front of the Ouachita orogenic belt, and they have been subjected to major tectonic events that dominated the south-central U.S. beginning with the Late Precambrian-Early Cambrian rifting through the Late Paleozoic convergent Ouachita orogeny.

The Arkoma basin is an arcuate structural feature that extends from the Gulf coastal plain in central Arkansas westward 400 km to the Arbuckle Mountains in south-central Oklahoma. The study area lies at the transition zone between the Arkoma basin and the Ouachita orogenic belt and could also be associated with northwest trending faults associated with the Southern Oklahoma aulacogen. The interpretation of the 3-D seismic data reveals an E-W zone of crustal weakness in the northern part of the study area, which could be a Late Paleozoic tectonic inversion of the extension faulting that developed during Cambrian rifting and later foreland basin development. The seismic interpretation reveals a compressive deformation of the Late Paleozoic strata related to the Ouachita orogeny. Magnetic boundaries such as faults and/or body edges extending

E-W, NE-SW and NW-SE have been delineated using magnetic edge detector techniques in the northern, southeastern, and western parts of the study area, respectively. The Euler magnetic depth estimation method delineated the same faults determined using magnetic edge detector techniques. The maximum depth to faults dominating the basement and/or the intrabasement features determined by the Euler's method is about 3850 m. The fault trends delineated by the seismic interpretation and those determined by the Euler's method and the edge detector techniques show a very clear correlation.

The Llano Uplift is a broad structural dome in central Texas with 2 to 3 km of structural relief relative to the subsurface Fort Worth and Kerr basins to the northeast and southwest. The Llano uplift appears like an island of Precambrian granitic and metamorphic rocks surrounded by Paleozoic and Cretaceous rocks. The current Llano uplift developed due to a variety of tectonic and structural processes. The initial uplift due to an arc-continent collision was followed by a continent-continent collision between the Laurentia and a southern continent during the Grenville orogeny. The extensional tectonism associated with the Cambrian rifting and the opening of the Gulf of Mexico played a pronounced role in the evolution of the Llano uplift. The compressional tectonism of the Late Paleozoic Ouachita orogeny as well as the Ouachita related foreland basins contributed to the rise of the Llano uplift area. The complete Bouguer gravity and reduced to pole total magnetic intensity (RTP) maps of the Llano uplift show anomalously high values. A number of short wavelengths maxima superimposed on a relatively broad, high gravity anomaly coincide with Llano uplift

area. The sources of the short wavelength anomalies can be related to shallow mafic bodies that were intruded into the uppermost crust during subduction of the Laurentia (North America continent) beneath a southern continent during the Grenville orogeny. The source of the broad, circular gravity anomaly appears to be related to a deeper geologic body situated in the middle crust. The RTP map reveals NW-SE trending magnetic highs that coincide with metamorphic rock exposures. Based on the gravity signature, the Llano uplift is interpreted to be independent terrane with physical and geological properties that differ distinctly from its surroundings.

The Meers fault is the southernmost element of the complex and frontal fault zone which separates the uplifted igneous rocks of the Wichita Mountains, and the Anadarko basin in southwest Oklahoma. Motion on the Meers fault represents continued activity on one of the largest structural features in North America. The Wichita uplift and the Anadarko basin, which are separated by the Meers fault and related subparallel fault strands, indicate significant intra-plate deformation along the trend of the Southern Oklahoma aulacogen. The interpretation of the gravity and magnetic data reveals clearer variations in the magnetic properties than densities of the rocks on both sides of the Meers fault. The high magnetic contrast on both sides of the Meers fault is mostly due to the Late Paleozoic movement, which juxtaposed Early Cambrian igneous rocks against Cambrian-Ordovician carbonate rocks. The magnetic expression of the Meers fault suggests that the fault can be traced in the subsurface for 21 km southeastward further beyond the clearly defined scarp and for 51 km northwestward where it branches and strikes more northerly. Thus, its total subsurface

extension is ~95 km. The seismic data provide impressive images of the structural complexity of the Wichita Thrust Front, and suggest that the Meers fault is a deep-seated high-angle thrust fault.

INTRODUCTION

This dissertation includes three separate chapters, each employing the geologic interpretation of geophysical datasets to reveal the tectonic and structural processes responsible for the evolution of three selected tectonic features in south-central U. S. The main aims of the current study are: (1) mapping and illumination of the basement structures of western Arkoma basin in Oklahoma and Arkansas, (2) determining and investigating the subsurface causative source bodies and/or structures responsible for the unexpected anomalous gravity and magnetic signature from Llano Uplift area as well as investigate the tectonic processes responsible for uplift of the Precambrian and Lower Paleozoic rocks, and (3) mapping the southeastern subsurface extension of the Meers fault.

Each chapter is planned to be a scientific paper by itself. These chapters are in different stages of preparation for publication. Chapter I on the basement structure of the Arkoma basin is ready for submission to the new journal of Interpretation. Chapter, II on the Llano uplift is being prepared for submission to the Geological Society of America journal Geosphere. Chapter III on the Meers fault is also in preparation for submission to Geosphere.

**CHAPTER I: INTEGRATED GEOPHYSICAL STUDIES OF THE BASEMENT
STRUCTURE OF THE ARKOMA BASIN,
OKLAHOMA AND ARKANSAS**

Abstract

We employed three-dimensional (3D) seismic, magnetic, and gravity data in an integrated approach to map the basement surface and the associated structural features in the western Arkoma basin of Oklahoma and Arkansas. The structural interpretation and seismic attributes reveal an E-W striking zone of intensive deformation or crustal weakness in the northern part of the study area. This zone of weakness may represent a Late Paleozoic tectonic inversion of the normal faulting (block faulting) that developed during Cambrian rifting and later foreland basin development. The structural interpretation also reveals a compressive deformation related to the Late Paleozoic Ouachita orogeny. We recognized a clear relationship between the Precambrian basement structures and the Paleozoic structural deformation and depositional history. Edge detector techniques applied to the magnetic data delineated magnetic boundaries (faults or body edges) that extend in E-W, NE-SW and NW-SE in the northern, southeastern, and western parts of the study area, respectively. The Euler magnetic depth estimation method also delineated major faults by showing clustering of the solutions along the fault trends. Euler's method shows a maximum depth value of about 3850 m to the faults that affect the basement and/or the intrabasement features. The fault trends obtained from seismic data interpretation show a very clear correlation with those determined by the Euler's method and the edge detector techniques.

Introduction

The basement surface is rarely well imaged in seismic surveys because most of them are designed to image shallower targets for hydrocarbon exploration. Another reason for the poor imaging or mapping of the basement is the rarity of wells that penetrate to the basement surface. Mapping the Precambrian basement structures is extremely useful because they are responsible for the processes controlling the formation of natural fractures and faults in the overlying sedimentary cover in basins. Precambrian basement structures in the continental United States strongly influenced later Proterozoic and Phanerozoic tectonics (e.g., Sims et al., 2005). The structures dominating the formation of the Ancestral Rocky Mountains, Laramide, and Sevier orogenies were strongly affected by intense deformation along zones of weakness in the Precambrian basement. During renewed tectonism, preexisting zones of weakness and structures are preferentially reactivated at the expense of formation of new ones (Holdsworth et al., 2001). The zones of weakness in the basement play a prominent role in localizing magmatism and ore deposits (Sims et al., 2002).

On a local basin scale, the basement structures in the Fort Worth basin are responsible for intrasedimentary features such as faults, fractures and collapse features in the Ellenberger Group and Viola Limestone, (Sullivan et al., 2005; Baruch et al., 2009; Elebiju et al., 2010). Moreover, hydrocarbon production from the fractured basement has attracted more attention to the need for better understanding of basement structures. This need is also underscored by commercial hydrocarbon accumulations around the world in reservoirs in fractured basement rocks (Gutmanis et al., 2010). In

addition, new hydrocarbon plays have developed in the Arkoma foreland basin and within the Ouachita orogenic belt (Fig. I.1), and petroleum accumulation may be possible in the Lower Paleozoic strata lying beneath the Ouachita thrust sheets well into the orogenic belt (Keller, 2009).

Basement-involved structures are common in the foreland and sub-thrust platform of the Ouachita orogeny. These basement structures are represented by fault blocks that developed before or during the Cambrian rifting. Many of these faults were reactivated by the Late Paleozoic tectonics, and they cut upward through the sedimentary cover (Thompson et al., 1995). In this study, we have integrated recently acquired 3D seismic, gravity, and magnetic data with geological information for mapping and illumination of the basement structures of western Arkoma basin in Oklahoma and Arkansas.

Location and geology

The Arkoma basin extends from central Arkansas westward for 400 km to the Arbuckle Mountains in south-central Oklahoma (Fig. I.1). The Ozark uplift and Northeast Oklahoma platform represent the natural northern boundary of the basin. The southern margin of the basin is marked by the Choctaw fault in Oklahoma and by Ross Creek fault in Arkansas, both of which define the cratonward margin of the Ouachita fold belt (Sutherland, 1988). The basin was once a part of a stable shelf along a passive continental margin, and it developed as a foreland basin related to Ouachita orogeny. Normal faults downthrown to the south that affect Lower Pennsylvanian and deeper rocks are abundant. Many folds and faults in the Arkoma basin were produced by

horizontal compressive forces related to the Ouachita orogeny (Keller, 2009). The compressive forces were directed north and northwest and decreased in intensity away from the Ouachita Mountains region (Eissa and Castagna, 2003).

The Ouachita rocks are divided into two main stratigraphic units known as Ouachita facies (Viele, 1989). The lower unit, known as preorogenic, was deposited in the Late Cambrian to Early Mississippian, and it includes two different facies (Fig. I.2). The first (off-shelf facies) is composed of deep-water shale, sandstone and chert that were deposited on the continental slope, and the second is composed of shallow-water carbonates that were deposited on the shelf. The upper, synorogenic unit is mainly composed of deep-water turbidites in the basin and deltaic sediments on the shelf (Viele, 1989). About ~6000 m of the Atokan sediments were deposited in the Arkoma basin. The thickness of the sedimentary section in Arkoma basin ranges from ~1000 m on the shelf at the north, to at least 9 km along the frontal zone of the Ouachita Mountains (Branan, 1968), to at least 10 km under the thrust sheets to the south (Mickus and Keller, 1992; Arbenz, 2008).

Tectonic history of the Arkoma basin-Ouachita orogenic belt province

The collisions of the Archean continents formed the Canadian Shield (Whitmeyer and Karlstrom, 2007). The addition of volcanic arcs and the accretion of oceanic terranes in the Paleoproterozoic built the lithosphere of the area known today as southern North America. The continental growth of southern North America ended with the Grenville orogeny (Mosher, 1998). A supercontinent known as Rodinia was the result of this continental growth. The geologic history important to the area of this study

began with the breakup of Rodinia around 600 Ma and the development of a rifted continental margin about 550 Ma (Keller et al., 1983; Kruger and Keller, 1986) (Fig. I.3). Oceans opened along the newly formed continental margins (Viele and Thomas, 1989). During the period that extends from the Cambrian to the lowermost Mississippian, two different sedimentary facies were deposited on the new margin. The first facies, known as shelf facies, is composed mainly of carbonate with minor shale and sandstone. The second facies, known as off-shelf is composed mainly of shale with minor limestone, sandstone and chert (Houseknecht and Matthews, 1985; Houseknecht, 1987).

The ocean basin began to close in the Devonian-Early Mississippian due to southward subduction beneath an approaching continental landmass often referred to as Llanoria. A magmatic arc developed along the northern margin of Llanoria, and the Ouachita orogenic belt began to form as an accretionary prism (Houseknecht and Matthews, 1985; Houseknecht, 1987).

A slow rate of sedimentation characterized the shelf area during the Mississippian and Early Atoka time, where carbonate, sandstone, and shale continued to be deposited in environments ranging from shallow to non-marine. The deep Ouachita (trench) and the remnant ocean basin were characterized by rapid deposition of flysch sediments. The ocean basin was closed due to the subduction and the accretionary prism was obducted onto the rifted continental margin (Dickinson, 1974). The continental margin experienced a flexural bending due to the attenuation of the continental crust and the load exerted by the obducted material. Consequently, many normal faults were created in the foreland (Houseknecht and Matthews, 1985; Houseknecht, 1987). Atoka

sediments, which represent the transitional stage between passive margin and foreland basin sedimentation, were deposited contemporaneously with the faulting. Finally, close to the end of Atoka time, the continuous advance of the subduction complex resulted in uplift of the thrust strata along the frontal thrust belt of the Ouachita and the formation of the foreland basin was complete (Houseknecht and Matthews, 1985; Houseknecht, 1987; Gangopadyay and Heydari, 1995).

Structural framework

The Ouachita Mountains are divided into three regional provinces depending on the structural elements (Arbenz, 2008) (Fig. I.1). Starting from the north to the south, these structural provinces are arranged as follows: (1) southern Arkoma basin fold belt, (2) frontal Ouachita thrust and fold belt, and (3) the Ouachita allochthon. The study area lies at the transition zone between the Arkoma basin and the Ouachita orogenic belt and could also be associated with northwest trending faults associated with the Southern Oklahoma aulacogen (e.g., Keller et al., 1983; Keller and Stephenson, 2007). A brief description of these tectonic (structural) provinces is given in the following paragraphs.

The southern Arkoma basin fold belt represents the northernmost division of the Ouachita orogenic belt (Fig. I.1). The southern Arkoma basin fold belt lies between the compressional structures to the far north, and the traces of the Choctaw and Ross Creek thrust faults to the south. The province is characterized by two structural levels separated by a detachment surface in the Atoka ductile shale (Arbenz, 2008). The first structural style is represented by block faulting due to tensional forces associated with the basin subsidence in the Early Pennsylvanian. Several E-W normal faults developed

due to the subsidence and the tensional forces (Branan, 1968; Houseknecht and Matthews, 1985). The faults were active during the Lower to Middle Atoka, resulting in a significant thickening of those strata especially over the downthrown blocks (Houseknecht and Matthews, 1985; Houseknecht, 1987). These faults are exposed in the northern parts of the basin, and they are obscured in the basin trough area. The majority of these faults are characterized by downthrows to the south (Branan, 1968; Houseknecht and Matthews, 1985). These faults strike parallel to the Ouachita orogenic belt and offset the basement and Lower Paleozoic sediments. Most of these faults broke previously undeformed continental crust while a few of them occurred due to the reactivation of the Early Paleozoic rifting related faults (Houseknecht and Matthews, 1985; Houseknecht, 1987). The second structural style is represented by compressional structures due to the Ouachita orogeny. The compressional structures include thrust faults and narrow, long anticlines and synclines parallel to the Ouachita orogenic belt strike (Branan, 1968). The folded section is underlain by thrust faults that ramp to the surface along many anticlinal crests (Houseknecht and Matthews, 1985; Houseknecht, 1987). In addition to the previous two structural styles, there are high angle thrust faults influencing the older and deeper rocks in the area of the basin trough. In contrast to the down-to-the-basin faults, these faults are upthrown on the south (Branan, 1968).

The northern boundary of *the frontal Ouachita thrust and fold belt* is represented by the Choctaw fault and the Ross Creek fault in Oklahoma and Arkansas, respectively (Arbenz, 2008) (Fig. I.1). The Ti-Valley and the Y-City faults define the southern boundary of this belt. The structural deformation of this belt was strongly controlled by the thickness of the Atoka sediments. The thick turbidite sandstones are associated with

broad synclines and massive thrust slabs. However, the thin sandstone sections are associated with narrow faulted folds and laterally limited thrust slices. The frontal thrust and fold belt terminates near Atoka, Oklahoma where the Choctaw and the Ti-Valley faults merge.

The structural styles of *the Ouachita allochthonous* province differ vertically in the stratigraphy (Fig. I.1). The older section, known as preorogenic, is mainly composed of ductile shale of pre-Pennsylvanian age. The younger section, the orogenic sequence, is composed of competent sandstone of Pennsylvanian age. The Ouachita allochthonous province is divided into four distinct sub-provinces (Arbenz, 2008).

The northern and central parts of the Arkoma basin lie in the continental foreland province. The continental foreland province extends northward to include the southern flank of the Ozark uplift and the southwest extension of the Northeast Oklahoma shelf. There are no compressional structures in this zone. The basement and the sedimentary rocks have been subjected to extensional faults due to the breakup and rifting of the southern margin of Laurentia (Thomas, 1977). An active phase of faulting influenced the platform rocks from the Early Atoka to the Desmoinesian synchronous with the down-warping of the basin flank. Faults striking NE-SW with downthrows to the south were active during the deposition of the Atoka Formation. Consequently, the subsidence of the basin and the accumulation rates accelerated. Some of these faults can be recognized beneath the Ouachita thrust and fold belt strata (Arbenz, 2008).

Figure I.4 shows a structural cross section across the Ouachita orogenic belt-Arkoma basin province.

The study area

The study area lies in the westernmost portion of the Arkoma basin in southeastern Oklahoma where it is bounded by the Arbuckle uplift to the west (Fig. I.1). The area occupies part of the transition zone between the Ouachita frontal zone and Arkoma basin. The Choctaw fault, the leading thrust of the Ouachita orogenic belt and the boundary between the Arkoma basin and the Ouachitas, separates two different structural and stratigraphic styles. To the north, the Upper Atoka-Desmoinesian deltaic strata are mostly deformed by broad, open folds and few faults. To the south of the fault, shallow-water carbonate and deep-water turbidite sediments of Morrowan-Lower Atoka are dominated by imbricate faults, isoclinal folds and overturned strata (Suneson, 1995). The blue rectangle in Figure 1 shows the boundaries of the area of our integrated analysis of drilling, geologic, seismic, magnetic and gravity data, while the red polygon (Fig. I.1) shows the boundaries of the 3D seismic survey that was provided for this study.

3D seismic data and seismic attributes

The Arkoma basin 3D seismic survey is located in southeastern Oklahoma, and it was acquired for imaging the Woodford Shale, Hunton Limestone and other targets (Fig. I.1). The 3D seismic volume was initially interpreted structurally by identifying the main faults as well as picking the tops of the Woodford Shale, Timbered Hill Group, and basement horizons. We generated volumetric attributes including the most positive and most negative principle curvatures as well as the reflector rotation volumes (e.g., Chopra 2001 a, b; Chopra and Marfurt, 2007).

The panoramic 3D view in Figure 5 shows the basement surface with intensive irregular topography due to a long period of exposure and weathering. The white arrow shows a clear unconformity between the basement rocks and the Paleozoic section. An area of severe deformation where some faults penetrate into and offset the basement is shown by the red ellipse. The seismic section A-A' shows structural reactivation of the basement normal faults (block faulting) as compressional structures (Fig. I.6). A prominent high angle reverse fault (F3) appears to be a principal rift fault that was reactivated as a reverse fault due to Late Paleozoic compression. In southern Oklahoma, a Proterozoic zone of weakness was possibly reactivated during the Cambrian rifting to create NW-trending normal faults, which were reactivated again as oblique strike-slip faults during the Pennsylvanian time (Thomas and Baars, 1995). High angle thrust faults, which dominate the older and deeper strata, occur near the Choctaw fault. To the southwest of the study area, the south-dipping Washita Valley thrust fault exposed the sedimentary rocks and Cambrian rift-related rhyolite in the hanging wall as well as Ordovician carbonates in the footwall (Puckett, 2011).

Seismic section A-A' also shows a relationship between the faults that displace the basement as well as Lower Paleozoic rocks and those displace the Upper Paleozoic rocks (Fig. 6). A thrust fault influencing the shallower Upper Paleozoic strata aligned vertically above the reactivated reverse fault F3 displacing the deeper strata of the Lower Paleozoic and the basement. This interpretation is supported by the fact that the Choctaw and Ross Creek faults originated near basement faults (Arbenz, 2008). Similarly, the F2 fault is a minor rift fault that was reactivated as a reverse one. Moreover, there is a distinct thickening of the Atoka Formation and the Late

Pennsylvanian strata over the down thrown blocks similar to normal growth faults that developed during the subsidence of the Arkoma basin (Houseknecht, 1987; Sutherland, 1988). Seismic section B-B' confirms the thickening of the Atoka Formation and the Late Pennsylvanian strata on the down thrown blocks (Fig. I.7). Fault F3 still appears to be a major rift fault that was reactivated as a reverse fault while the fault F2 appears to be a minor rift (normal) fault in the B-B' seismic section. Moreover, seismic section C-C' (Fig. I.8) confirms the previously mentioned relationship between the shallower compressional structures and the deeper rifting faults as well as the relationship between the thickening of the Late Paleozoic strata and the downthrown blocks of the Early Paleozoic strata.

Coherence and curvature seismic attributes are powerful tools for optimizing seismic interpretations. These seismic attributes have the ability to reveal the structural deformation and depositional history (Chopra and Marfurt, 2007b). Coherence attributes volume reveal subtle faults regardless of their strike. Low coherence lineaments along fault planes and damaged areas result from discontinuities of trace-to-trace coherence of seismic traces (Chopra, 2001b). In contrast, curvature attributes enable interpreters to delineate small flexures and folds (Chopra and Marfurt, 2007b). Specifically, curvature shows subtle continuous flexures not seen by coherence. The reflector rotation seismic attribute measures changes in dip across wrench faults. We co-rendered the seismic volume with the reflector rotation and the most positive and most negative principle curvature volumes to recognize the different structural styles dominated the area.

Figure I.9 shows vertical slice DD' through the seismic amplitude co-rendered with the most-positive and most-negative principle curvatures, and time slices through the reflector rotation co-rendered with the most-positive and most-negative principle curvatures. The anticlinal features and up-thrown sides of faults show up as red while the synclinal features and downthrown sides show up as blue. In order to confirm the relationship between the Precambrian basement structures and the Paleozoic ones, we generated successive time slices ranging from 2.0 s to 1.0 s at 0.2 s increments. The shallower structural features dominating the Late Paleozoic align vertically above the deeper ones dominating the basement and the Early Paleozoic at the high deformed area of the Olney-Bromide fault. Moreover, the Olney-Bromide fault that penetrates deeply into the basement shows up clearly at deeper levels (Figs. I.9A-D) and diminishes at shallower levels (Figs. I.9A-F). In contrast, the Choctaw thrust fault shows up clearly at shallower levels (Figs. I.9D-F).

The reflector rotation attribute reveals the faults as lineaments as well as the direction of the rotation of the faulted blocks (Fig. I.10A). The Olney-Bromide occurs as an E-W lineament with faulted blocks rotates anticlockwise (down to the left) shown in white while the blocks rotates clockwise (down to the right) are shown in black. This could be interpreted as a compressional structure associated with a strike-slip component as suggested by Thomas and Baars (1995). Curvature shows up-thrown sides in red and the downthrown sides in blue (Fig. I.10B).

The vertical slice FF' through the seismic amplitude and time slice 1.4 s through the reflector rotation show an unnamed thrust fault displacing the shallow Late Paleozoic strata at the area north of the Olney-Bromide fault area (Fig. I.11A). The up-

thrown side of the thrust fault shows up as red in the vertical seismic slice co-rendered with the most-positive and most-negative principle curvatures (Fig. I.11B). Figure I.12 shows a zoomed in view of Figure I.11, and the unnamed thrust fault shows up clearly.

Gravity and magnetic data analysis

Gravity and magnetic data were obtained from a database maintained by the University of Texas at El Paso's Department of Geological Science through the website research.utep.edu/paces. The construction of this database was a large international cooperative effort and involved some modernization of data reduction procedures (Keller et al., 2002, 2006; Hinze et al., 2005). The two datasets, Complete Bouguer anomaly and total magnetic intensity, were gridded for mapping and filtering. The Bouguer gravity map was constructed with a grid size of 5 km while the total magnetic intensity was gridded at 2 km. Both of the grids were subjected to some filtering and edge enhancement techniques to obtain maps for optimum interpretation. The Bouguer gravity grid was subjected to regional-residual separation to create the residual map used to construct density models. The grid was upward continued to 40 km and the result was subtracted from the Bouguer anomaly grid to produce a residual anomaly map that was used in the modeling which is below. The Bouguer gravity map shows an extremely low gravity anomaly related to the Arkoma basin (AB) and remarkably high anomalies due to the Wichita uplift (WU), Arbuckle uplift (AU) and Ouachita interior zone (OIZ) (Fig. I.13). In figure I.13, the black rectangle shows the boundaries of the total magnetic intensity map, and the red polygon shows the location of the 3D seismic survey. The total magnetic intensity grid was reduced to the pole (RTP) to remove the

effects of magnetic inclination (Fig. I.14). Then edge detector techniques and the Euler depth estimation method were applied to the RTP grid.

Edge detector techniques

The total horizontal derivative and tilt derivative of the magnetic data are powerful tools for delineating the edges or boundaries of geologic bodies. The maps resulted from the application of these techniques show clear boundaries of geologic bodies or faulted blocks revealed by contrasts in the magnetic anomaly signatures on both sides of the boundaries.

The edges of the magnetized or high-density bodies have often been delineated by the horizontal derivatives of the potential field data, and the data should first be corrected for the inclination of the Earth’s magnetic field (Lahti and Karinen 2010). The total horizontal derivative peaks over the edges and is near zero over the body (Miller and Singh, 1994). This method has been commonly used to locate the steep gradients associated with vertical boundaries such as faults (Blakely and Simpson, 1986).

The total horizontal derivative (THD) magnitude of the magnetic data grid was calculated using the standard formula (Verduzco et al., 2004)

$$THD = \sqrt{\left(\frac{dT}{dx}\right)^2 + \left(\frac{dT}{dy}\right)^2} \dots\dots\dots (1)$$

where, T is the total magnetic intensity of the magnetic field data.

The total horizontal derivative map shows clear magnetic boundaries, which may coincide with the E-W trending Olney-Bromide fault, the NE-SW trending Choctaw fault, and a NW-SE striking unknown fault, see the white arrows (Fig. I.15A).

The NW-SE trending unknown fault might be associated with the Southern Oklahoma aulacogen.

The tilt derivative can be defined as the ratio of the first vertical derivative to the total horizontal derivative of the potential field. The technique can delineate sources in areas of low gradients. In contrast to the total horizontal derivative, the tilt derivative has high positive value over the source body, close to zero values near the edge, and a negative value outside the source region (Miller and Singh, 1994). Salem et al., (2007) used the zero contours to locate the magnetic body edges. They also calculated the depth to the magnetic body by measuring the distance between the zero and the +45° or -45° contour lines.

The tilt derivative (TD) technique was also applied to the magnetic data using the standard formula of (Verduzco et al., 2004):

$$TD = \tan^{-1} (VD/THD) \dots\dots\dots (2)$$

where, VD is the vertical derivative and THD is the total horizontal derivative of the magnetic data, respectively.

The tilt derivative map of the study area reflects the same boundaries shown by the THD map by showing close to zero values at or near the edges of the magnetic source bodies or the fault planes (Fig. I.15B).

Euler depth estimation method

The Euler deconvolution method can be used to determine the location and depth to magnetic sources (Thompson, 1982). This method delineates the magnetic

boundary or fault trends and recognizes the geometry of the magnetic source (Reid et al., 1990). Euler's homogeneity relation can be written as:

$$(x - x_0)\partial T/\partial x + (y - y_0)\partial T/\partial y + (z - z_0)\partial T/\partial z = N(B-T) \dots\dots\dots(3)$$

where, T is the total field measured at the position (x, y, z). The source lies at the position (x₀, y₀, z₀). B is the regional field or background value, and N is the degree of homogeneity, also known as the structural index (Thompson, 1982).

After some testing, the Euler solutions in this study were determined using a structural index value of zero (S.I. = 0.0) in order to emphasize faults as magnetic contacts. The result (Fig. I.16) shows clustering of magnetic source solutions along an E-W trend to the north, which appears to coincide with the Olney-Bromide fault. Another cluster striking NE-SW in the southeastern area appears to coincide with the Choctaw fault. There is also a NW-SE cluster to the west, which may be related to the previously mentioned unknown fault (see the blue arrows, Fig. I.16). In addition to revealing the previously mentioned fault trends, the depth to the basement was calculated using the Euler depth estimation method. The Euler depth to basement estimates show a maximum of about 3850 m that may reflect the depth to the faults that penetrate deeply into the basement or may be related to intrabasement features. This value shows very good correlation to the depth value to the basement at the well number 13 (Table 2) that has depth to the basement of about 4000 m.

We superimposed the results obtained from the application of Euler's method on both the total horizontal derivative and the tilt derivative maps of the magnetic data. The resulting figures show very good correlation between the Euler solution clusters and the edges of the magnetic source bodies determined by the edge detector techniques (white arrows, Figs. I.17A and B).

Integration of results from seismic and magnetic data

The results from the Euler solution cluster plot and edge detector methods show a considerable correlation with those obtained from the interpretation of the 3D seismic data and seismic attributes. The E-W striking Olney-Bromide fault and the NE-SW striking Choctaw fault are shown by a time slice through the coherence volume (Fig. I.18A). These two fault trends show a very good matching with those shown by the Euler solution cluster plot and the edge detector methods (white arrows, Fig. I.18B).

Modeling

The interpretation of gravity and magnetic data usually includes the modeling process as a final step. This process should include all relevant and reliable data that may help constrain the model (Williams and Finn, 1985). Modeling uses information from the different techniques to derive estimates of the variations in one or more possible physical properties such as density or magnetic susceptibility distributions across a specific region in the study area as well as the cause of such distribution. Any potential field model provides a non-unique solution (Jones-Cecil, 1995), but when

combined with other geological and geophysical information, the models are usually very useful (Saltus and Blakley, 2011).

Two local density models along two profiles across the residual gravity map after upward continuation to 40 km were constructed (Fig. I.19). The two profiles, AB and CD, extend NE-SW and NW-SE, respectively. Two datasets from wells that penetrate deeply to the tops of the Arbuckle Group (Table I.1) and the basement (Table I.2) were used to constrain the models. The approximate thicknesses of the different stratigraphic units and their densities were obtained from the literature and regional gravity models. The models reflect the subsurface distribution of the different blocks with their densities as well as the structural styles influencing the area.

The first model shows an increase in the depth to the basement surface from SW to NE (Fig. I.20). The basement is exposed in the Arbuckle Mountains area to the southwest, and it deepens to the northeast where its depth reaches 4000 m. The large positive gravity anomaly at the far southwest is probably the result of deeply buried mafic igneous rocks from the Cambrian rifting at the core of Arbuckle Mountains (Kruger and Keller, 1986). The broad negative anomaly along the middle portion of the profile results from the thickening of the Late Paleozoic strata in the Arkoma basin. To the far northeast, there is a relatively small positive anomaly coinciding with the thick sedimentary cover in the Arkoma basin (AB). This positive anomaly can be explained by the presence of a mafic intrusion of unknown age.

The second model shows a positive gravity anomaly coinciding with or near the Coalgate anticline to the northwest (Fig. I.21). The positive anomaly may be related to the thinning of the low-density clastic rocks of the Middle-Late Pennsylvanian. To the

far southeast, there is a positive anomaly that may be related to the existence of buried mafic intrusions in the core of the Arbuckle Mountains and/or due to igneous and metamorphic rocks of the Ouachita interior zone. A negative anomaly exists between the two positive ones. The negative anomaly is the result of thickening of the low-density clastic sediments of the Atoka and Desmoinesian that fill the Lehigh syncline.

Conclusions

The integrated approach adopted in this study optimized the interpretation process and the results. The 3-D seismic data provides a new detailed view of the basement structures and how they relate to younger features. The basement rocks in the area were subjected to intense deformation, as well as deep erosion in some places, during extension in the Cambrian that was a reflection of the breakup of Rodinia also the Late Paleozoic Ouachita orogeny and tectonic inversion of the Southern Oklahoma aulacogen. Thus, normal faults (extensional block faulting) dominate the basement and the Lower Paleozoic rocks while compressional structures dominate the Upper Paleozoic rocks. E-W and NE-SW trending faults were identified that probably represent a tectonic (structural) reactivation of the Cambrian rift faults as compressional thrust faults of the Late Paleozoic Ouachita orogeny. Northwest trending faulting in the western portion of the study area is probably related to the Cambrian rifting in the Southern Oklahoma aulacogen and subsequent tectonic inversion in the Late Paleozoic to form the Arbuckle uplift. The basement structures clearly influenced the Paleozoic structures and the depositional history of the Arkoma basin.

Seismic attributes, Euler depth estimate cluster plots and edge detector techniques enhance the definition of E-W and NE-SW striking faults. Fault trends determined by the Euler depth estimation method show remarkably strong correlation to those obtained from seismic data. The depth to the basement increases from the southwest to the northeast across the study area. The maximum depth to basement value of about 3850 m agrees well with the limited drilling data that is available and is a reflection of faults that penetrate deeply into the basement and/or intrabasement structures. These relatively detailed local results provide useful information for broader analyses of the complex structural relations in the region where the Ouachita orogenic belt intersects the Southern Oklahoma aulacogen.

Table I.1: Wells penetrate to the top of the Arbuckle Group.

No.	Well Name	County	Arbuckle Subsea ft.	Surface Elevation ft.	Latitude	Longitude
1	Texaco Incorporated Burnett Era Est Unit 29-1	Pittsburg	-15,858	832	34.60877	-95.84774
2	Devon Energy Prod Mullens 3-29	Pittsburg	-11,810	712	34.78561	-95.85711
3	Hamilton Bros Oil Co Blue Creek 1-8	Pittsburg	-12,920	1,059	34.66240	-95.85998
4	Hamilton Bros Oil Co Pine Mountain 1-35	Atoka	-14,142	858	34.60405	-95.90378
5	Sonat Expl Inc Phipps A 1	Pittsburg	-12,657	761	34.69928	-95.95760
6	Arco Oil & Gas Corp Ingersoll 1-19	Atoka	-18,741	791	34.54097	-95.97676
7	Texinia O & G Inc Brisco W H 1-13	Atoka	-12,966	584	34.37818	-96.09800
8	Park Ave Expl Corp Jacobson 1a-26	Coal	-15,205	705	34.52769	-96.12160
9	Sohio Natural Res Co Taylor 1	Atoka	-13,214	584	34.29164	-96.13215
10	Sun Oil Company R H Crim 1	Coal	-10,971	594	34.56237	-96.16665
11	Exxon Co Usa A Mullin 1	Atoka	-9,777	553	34.25261	-96.17368
12	Arkla Expl Co Carr Estate 1-13	Atoka	-9,469	679	34.37935	-96.20297
13	Daube Expl Co Marathon 1	Atoka	686	844	34.21390	-96.21379
14	Helmerich&Payne Inc Ridgeway 1-5	Atoka	-646	636	34.24190	-96.27856
15	Wentworth Oper Co Mowdy 1	Coal	-6,602	662	34.49532	-96.30095
16	Devon Energy Prod Double 5 Ranch 2-10swd	Coal	-7,191	889	34.74456	-96.23238
17	Newfield Ex Mid-Con Davis 228 Swd	Hughes	-7,635	831	34.78892	-96.25132
18	Eland Energy Inc Saber Swd 1-5	Hughes	-7,279	876	34.84824	-96.26761

Table I.2: Wells penetrate to the top of the basement.

No.	Well Name	County	Surface Elevation ft.	Basement Subsea ft.	Latitude	Longitude
1	M. W. Bowers Moore 1	Johnston	675	535	34.26766	-96.47956
2	Carl (Ada) Wolff Laughlin 1	Johnston	635	420	34.20584	-96.47517
3	Sun Oil Co. Ora A Peters 1	Johnston	805	805	34.34121	-96.44904
4	Mcmillen & Allen Brown 1	Johnston	700	273	34.22881	-96.43662
5	Atlantic Refining Co. Core Hole 2	Johnston	603	258	34.16994	-96.41841
6	Wayne Roberts (Sutherland & Piranio) Ayers 1	Atoka	685	680	34.30890	-96.37299
7	Thomas E. Berry Audie Evans 1	Atoka	662	642	34.27139	-96.35322
8	National Oil Co. Bonner 1	Atoka	641	641	34.25676	-96.30920
9	Dillingham Oil Co. Powledge 2	Atoka	680	242	34.19318	-96.29255
10	Helmerich & Payne Inc. Ridgeway 1-5	Atoka	634	-5,456	34.24192	-96.27880
11	Dillingham Oil Co. Dufur 1	Atoka	630	215	34.17470	-96.23756
12	Hamon Jake L. Crossland 1	Atoka	522	-7,458	34.24591	-96.21750
13	Arco Browne 1-28	Pittsburg	967	-13,023	34.97017	-95.51420

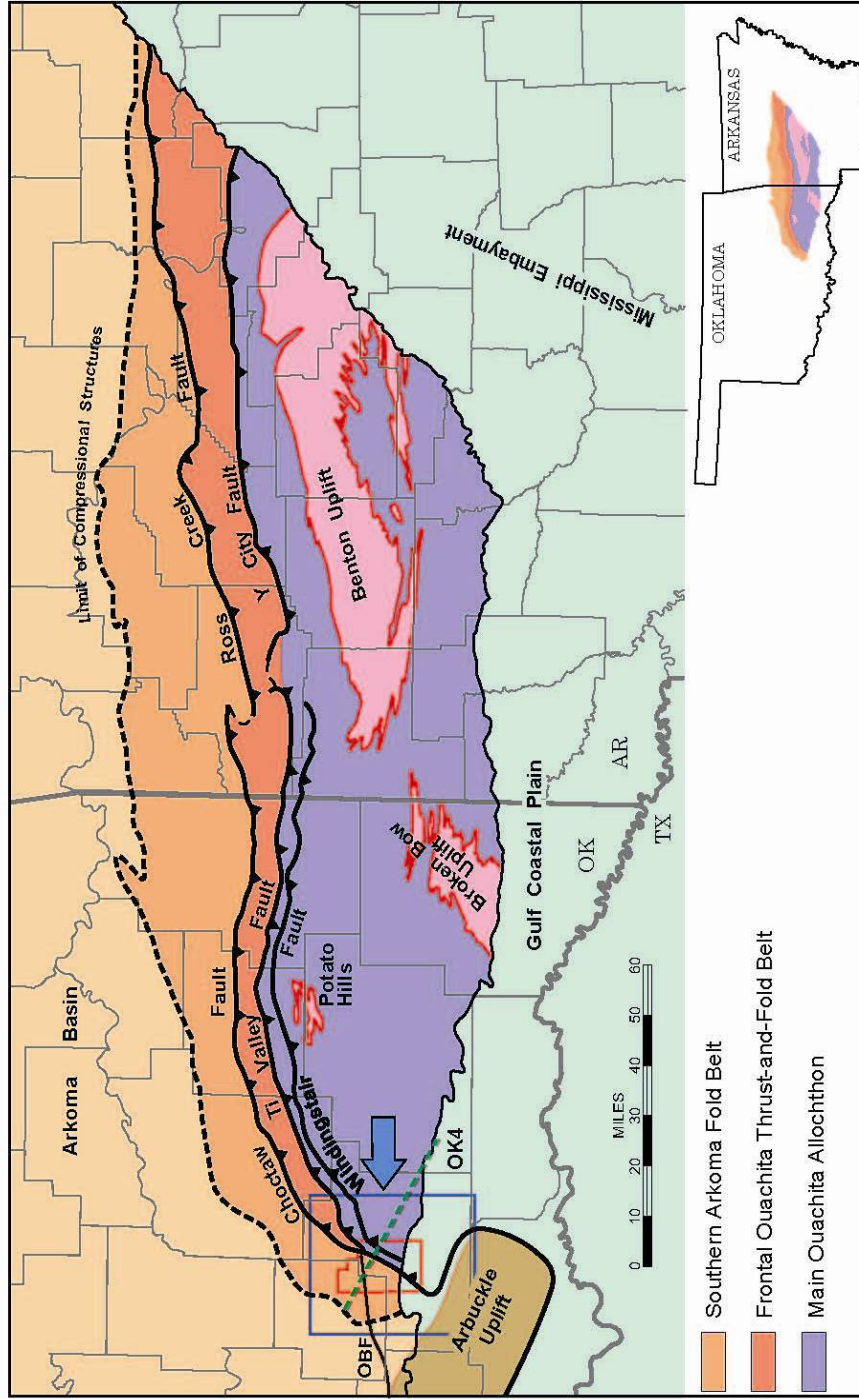


Figure 1.1: Index map of the study area showing the main structural subprovinces of the Arkoma basin-Ouachita orogenic belt province. The blue rectangle shows the boundary of the total magnetic intensity map, and the red polygon shows the boundary of the 3D seismic survey. OBF refers to the Olney-Bromide fault, and OK4 refers to structural cross section shown in dashed green color across the study area, (Modified from Arbenz, 2008).

		North American Continental Platform Section					Ouachita Deep-Water Facies						
		Arbuckle Facies Arkoma Basin Section		Deep-Water Facies Foredeep Section		Ouachita Basin Section							
Tertiary-Quaternary		Sedimentary formations (undivided)		TQ				Tertiary-Quaternary					
Cretaceous		Sedimentary formations (undivided); intrusives		K K _i				Cretaceous					
P e n n s y l v a n i a n	D e s m o i n e s i a n	Senora Formation		IPs				D e s m o i n e s i a n					
		Stuart Formation		IPst									
		Thurman Formation		IPt									
		Boggy Formation		IPbg									
		Bluejacket Sandstone Member		IPbj									
		Savanna Formation		IPsv									
		McAlester Formation		IPma									
		Hartshorne Formation		IPh									
		A t o k a	Atoka Formation		IPa		Atoka Formation		IPa				
					Atoka Formation (IPa) { Upper IPau Middle IPam Lower IPal								
	M o r r o w a n	Wapanucka Formation		IPw		Wapanucka Formation		IPw					
		Springer Group and Union Valley Formation (undivided)		IPm		Johns Valley Shale		IPjv					
M i s s i s s i p p i a n	C h e s t e r i a n	Caney Shale		Morrowan and Caney Shale (undivided)		MIPcm		Jackfork Group		IPj			
	M e r a m e c i a n							Stanley Group		Ms			
	O s a g e a n							Arkansas Novaculite		Da			
D e v o n i a n	K i n d e r h o o k i a n	Woodford Shale		Woodford Shale		Dw		Upper		Osagean			
	M i d d l e									Lower		Middle	
	L o w e r									Hunton Group		OsDh	
S i l u r i a n	U p p e r	Sylvan Shale		Sylvan Shale		Osy		Blaylock Sandstone		Sb			
	L o w e r							Polk Creek Shale		Opc			
O r d o v i c i a n	U p p e r	Viola Group		Ov		Viola Group		Ov		Upper			
	M i d d l e	Simpson Group		Os		Simpson Group		Os		Middle			
		Arbuckle and Timbered Hills Groups (undivided)		€Oa		Arbuckle and Timbered Hills Groups (undivided)		€Oa		Lower			
	L o w e r	Womble Shale		Ow		Womble Shale		Ow		Middle			
C a m b r i a n	U p p e r	Blakely Sandstone		Oby		Blakely Sandstone		Oby		Middle			
		Mazam Shale		Om		Mazam Shale		Om		Lower			
		Crystal Mountain Sandstone		Ocm		Crystal Mountain Sandstone		Ocm		Lower			
		Collier Shale		€Oc		Collier Shale		€Oc		Upper			
Precambrian		Continental Basement (granite, rhyolite)		P-€						Precambrian			

Figure I.2: Figure: Stratigraphic section of Arkoma basin-Ouachita orogenic belt province from Arbenz (2008).

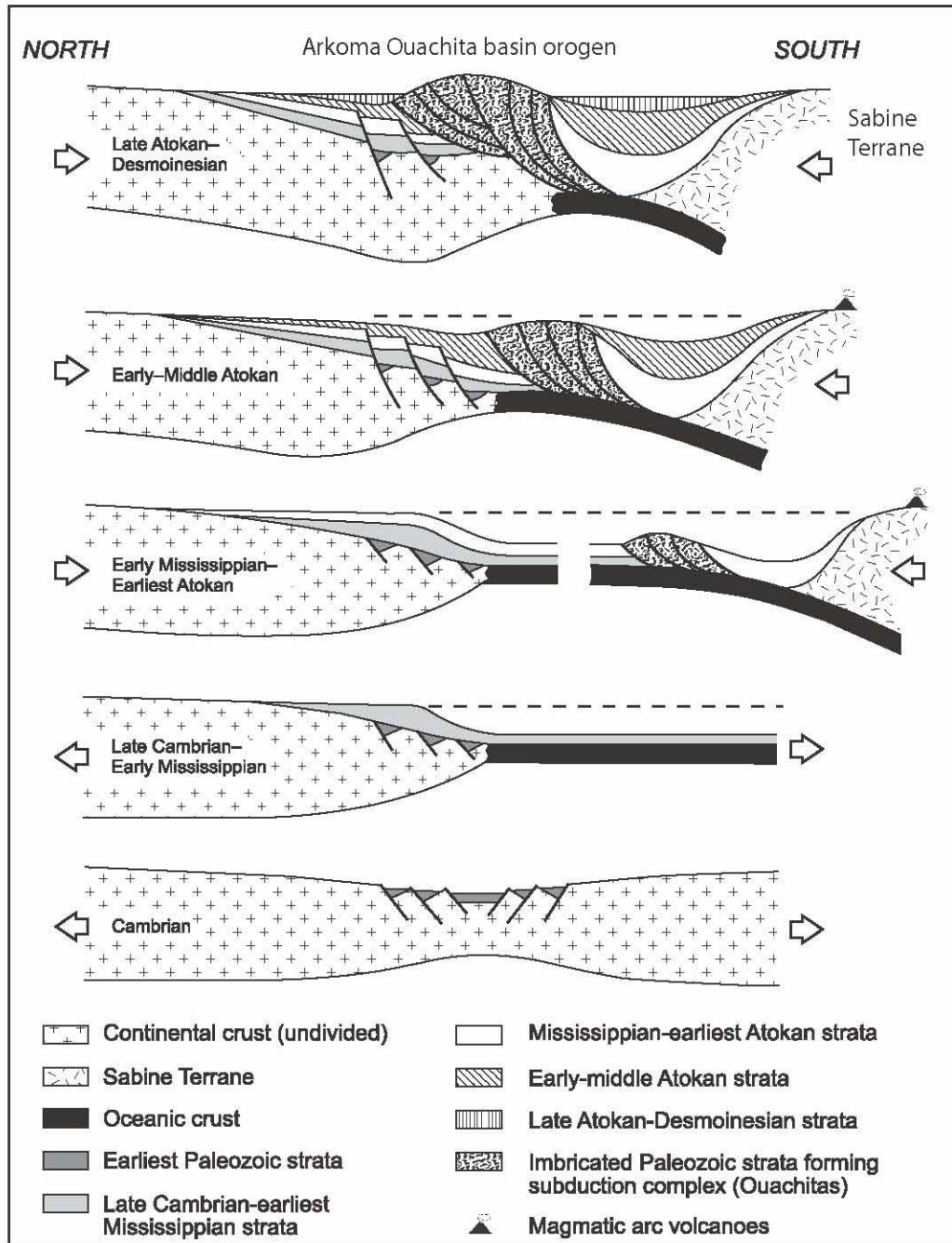


Figure I.3: Tectonic evolution of the Arkoma basin and the Ouachita orogenic belt, from Keller (2009) after Houseknect and Mathews (1985).

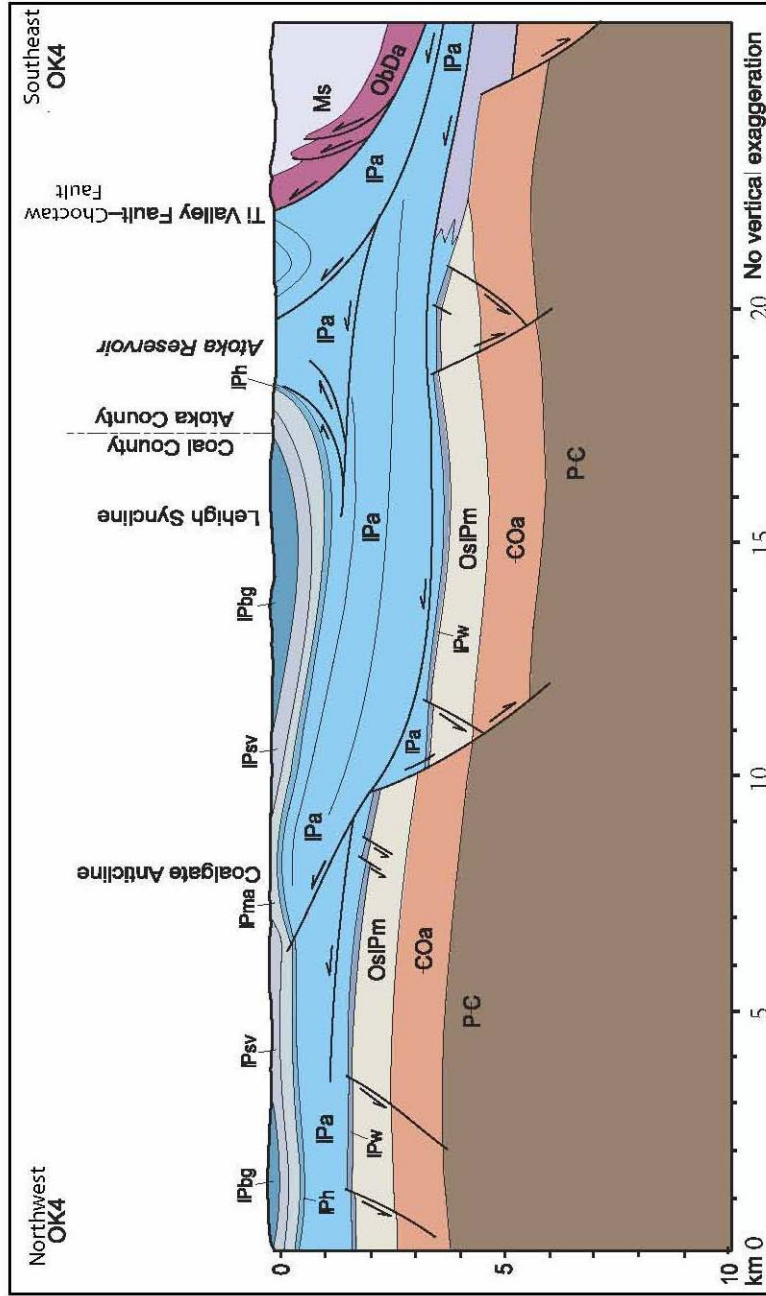


Figure I.4: Structural cross section OK4 across Ouachita Orogenic belt, modified from Arbenz (2008).

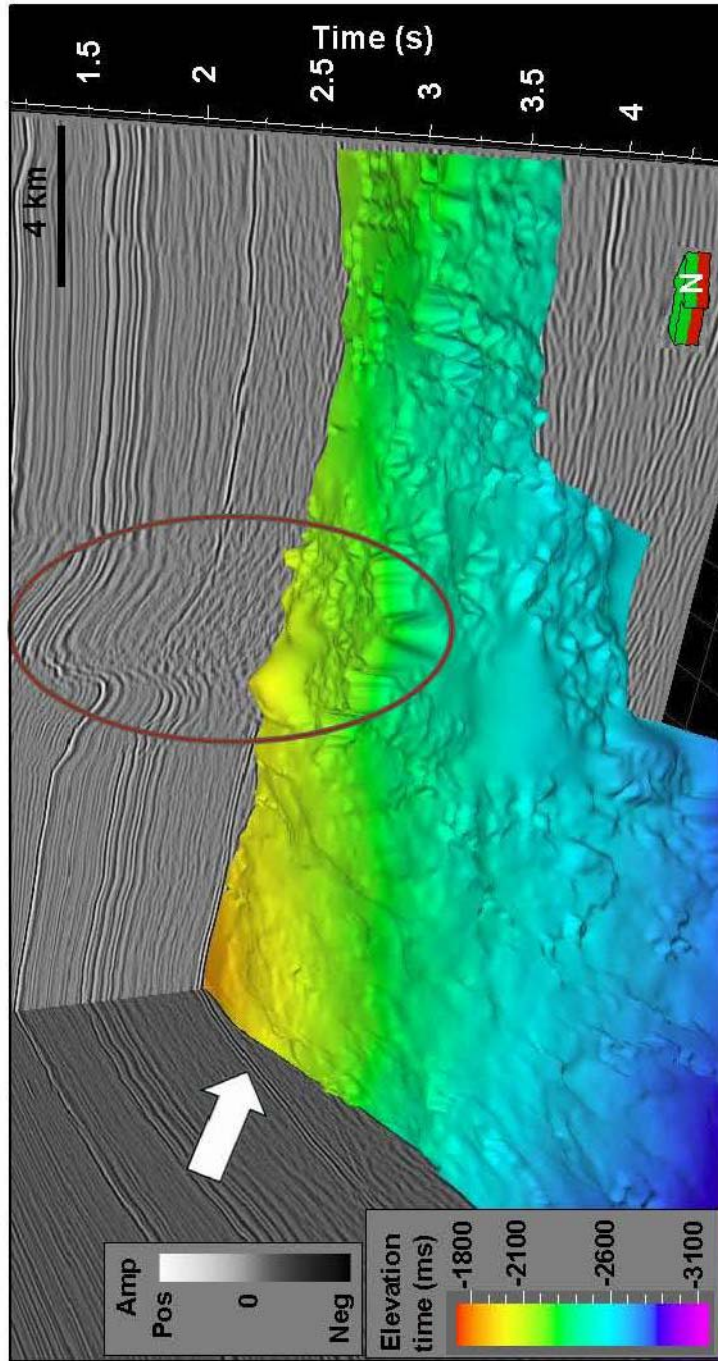


Figure I.5: 3D view showing the basement surface with intensive deformation due to tectonic inversion. The white arrow shows an unconformity surface between the basement and the Lower Paleozoic strata. The red ellipse shows an area of severe deformation.

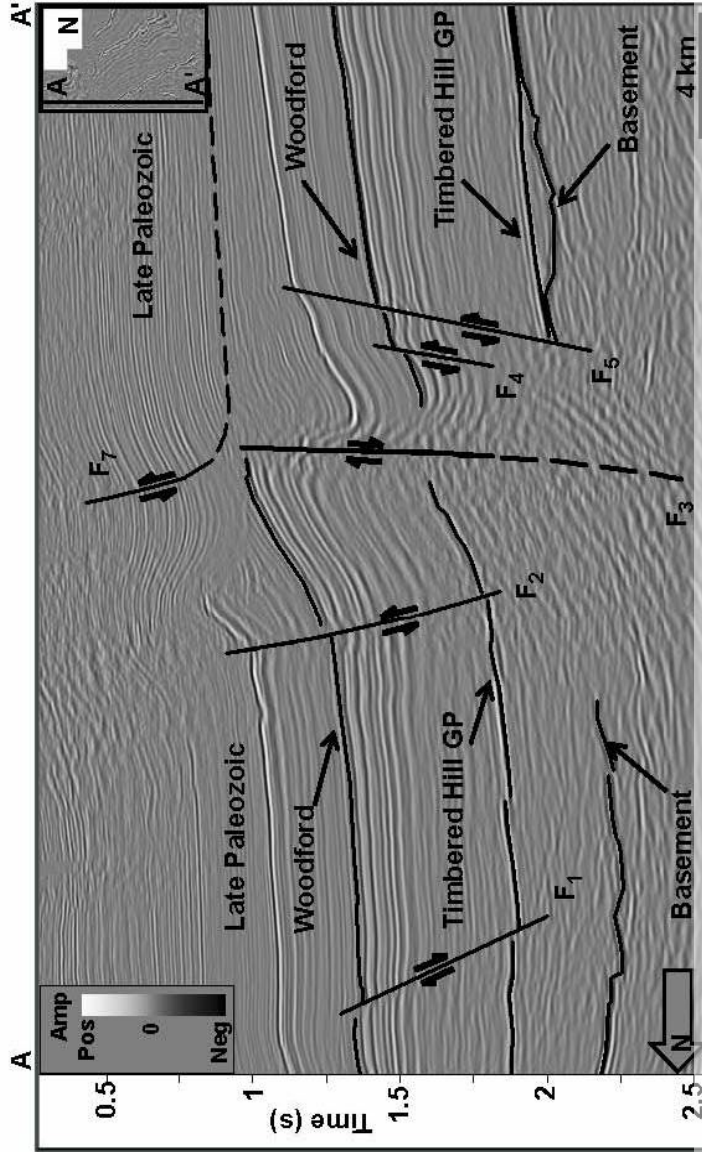


Figure I.6: Seismic section AA' showing an area of intensive deformation where some basement normal faults were reactivated as reverse faults (F2 and F3). The shallower Late Paleozoic thrust fault (F7) aligns vertically above the deeper basement fault. A distinct thickening of the Late Paleozoic strata is noticed above the downthrown blocks.

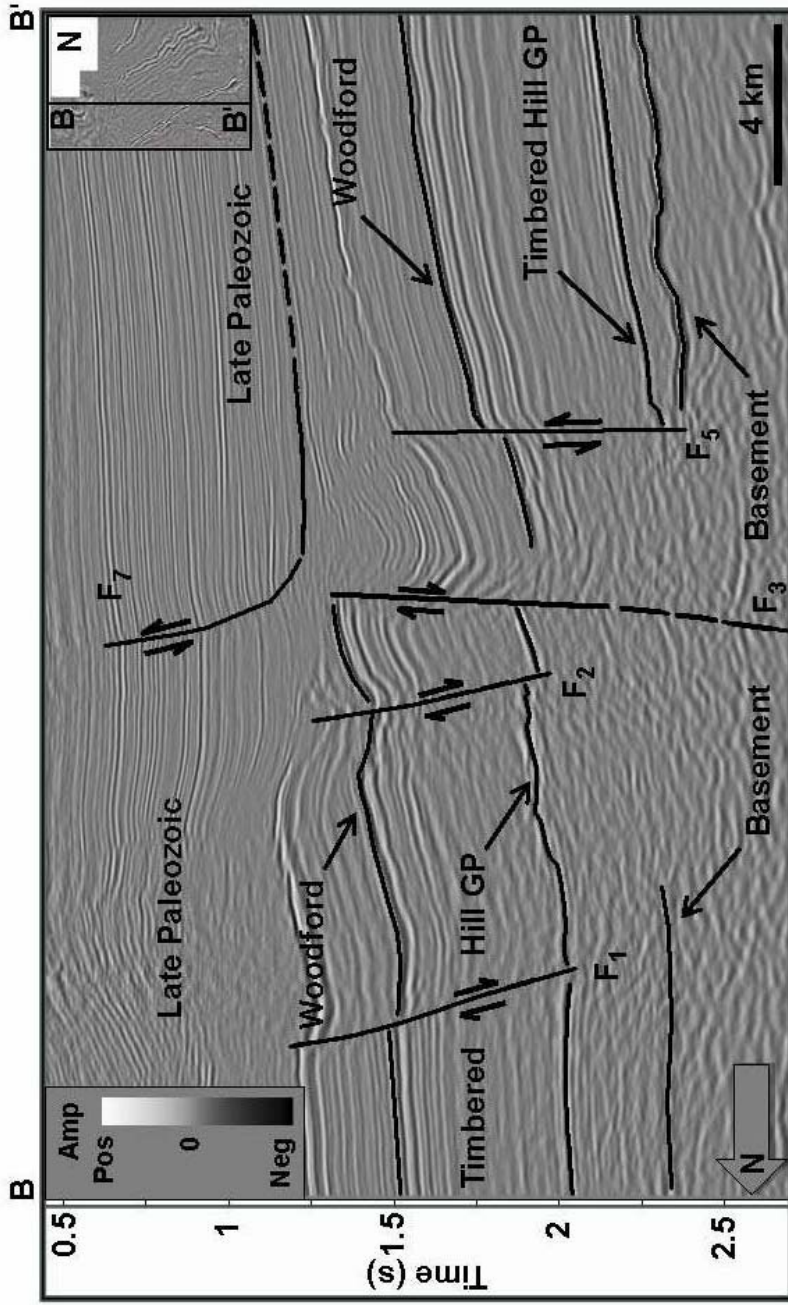


Figure I.7: Seismic section BB' showing the same area of intensive deformation where the master rift fault F3 was reactivated as a reverse fault. The fault F2 is normal in this seismic section. The seismic section BB' shows thicker Late Paleozoic strata above the downthrown blocks than those in the section AA'.

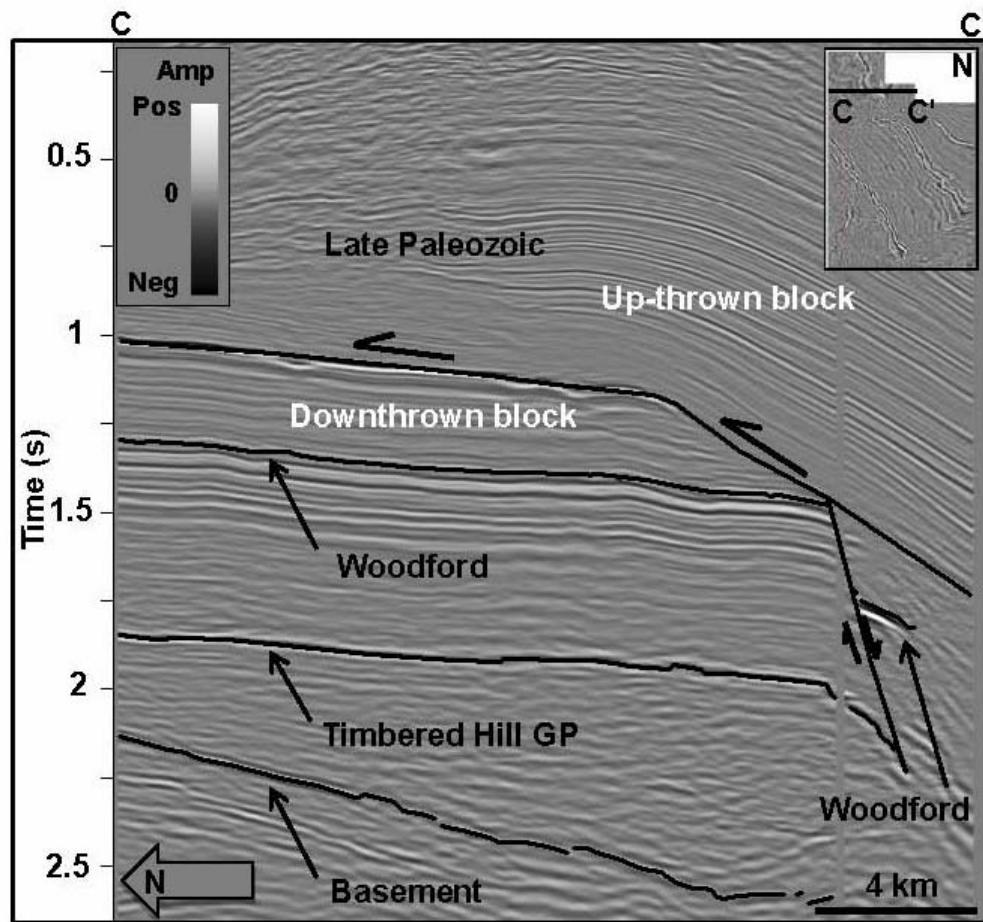


Figure I.8: Seismic section CC' showing the alignment of a thrust fault above the deeper normal fault as well as thickening of the Late Paleozoic strata above the downthrown blocks.

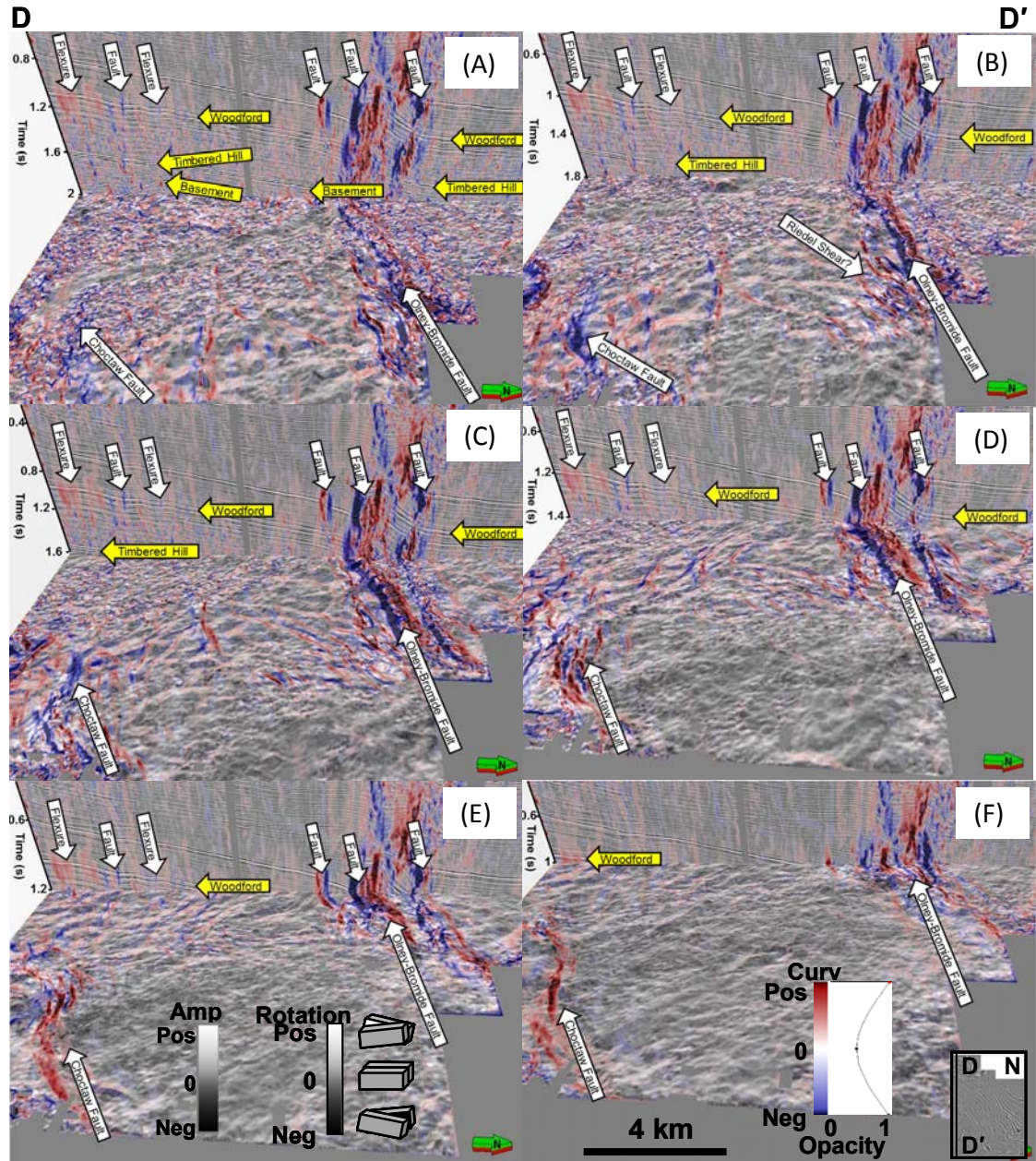


Figure I.9: Vertical slice DD' through the seismic amplitude and most-positive and most-negative principle curvatures, and time slices at (a) $t=2.0$, (b) $t=1.8$, (c) $t=1.6$, (d) $t=1.4$, (e) $t=1.2$ and (f) $t=1.0$ s through the reflector rotation co-rendered with the most-positive and most-negative principle curvatures showing different structural deformation. Anticlinal features and the up-thrown sides of faults show up as red. Synclinal features and the downthrown sides of faults show up as blue.

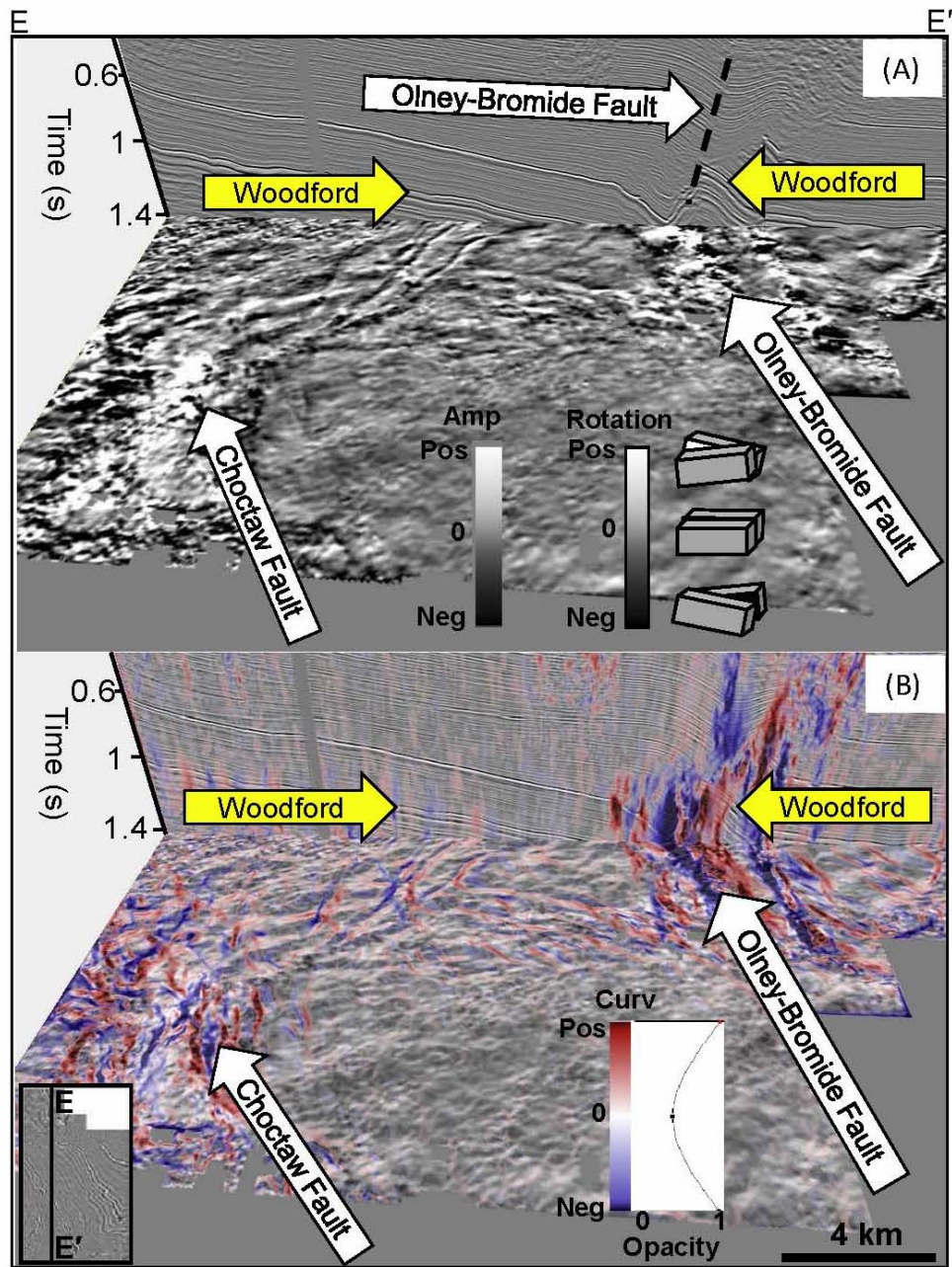


Figure I.10: (A) Vertical slice EE' through seismic amplitude and a time slice at $t=1.4$ s through reflector rotation showing the Olney-Bromide and Choctaw faults. (B) The same slices but co-rendered with most-positive and most-negative principal curvature.

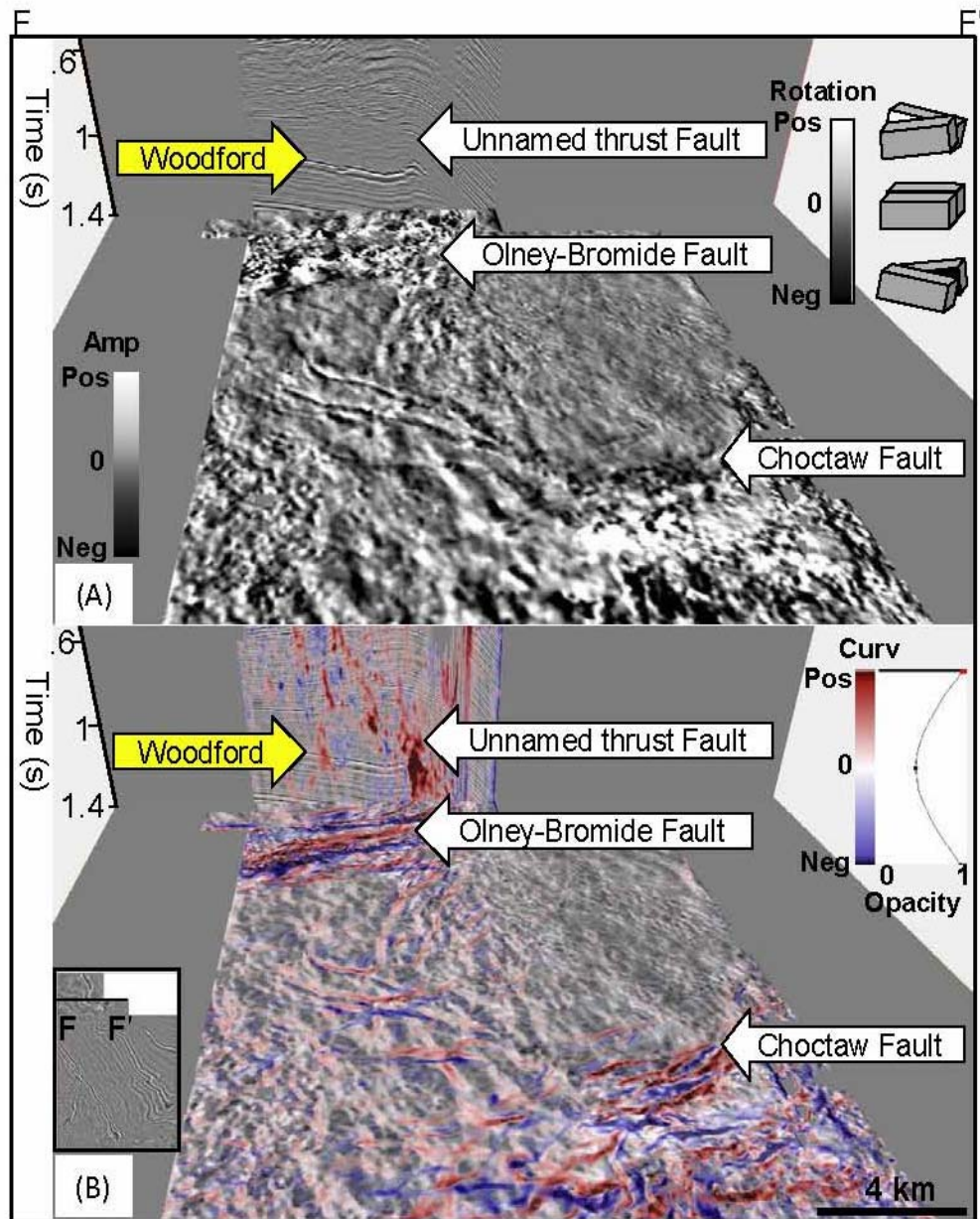


Figure I.11: (A) Vertical slice FF' through seismic amplitude and a time slice at $t=1.4$ s through reflector rotation showing the Olney-Bromide and Choctaw faults as well as unnamed thrust fault at the most northern part. (B) The same slices but co-rendered with the most-positive and most-negative principal curvature.

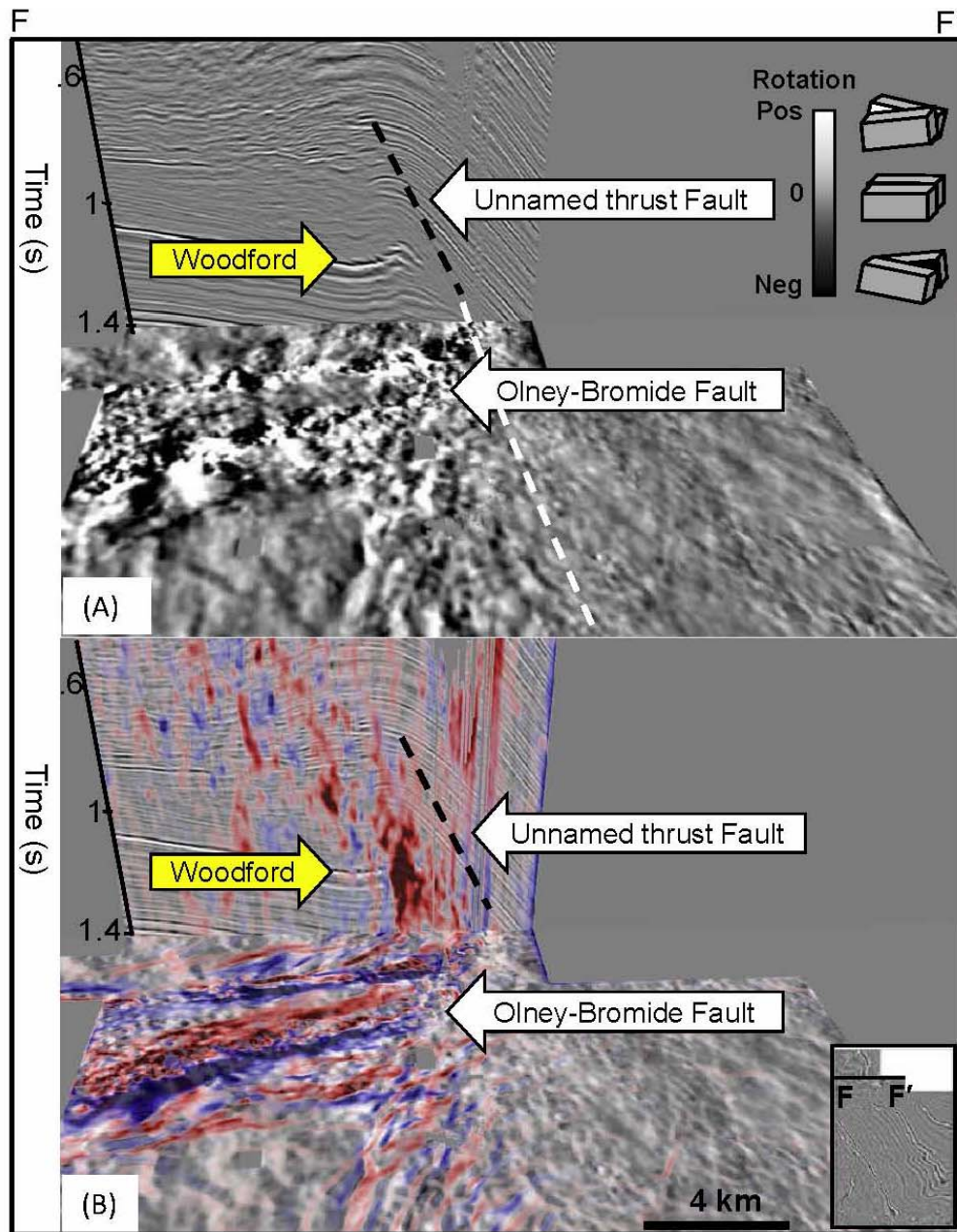


Figure I.12: Figure 12: (A) A zoomed in view of figure 11 showing the unnamed thrust fault clearly. (B) The same slices but co-rendered with most-positive and most-negative principal curvature showing the up- thrown side of the thrust fault as red.

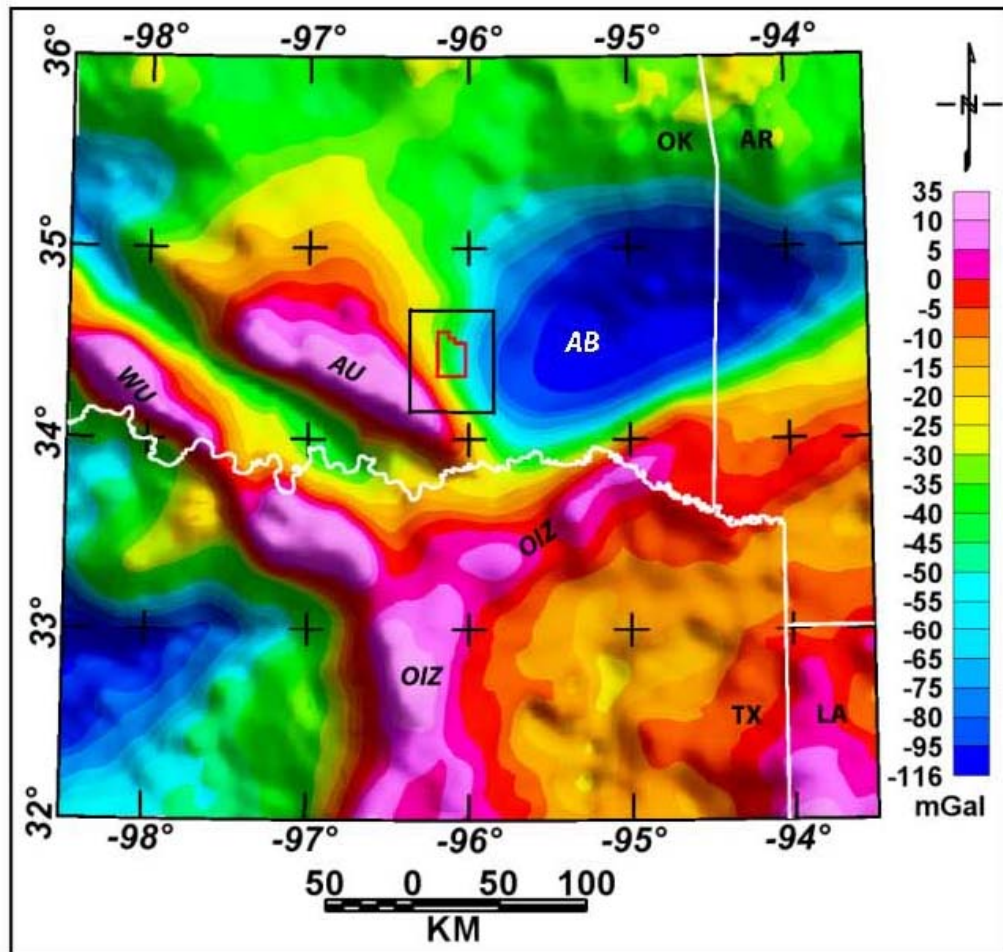


Figure I.13: Bouguer gravity map of the Arkoma basin and its surrounding showing very low gravity anomaly related to the Arkoma basin (AB) and very high anomalies due to the Wichita Uplifts (WU), Arbuckle Uplifts (AU) and Ouachita interior zone (OIZ). The black rectangle shows the boundaries of the total magnetic intensity map and the red polygon shows the boundaries of the seismic survey.

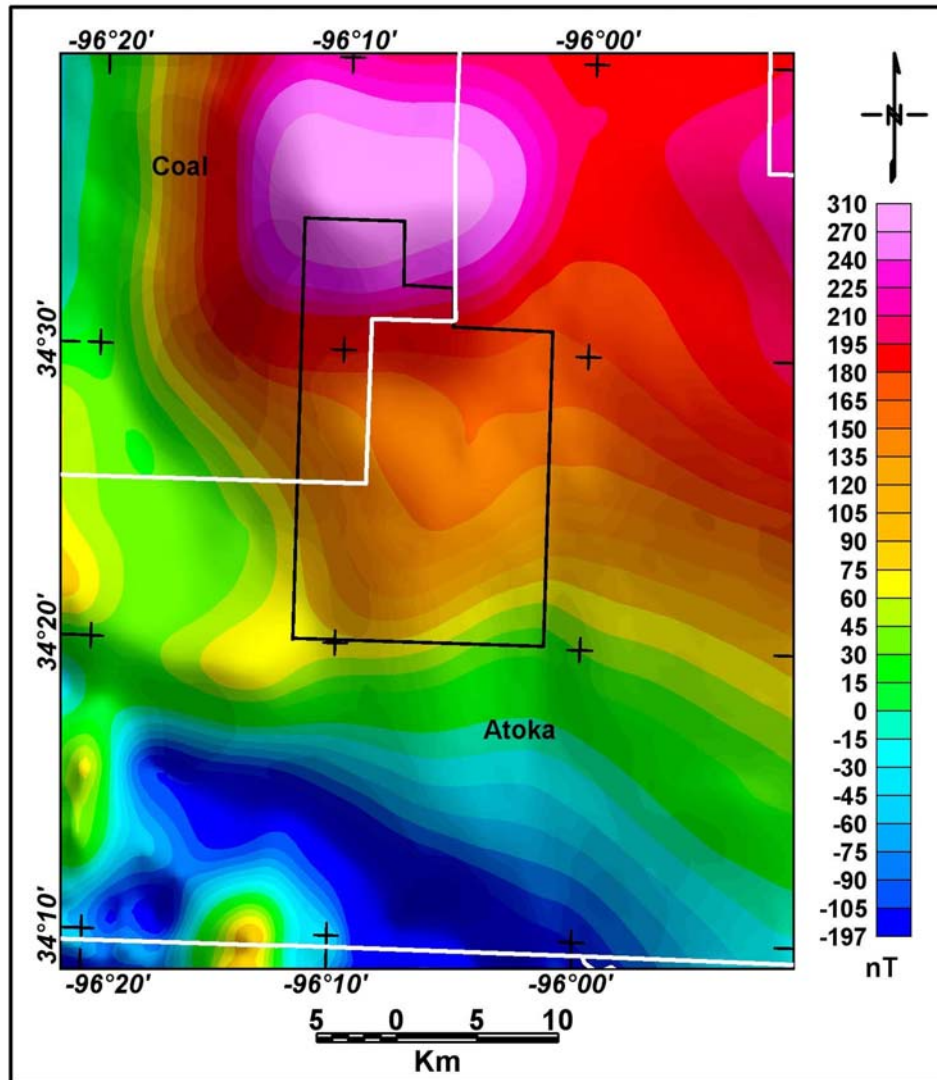


Figure I.14: The reduced to pole total magnetic intensity map of the study area showing the seismic survey boundaries (black polygon).

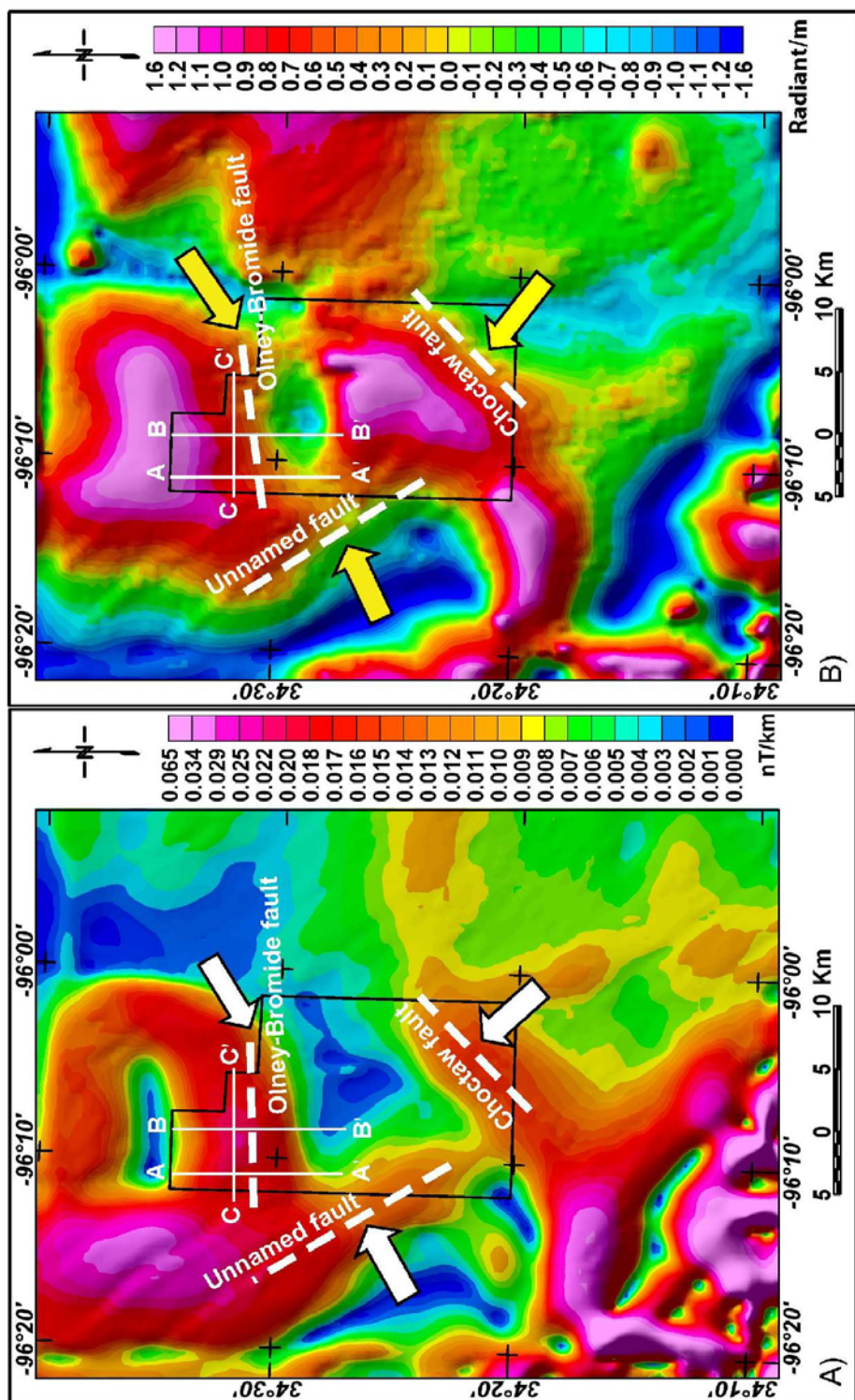


Figure I.15: The total horizontal derivative of the magnetic data (A) showing magnetic maxima above the magnetic edges or the faults (white arrows). The tilt derivative (B) showing low or close to zero magnetic values above the edges or the faults (yellow arrows). AA', BB' and CC' are seismic sections in Figures 6, 7 and 8.

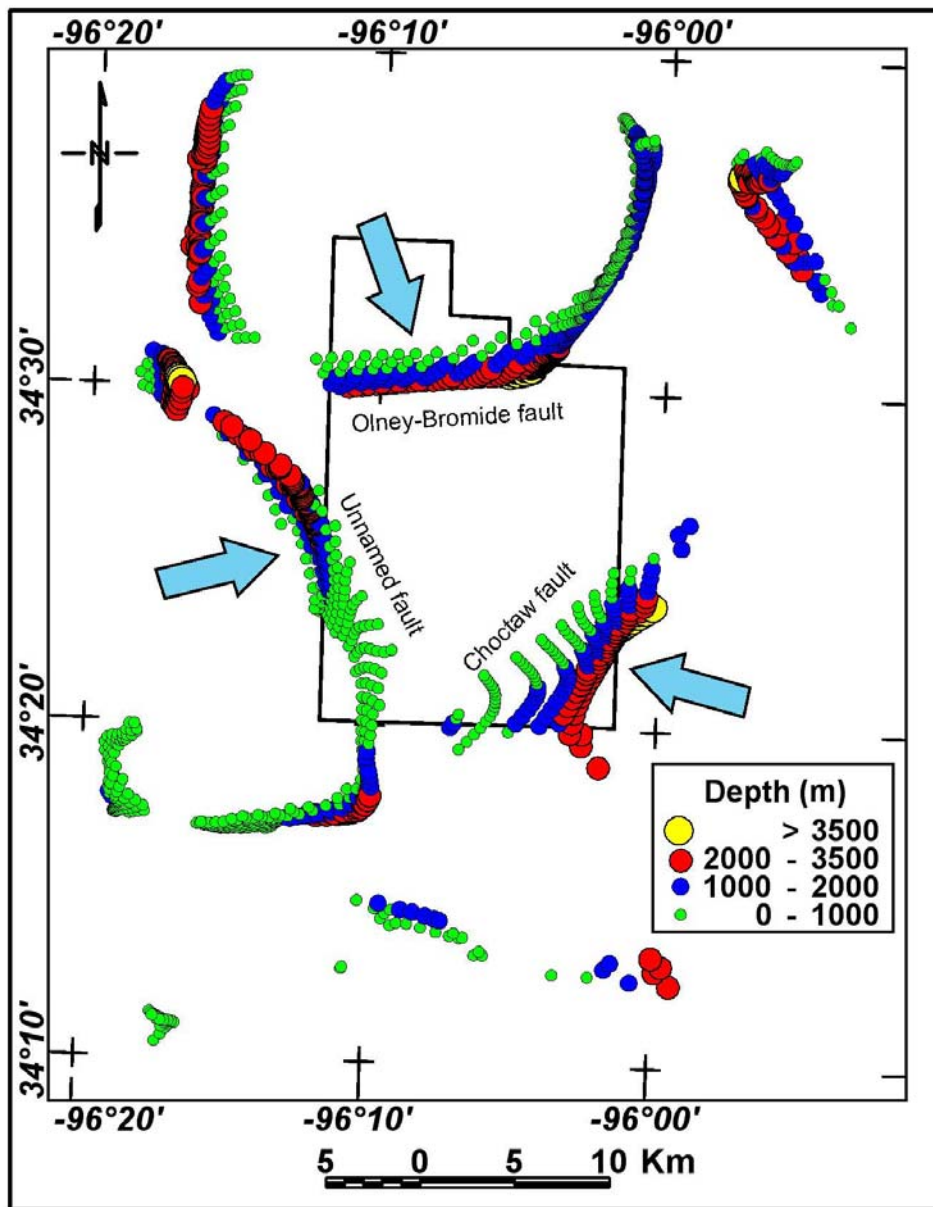


Figure I.16: Euler solution plot using structural index (SI=0.0 faults). The plot shows three clusters along EW trend at the north, NE-SW trend at the southeast, and NW-SE at the west. These clusters coincide with the Olney-Bromide fault, Choctaw fault and unnamed fault, respectively (blue arrows).

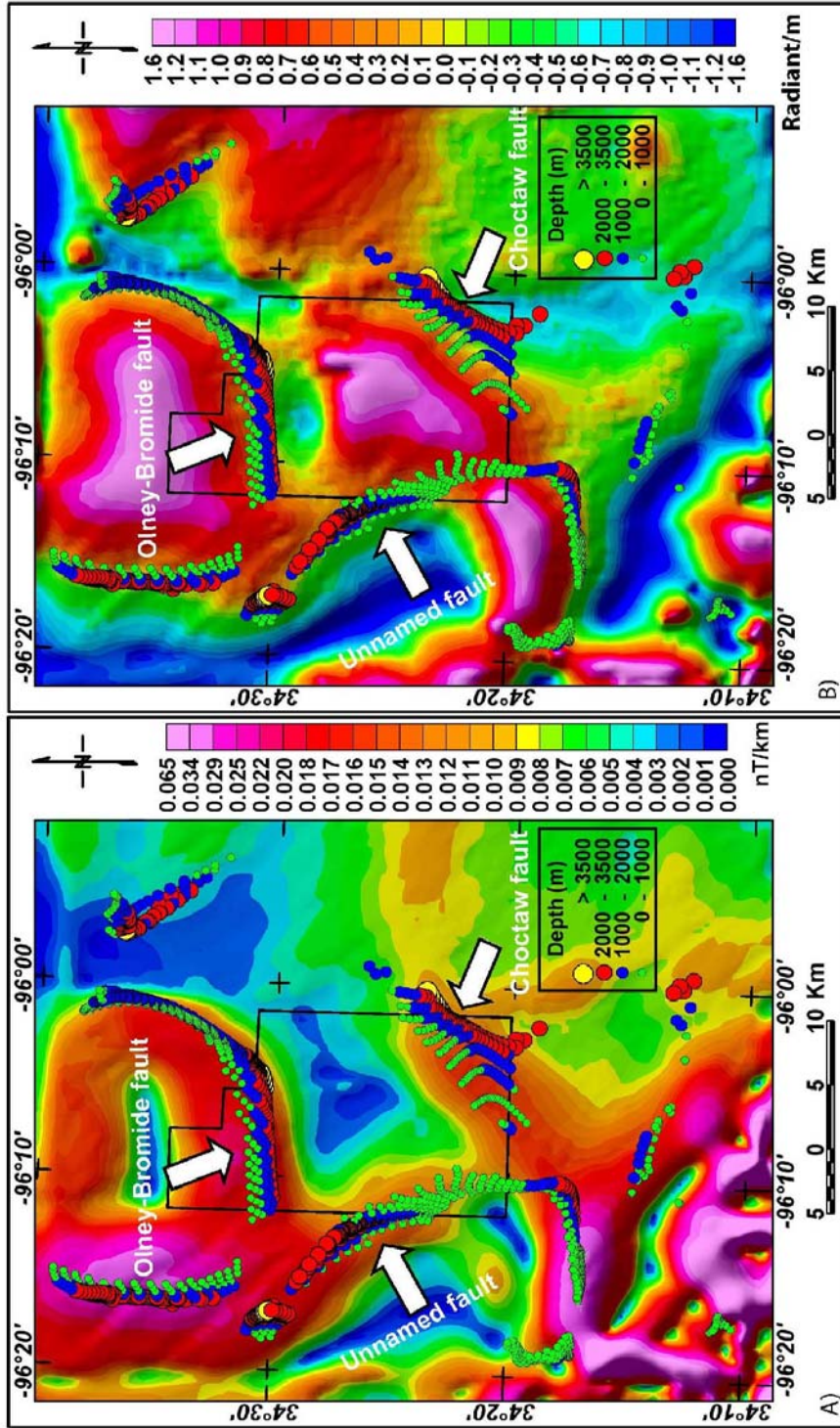


Figure I.17: The Euler solution cluster plots superimposed on the total horizontal derivative (A) and tilt derivative (B) of the magnetic data. The cluster plots coincide with the fault trends or the edges of the magnetic source bodies (white arrows).

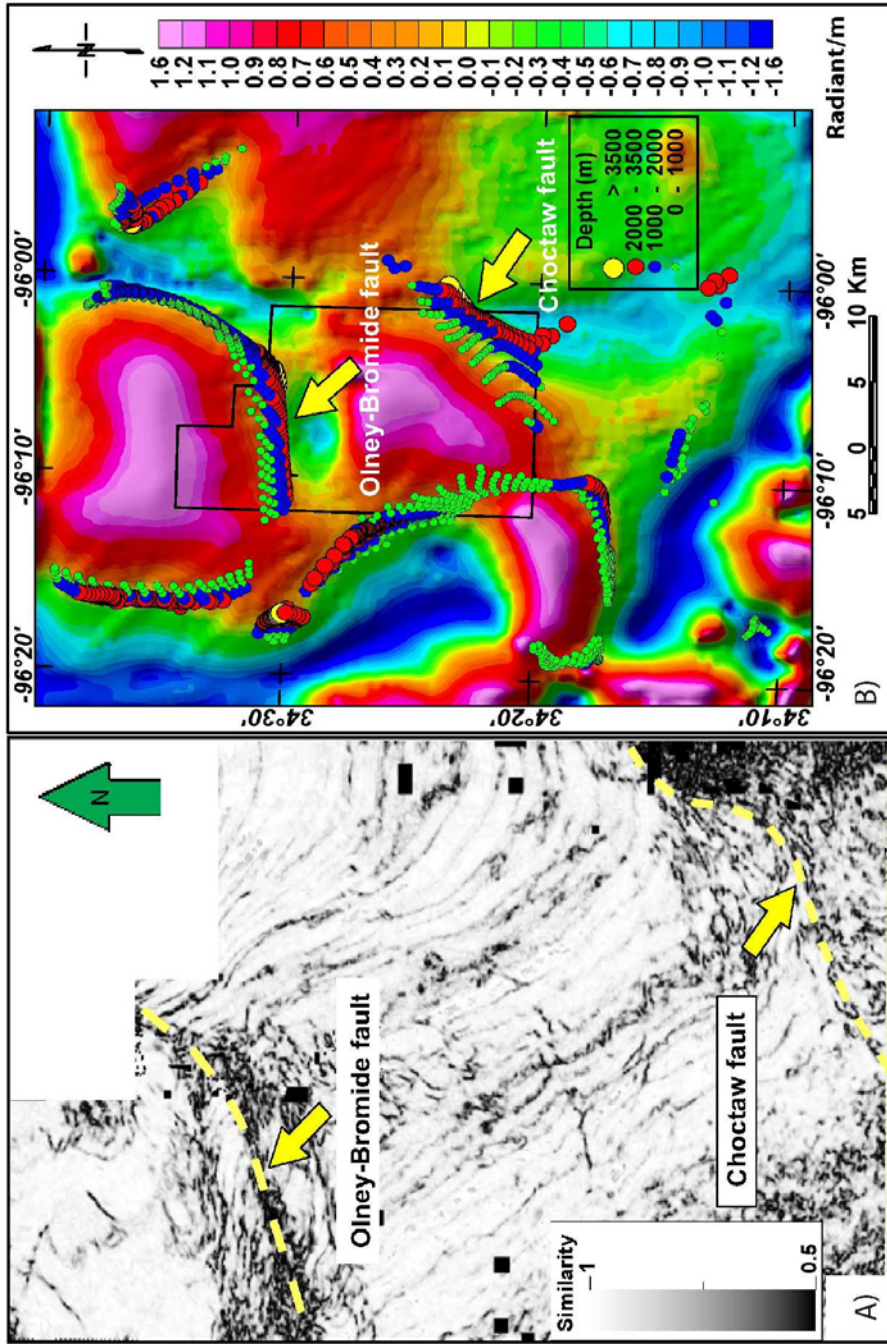


Figure 1.18: Time slice at 1470 ms through the coherence volume (A) and the Euler solution cluster plot superimposed on tilt derivative of the magnetic data (B) showing a strong correlation between the fault trends from the seismic data and those from Euler's methods and the edge detector technique (yellow arrows).

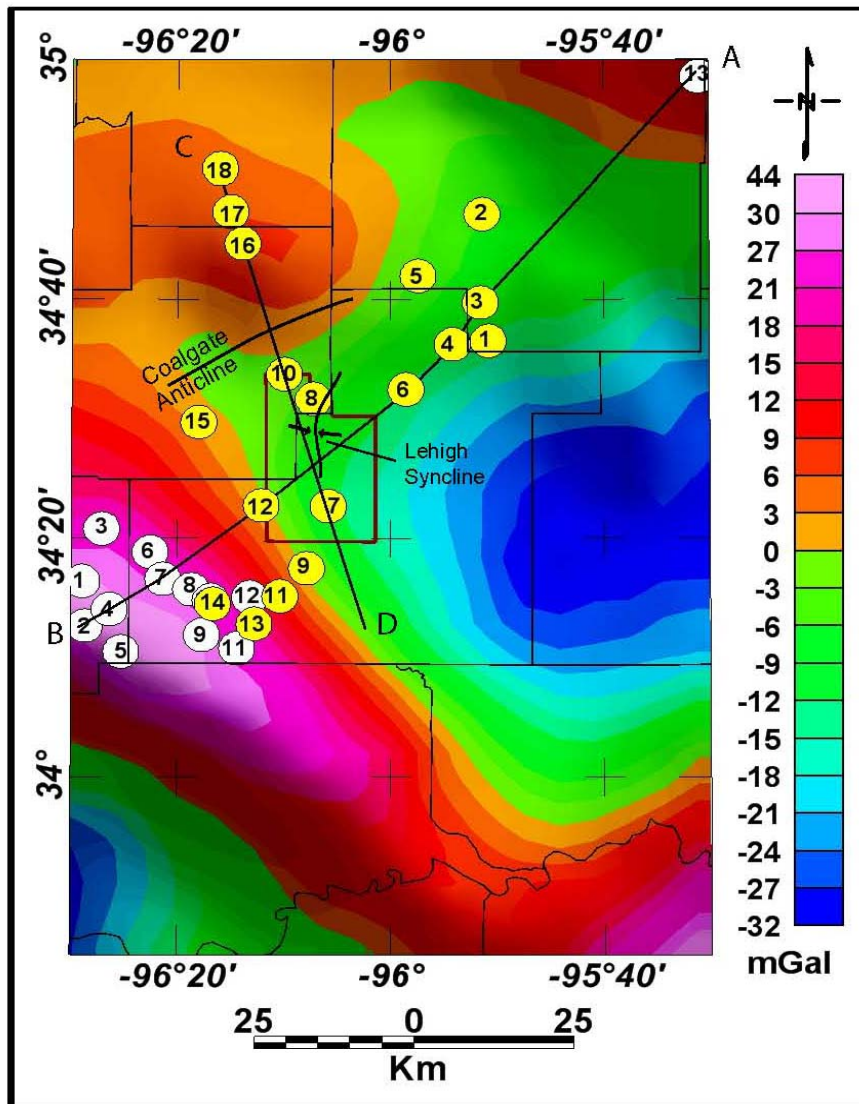


Figure I.19: Residual gravity map after upward continuation to 40 km showing the location of the wells and two selected profiles for the density models. Wells penetrating to the top of the basement are shown in white, and those penetrating to the top of the Arbuckle are shown in yellow.

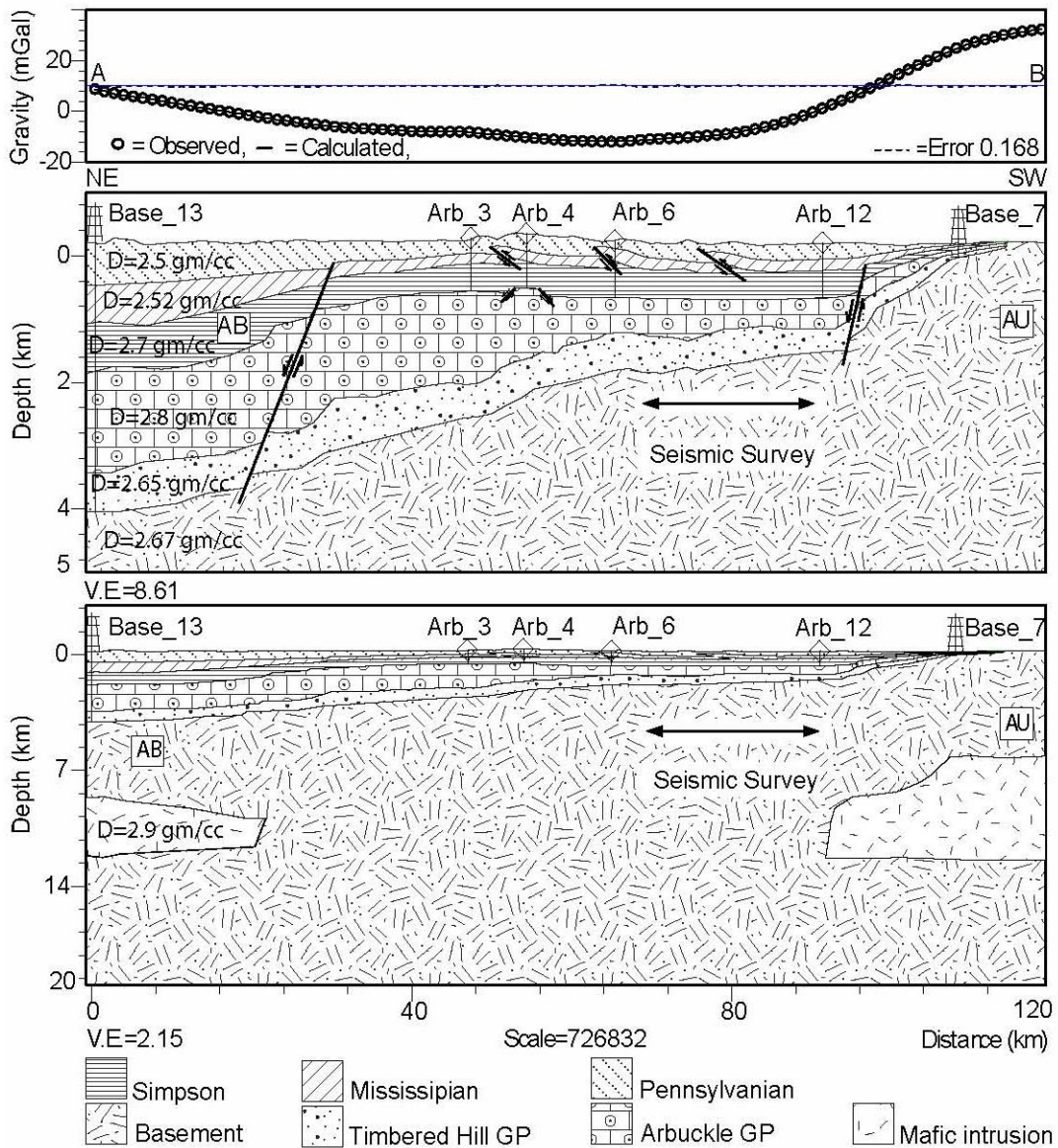


Figure I.20: Local gravity model along the profile AB extending NE-SW. The positive anomaly at the southeast is due to mafic rocks at the core of Arbuckle Uplift (AU). The broad negative anomaly at the middle part coincide with the thickening of the Late Paleozoic strata and the due to thickening of the Paleozoic rocks in Arkoma basin (AB). D refers to the densities of the different stratigraphic units. Arb_3, 4 and 6 refer to the wells that penetrate to the top of the Arbuckle Group, and Base_7 and 13 refer to wells that penetrate to the basement.

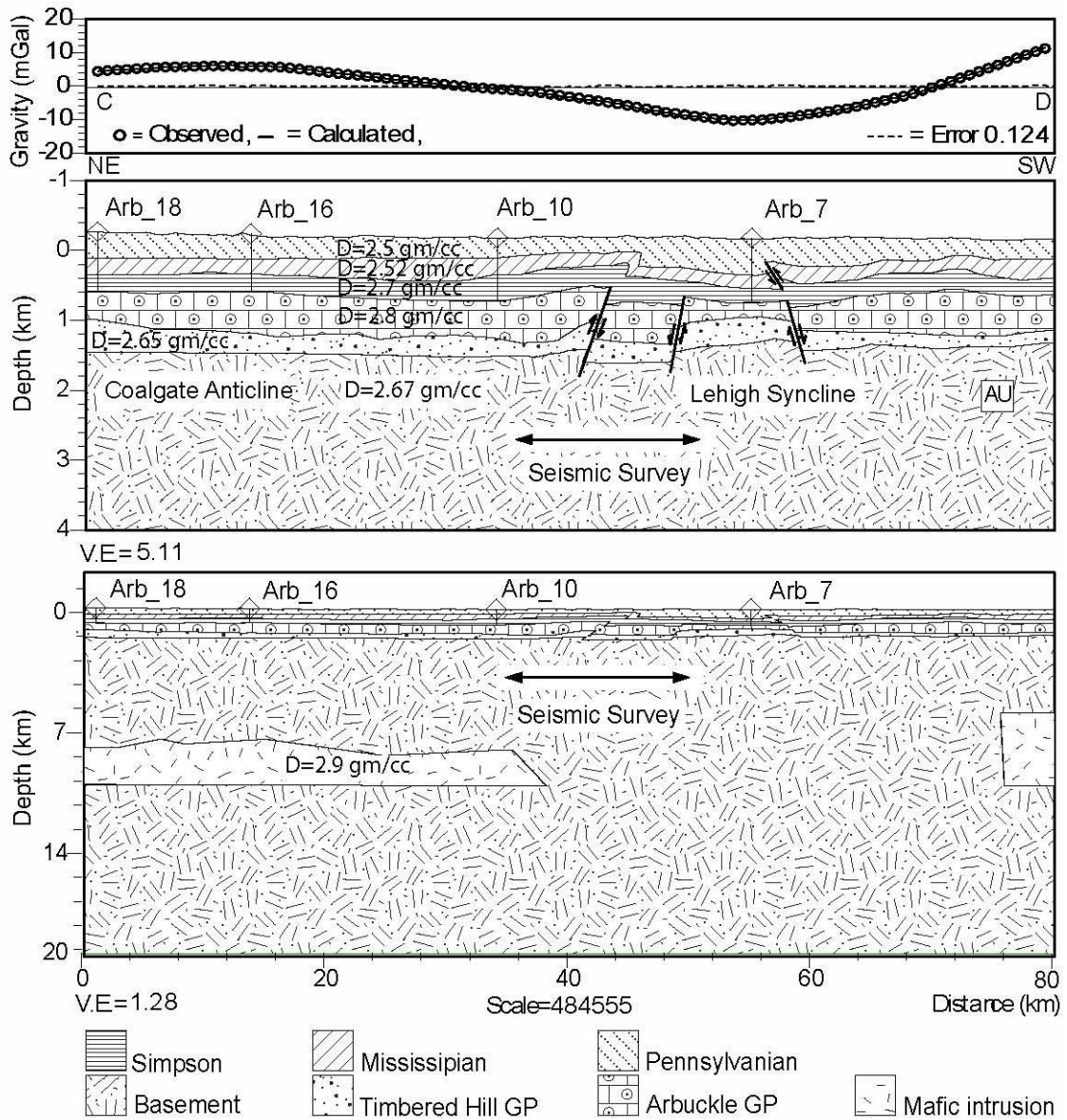


Figure I.21: Local gravity model along the profile CD extending NW-SE. The positive anomaly at the northwest is due to thinning of the Late Paleozoic strata and due to shallowing of the basement. The positive anomaly at the southeast is due to mafic rocks at the core of Arbuckle Uplift (AU). The negative anomaly may result from thickening of the Late Paleozoic strata in Lehigh syncline.

REFERENCES

- Arbenz, K. J., 2008, Structural framework of the Ouachita Mountains, in Suneson, N. H., (ed.), Stratigraphic and structural evolution of the Ouachita Mountains and Arkoma basin, southeastern Oklahoma and west-central Arkansas: Applications to petroleum exploration: 2004 Field Symposium. Oklahoma Geological Survey, Circular 112A, the Arbenz-Misch/Oles Volume, p. 1-40.
- Baruch, E., O. O. Elebiju, and R. Perez, 2009, Geophysical evidence of basement controlled faulting in the Ellenberger group and Viola limestone, Fort Worth basin, Texas: 79th annual meeting of the Society of Exploration Geophysicists, expanded abstract, no. 28, p. 995-999.
- Blakely, R. J., and R. W. Simpson, 1986, Approximating edges of source bodies from magnetic or gravity anomalies: *Geophysics*, v. 51, no. 7, p. 1494–1498.
- Branan, C. B., Jr., 1968, Natural gas in Arkoma basin of Oklahoma and Arkansas: *AAPG Bulletin*, v. 52, p. 1616-1635.
- Chopra, S., 2001a, Integrating coherence cube imaging and seismic inversion: *The Leading Edge*, v. 20, p. 354-362.
- Chopra, S., 2001b, Integrating coherence cube imaging and seismic attributes: *Canadian Society of Exploration Geophysicists, Recorder*, v. 26. no. 10, p. 20-22.
- Chopra, S. and K. J. Marfurt, 2007, Seismic curvature attributes for mapping faults/fractures, and other stratigraphic features: *Canadian Society of Exploration Geophysicists, Recorder*, v. 32. no. 10, p. 37-41.
- Dickinson, W. R., 1974, Plate tectonics and sedimentation, in Dickinson, W. R. (ed.), *Tectonics and sedimentation: Tulsa, Oklahoma, Society of Economic Paleontologists Mineralogists, Special Publication*, v. 22, p. 1-27.
- Eissa, M. A., and J. P. Castagna, 2003, Case study: AVO analysis in a high-impedance Atoka sandstone (Pennsylvanian), north Arkoma basin, McIntosh County, Oklahoma: *The Leading Edge*, v. 22, p. 988-997.

- Elebiju, O. O., G. R. Keller, and K. J. Marfurt, 2010, Investigation of links between Precambrian basement structure and Paleozoic strata in the Fort Worth basin, Texas, U.S.A., using high-resolution aeromagnetic, HRA data and seismic attributes: *Geophysics*, v. 75, p. 157-168.
- Gangopadhyay, T., and E. Heydari, 1995, Compositional variation and tectono-sedimentary conditions of the Atoka deltaic sediments, Arkansas: *Gulf Coast Association of Geological Societies Transactions*, v. 45, p. 203-210.
- Gutmanis, J., T. Batchelor, and Colleagues of GeoScience Limited, 2010, Hydrocarbon production from fractured basement formations: GeoScience Limited, 40 p. http://www.geoscience.co.uk/assets/file/ReservoirsinFracturedBasementVer_JCG.pdf (accessed July 2012)
- Hinze, W. J., C. Aiken, J. Brozena, B. Coakley, D. Dater, G. Flanagan, R. Forsberg, T. Hildenbrand, G. R. Keller, and J. Kellogg, 2005, New standards for reducing gravity data: The North American gravity database: *Geophysics*, v.70, p.25-32.
- Holdsworth, R. E., M. Stewart, J. Imber, and R. A. Strachan, 2001, The structure and tectonic evolution of reactivated fault zones-a review and case study: Geological Society of London, Special Publication 184, p. 115-137.
- Houseknecht, D. W. and S. M. Matthews, 1985, Thermal maturity of Carboniferous strata, Ouachita Mountains: *AAPG Bulletin*, v. 69, p. 335-345.
- Houseknecht, D. W., 1987, The Atoka formation of the Arkoma basin: Tectonic, sedimentology, thermal maturity, sandstone petrology: Tulsa Geological Society Short Course Notes, 72 p.
- Jones-Cecil, M., 1995, Structural controls of Holocene reactivation of the Meers fault, southwestern Oklahoma, from magnetic studies: *Geological Society of America Bulletin*, v. 107, p. 98-112.
- Keller, G. R., 2009, Some thoughts on the structure and evolution of the Ouachita Mountains-Arkoma Basin region, *Oklahoma Geology Notes*, v. 69, no.1, p. 4-12.

- Keller, G. R., E. G. Lidiak, W. J. Hinze, and L. W. Braile, 1983, The role of rifting in the tectonic development of the midcontinent, USA: *Tectonophysics*, v. 94, p. 391-412.
- Keller, G. R., T. G. Hildenbrand, R. Kucks, D. Roman, and A. M. Hittelman, 2002, Upgraded gravity anomaly base of the United States: *The Leading Edge*, v. 21, p.366-367.
- Keller, G. R., T. G. Hildenbrand, R. Kucks, M. Webring, Allen Briesacher, Kristine Rujawitz, A. M. Hittelman, Dan Roman, Dan Winester, R. Aldouri, Roberto Torres, W. J. Hinze, Ann Gates, and John Seeley, 2006, A community effort to construct a gravity database for the United States and an associated web portal, *in*, Sinha, A. K. (ed.), *Geoinformatics: Data to Knowledge*: Geological Society of America, Special Paper 397, p. 21-34.
- Keller, G. R. and R. A. Stephenson, 2007, The Southern Oklahoma and Dniepr-Donets aulacogens: a comparative analysis, *in* Hatcher, R. D., Jr., Carlson, M. P., McBride, J. H., and Martínez Catalán, J. R. (eds.), *The 4D Framework of Continental Crust*: Geological Society of America, Memoir 200, p. 127-143.
- Kruger, J. M., and G. R. Keller, 1986, Interpretation of crustal structure from regional gravity anomalies, Ouachita Mountains area and adjacent Gulf Coastal Plain: *AAPG Bulletin*. v. 70, no. 6, p. 667-689.
- Lahti, I., and T. Karinen, 2010, Tilt derivative multiscale edges of magnetic data. *The Leading Edge*, v. 29; p. 24-29.
- Mickus, K. L., and G. R. Keller, 1992, Lithospheric structure of the south-central U.S.: *Geology*, v. 20, p. 335-338.
- Miller, H. G., and V. Singh, 1994, Potential field tilt; a new concept for location of potential field sources: *Journal of Applied Geophysics*, v. 32, p. 213-217.
- Mosher, S., 1998, Tectonic evolution of the southern Laurentian Grenville orogenic belt: *Geological Society of America Bulletin*; v. 110, p. 1357-1375.
- Puckett, R. E. Jr., 2011, A thick sequence of rift-related basalts in the Arbuckle Mountains, Oklahoma, as revealed by deep drilling: *Shale Shaker*, v. 61, p. 207-216.

- Reid, A. B., J. M. Allsop, H. Granser, A. J. Millett, and I. W. Somerton, 1990, Magnetic interpretation in three dimensions using Euler deconvolution: *Geophysics*, v. 55, p. 80-91.
- Salem, A., S. Williams, J. D. Fairhead, D. Ravat, and R. Smith, 2007, Tilt-depth method: A simple depth estimation method using first order magnetic derivatives. *The Leading Edge*, v. 26, p. 1502–1505.
- Saltus, R. W. and R. J. Blakely, 2011, Unique geologic insights from “non-unique” gravity and magnetic interpretation: *Geological Society of America Today*, v. 21, no. 12, p. 4-11.
- Sims, P. K., H. J. Stein, and C. A. Finn, 2002, New Mexico structural zone - an analog of the Colorado mineral belt: *Ore Geology Reviews*, v. 21, p. 211-225.
- Sims, P. K., R. W. Saltus, and E. D. Anderson, 2005, Preliminary Precambrian basement structure map of the continental United State - an interpretation of geologic and aeromagnetic data: *United States Geological Survey Open-File Report 2005-1029*. 31p.
- Sullivan, E. C., K. J. Marfurt, A. Lacazette, and M. Ammerman, 2005, Application of new seismic attributes to collapse chimneys in the Fort Worth basin: *Geophysics*, v.71, no. 4, p. 111-119.
- Suneson, N. H., 1995, Structural interpretation of the Arkoma basin-Ouachita Mountains transition zone, southeastern Oklahoma: a review, in Johnson, K. S., (ed.), *Structural styles in the southern Midcontinent, 1992 symposium*: Oklahoma Geological Survey Circular 97, p. 259-263.
- Sutherland K. P., 1988, Late Mississippian and Pennsylvanian depositional history in the Arkoma basin area, Oklahoma and Arkansas: *Geological Society of American Bulletin*, v. 100, p. 1787-1802.
- Thomas, W. A., 1977, Evolution of Appalachian-Ouachita salient and recesses from reentrants and promontories in the continental margin: *American Journal of Science*, v. 277, p. 1233-1278.

- Thomas, W. A., and D. L. Baars, 1995, The paradox transcontinental fault zone, in Johnson, K. S., (ed.), Structural styles in the southern Midcontinent, 1992 symposium: Oklahoma Geological Survey Circular 97, p. 113-118.
- Thompson, D. T., 1982, EULDPH: A new technique for making computer-assisted depth estimates from magnetic data: *Geophysics*, v. 47, p. 31-37.
- Thompson, T. L., B. W. Hawley, J. R. Howe, and S. P. Gay, 1995, Basement influence on the structural geology of southern Oklahoma inferred from residual aeromagnetic maps, in Johnson, K. S. (ed.), Structural styles in the southern Midcontinent, 1992 symposium: Oklahoma Geological Survey, Circular 97, p. 13-14.
- Verduzco, B., J. D. Fairhead, C. M. Green, and C. MacKenzie, 2004, New insights into magnetic derivatives for structural mapping: *The Leading Edge*, v. 23, p. 116–119.
- Viele, G. W., 1989, The Ouachita orogenic belt, in Hatcher, R. D., Jr., Thomas, W. A., and Viele, G. W. (eds.), *The Appalachian-Ouachita Orogen in the United States: Geological Society of America, The Geology of North America*, v. F-2, p. 555-561.
- Viele, G. W. and W. A., Thomas, 1989, Tectonic synthesis of the Ouachita orogenic belt, in Hatcher, R. D., Jr., Thomas, W. A., and Viele, G. W. (eds.), *The Appalachian-Ouachita Orogen in the United States: Geological Society of America, The Geology of North America*, v. F-2, p. 695-728.
- Whitmeyer, S. J., and K. E. Karlstrom, 2007, Tectonic model for the Proterozoic growth of North America: *Geological Society of America: Geosphere*, v. 3, p. 220-259.
- Williams, D. L., and C. Finn, 1985, Analysis of gravity data in volcanic terrain and gravity anomalies and subvolcanic intrusions in the Cascade Range, U. S. A., and at other selected volcanoes, in Hinze, W. J., M. F. Kane, N. W. O'Hara, M. S. Reford, J. Tanner, and C. Weber, (eds.), *The utility of regional gravity and magnetic anomaly maps*, Tulsa, Oklahoma, Society of Exploration Geophysicists, p. 361-374.

CHAPTER II: UPPER CRUSTAL STRUCTURE OF THE LLANO UPLIFT: AN INTEGRATED GEOPHYSICAL INVESTIGATION

Abstract

The Llano uplift is a broad structural dome in central Texas exhibiting the largest exposure of the Mesoproterozoic igneous and metamorphic rocks in the south-central United States. The Mesoproterozoic rocks of the Llano uplift, in addition to other small exposures in west Texas and northern Mexico comprise the western extension of the Grenville orogenic belt. The Llano uplift is an extensive outcrop of granitic and metamorphic rocks surrounded by Paleozoic and Cretaceous rocks. The complete Bouguer gravity and reduced-to-pole total magnetic intensity (RTP) anomaly maps of the Llano uplift show anomalously high values. The complete Bouguer gravity map shows short wavelength, high anomalies that are superimposed on a relatively broad, circular, high anomaly. These short wavelength anomalies are shown to be related to small, shallow intrusions of mafic rocks into metamorphic rocks of the uppermost crust as well as emplacement of ophiolitic material during subduction of Laurentia (North America) beneath a southern continent during the Grenville orogeny. We interpret the broad, circular high gravity anomaly to be related to a source in the middle crust due to invasion of the thickened Laurentia crust by basaltic magma derived from the mantle. The RTP map shows NW-SE high magnetic trends coinciding with the folded metamorphic exposures. The gravity anomaly signature suggests that the Llano uplift is an independent terrane with physical and geological properties that differ distinctly from its surroundings, and its subsurface extension is larger than the surface

exposure. This terrane could be an island arc that is older than the Grenville orogeny. The current Llano uplift shape developed due to many successive tectonic and structural processes through its geological history. The initial uplift resulted from an arc-continent collision that was followed by a continent-continent collision between the Laurentia and a southern continent during the Grenville orogeny in the Mesoproterozoic. The multiple phases of extension associated with Cambrian rifting and the Mesozoic opening of the Gulf of Mexico contributed to the evolution of the Llano uplift. The compressional tectonics of the Late Paleozoic Ouachita orogeny and associated foreland basins played pronounced roles to raise the Llano uplift area. A number of active structural arches contributed to modify the form of the uplift.

Introduction

The Llano uplift is located in central Texas (Fig. II.1), and it exposes a large dome of Precambrian basement. The igneous and metamorphic exposures of the Llano uplift represent the largest tract of Mesoproterozoic crystalline rocks in the south-central United States. The Precambrian igneous and metamorphic rocks are overlain and rimmed by Paleozoic and Cretaceous sedimentary rocks. However, the Bouguer gravity and reduced-to-pole total magnetic intensity maps of Llano uplift area produced in this study show anomalously high values. In particular, the exposed rocks in the Llano uplift are not the source of the high gravity anomaly.

The current study aims to integrate the gravity, magnetic and all available geological data to determine and characterize the subsurface bodies and/or structures responsible for the unexpected anomalously high gravity and magnetic signatures of the

Llano uplift area. In addition, we try to explain the tectonic and/or structural processes responsible for uplift of the Precambrian and Lower Paleozoic rocks of the Llano uplift relative to their equivalents outside the uplift area.

Geology and tectonic setting

The Mesoproterozoic exposures of Llano uplift, in addition to small exposures in west Texas and northern Mexico represent the western continuation of the Grenville orogenic belt (e.g. Mosher, 1998) (Fig. II.1). The uplift exposes multiple deformed Mesoproterozoic metamorphic rocks intruded by syn-tectonic to post-tectonic granites (Mosher et al., 2008) (Fig. II.2). The metamorphic rocks consist mainly of schists, gneisses, and metaigneous rocks, and they comprise nearly three fifths of the Precambrian rocks. The granitic rocks consist of foliated granitic intrusions as well as coarse-grained and medium to fine-grained granites, and they comprise the remaining two fifths of the Precambrian rocks. The Precambrian exposures look like an island of igneous and metamorphic rocks rimmed by Paleozoic and Cretaceous sedimentary rocks (Barnes, 1988).

Stratigraphy

The Precambrian rocks of the area are represented by three metamorphic domains and intrusive rocks that crosscut one or more domains (e.g. Mosher, 1998; Mosher et al., 2008) (Fig. II.3). The first metamorphic domain is known as the Valley Spring Gneiss, and it is a polydeformed granitic gneiss terrane that consists of supracrustal and plutonic rocks (Reese et al., 2000). The second domain, Packsaddle

Schist, consists of metavolcanic and metasedimentary supracrustal rocks intruded by younger granite and sills. The third domain, Coal Creek, consists of tonalitic to dioritic arc terrane and ophiolitic rocks. Coal Creek is interpreted as obducted oceanic crust, and it is present only in the eastern uplift (Roback, 1996). Two main periods of igneous activity affected the uplift. The first period is represented by foliated granitic rocks that intruded the entire uplift except the Coal Creek domain (Walker, 1992). The foliated granitic rocks are abundant in the Packsaddle and Valley Spring domains (Mosher, 1998). The second period of the igneous activity is represented by the coarse-grained Town Mountain granite and associated medium to fine-grained granite plutons that intruded the metamorphic rocks across the entire uplift (Walker, 1992).

The Cambrian rocks are represented by the Riley and Wilberns Formations of the Moore Hollow Group (Fig. II.3). The Riley Formation was deposited during the period extending from the Middle to Late Cambrian, and it consists of the Hickory Sandstone, Cap Mountain and Lion Mountain Members. The Hickory Sandstone Member was unconformably deposited on the irregular Precambrian surface, and consists of a mixture of terrestrial and marine sandstones, siltstones, and mudstones (Krause, 1996). The thickness of the Hickory Member is controlled by the topography of the Precambrian surface (Barnes and Bell, 1977). The Hickory Sandstone thins on the Llano uplift and thickens away from the uplift in all directions (Standen and Ruggiero, 2007). The Cap Mountain Member consists mainly of limestone with considerable amounts of sandstone, and it unconformably overlies the Hickory Sandstone (Preston et al., 1996). The Lion Mountain Member consists of sandstone, sandy limestone and limestone (Barnes and Bell, 1977). The Wilberns Formation

includes four members. The Welge Sandstone consists mainly of marine sandstone, and unconformably overlies the Lion Mountain Member (Barnes and Bell, 1977; Preston et al., 1996). The Morgan Creek Limestone consists of limestone with interbeds of silty limestone, and unconformably overlies the Welge Sandstone Member. The Point Peak Shale consists of siltstones, thinly bedded limestones and shale (Barnes and Bell, 1977). The San Saba Limestone, the upper most member of the Wilberns Formation consists mainly of limestones and dolomite (Preston et al., 1996).

The Ordovician rocks are represented by the Honeycut, Gorman and Tanyard Formations of the Ellenburger Group (Fig. II.3). The group consists mainly of dolomite that transits into massive limestone (Cloud and Barnes, 1948). The group was subjected to various degrees of karstification and erosion. The Silurian-Mississippian sediments were not deposited in the area or they were deposited and subsequently eroded. The Pennsylvanian rocks were deposited unconformably on the rocks of the Ellenburger Group (Preston et al., 1996). The Pennsylvanian rocks are represented by the Marble Falls and Smithwick Formations of the Bend Group. The Marble Falls Formation is divided into two units; the lower one is a massive limestone, and the upper one is a very fine-grained limestone interbedded with shales (Carrell, 2000). The Smithwick Formation unconformably overlies the Marble Falls Formation, and it consists mainly of shale. Cretaceous limestones which are underlain by sand and shale capped the hills that surround the Llano uplift area from the east, south and west (Preston et al., 1996).

Structural setting

The Llano uplift is a huge structural dome exposing Precambrian rocks in central Texas (e.g. Preston et al., 1996; Standen and Ruggiero, 2007). The dip of the sedimentary rocks overlaying the Precambrian rocks follows a radial pattern outward from the dome, and it varies greatly. The Cretaceous rocks have a gentle dip ranging from a few feet to hundred feet per mile while the Paleozoic rocks have more variable dip ranging from tens to hundreds of feet per mile (Barnes and Bell, 1977; Preston et al., 1996).

The Llano uplift area is divided into eastern, central and western uplifts by major sets of normal faults (Mosher et al., 2008) (Fig. II.2). These faults are of Pennsylvanian age, and they cut the Paleozoic and Precambrian rocks (Standen and Ruggiero, 2007). Some of these faults might be related to the uplift process while others are related to the Ouachita orogeny. The normal faults are interpreted to have formed as a result of the bending of the continental plate due to the increasing of the vertical loads exerted by the Ouachita thrust sheets close and parallel to the continental margin (Johnson, 2004). The majority of these faults trend northeast-southwest, but many of them trend in all other directions. The throws of these faults range from few feet to 500 feet (Preston et al., 1996).

Tectonic evolution of the Llano uplift

Many tectonic events contributed to the geological and structural evolution of the Llano uplift. These tectonic events include two major orogenies, extensional faulting, and erosion (Ewing, 1991). The Precambrian rocks of the Llano uplift

experienced a long history of tectonic activity that began with arc-continent collision that slightly preceded the continental collision of the Grenville orogeny and the formation of the supercontinent called Rodinia (Fig. II.4, Mosher et al., 2008). The subduction of the Laurentian continental margin led to a collision of an arc-continent and obduction of an ophiolite. An island arc terrane (Coal Creek Domain) collided first with the southern continent and they were subducted together northward beneath Laurentia (Mosher, 1998). However, Mosher et al. (2008) reported that the island arc terrane collided with Laurentia, and they were subducted as a package beneath the southern continent. This was followed by a continent-continent collision, crustal thickening and uplift. The subduction of the continental crust beneath the southern continent and the slab breakoff resulted in buoyancy force that contributed to the uplift process (Mosher et al., 2008). Deep-crustal material was obducted during the continental collision (Bickford et al., 2000). Consequently, the upwelling of the asthenosphere and underplating of basaltic magmas resulted in melting of the lower continental crust and intrusion of juvenile granitic bodies (Mosher et al., 2008). Magma, derived from the mantle, invaded and underplated the newly thickened continental crust, and it served as the heat source for generating granitic magma (Huppert and Sparks, 1988; Barker and Reed, 2010). The Llano uplift crust was subjected to poly-metamorphism and deformation associated with the collision process. Three metamorphic cycles can be identified in the area; high, medium and low grade metamorphic facies (Walker, 1992; Mosher et al., 2008). The metamorphism took place at the depth of about 50-70 km in the western uplift as well as 42-46 km in the eastern uplift (Mosher et al., 2008). This means that the subduction along the eastern uplift took

place at higher structural levels. The poly-phases of deformation resulted in folding of the metamorphic rocks. Isoclinal folds with southeast striking axis are the predominant structures (Mosher, 1998; Mosher et al., 2008).

The Grenville orogeny ended with the continental collision which resulted in crustal thickening and uplift of the area of Llano uplift of about 6 to 7 km (Garrison, 1981). The thickness of the crust was not uniform through the entire uplift. The crust of the western uplift may have been thicker than the eastern uplift since it represents a continental-continental collision while the eastern uplift represents an arc-continent collision (Mosher, 1998; Mosher et al., 2008). The continental crust was at least 10 km thicker at the time of the emplacement of the granites. The initial uplift was followed by intensive deep erosion which removed 10 km of the Precambrian rocks in the Llano uplift region (Barker and Reed, 2010). Based on a synthesis of seismic refraction, reflection and surface wave studies by Braile et al. (1989), the crust of the Llano uplift region is ~ 40 km thick and thins significantly in the Coastal Plain area. However, other periods of uplift must have occurred during the Cambrian break-up of Rodinia, the Ouachita orogeny and even the opening of the Gulf of Mexico.

Rodinia began to break up apart around 600 Ma, and a rifted margin developed by 550 Ma (Keller et al., 1983; Kruger and Keller, 1986). New oceans opened along the newly formed continental margins with a predominance of passive margin deposition during the period extending from the Cambrian to the lowermost Mississippian (Viele and Thomas, 1989). A thick sequence consisting mainly of carbonates with minor shale and sandstone was deposited on the shelf, and it is known as shelf facies. The Ouachita facies, known also as off-shelf facies, consists mainly of shale with minor limestone,

sandstone and chert, and was deposited in a deep water environment (Houseknecht and Matthews, 1985; Houseknecht, 1987). Southward subduction beneath an approaching continental landmass known as Llanoria began to close the ocean basin in the Devonian-Early Mississippian time, and the Ouachita orogenic belt began to form partly as an accretionary prism (Houseknecht and Matthews, 1985; Houseknecht, 1987). The approaching subduction complex closed the ocean basin and obducted the accretionary prism onto the rifted continental margin (Dickinson, 1974). Consequently, the southern margin of Laurentia changed from an Early to Middle Paleozoic passive continental margin dominated by carbonate shelf buildup to a Late Paleozoic active margin characterized by clastic sedimentation, and formation of flexural foreland basins (Viele and Thomas, 1989).

The Ancestral Rocky Mountains and related foreland uplifts developed as intraplate deformation in response to the collision between North America continent and a southern continent that produced the Ouachita orogeny (Kluth and Coney, 1981). The timing of the structural activity in the Ancestral Rocky Mountains was synchronous with the deformation in the Ouachita and Southern Oklahoma aulacogen regions (Frezon and Dixon, 1975). The deformation spread southwestward from the Ouachita area, and the Llano area was uplifted (Freeman and Wilde, 1964). The foreland uplifts have great structural relief and are characterized by high-angle reverse faults. This suggests that the largest component of movement along these faults was vertical, although strike-slip components are documented (Kluth and Coney, 1981). This can be interpreted by the reactivation of the pre-existing zones of weakness that developed before or during the Late Precambrian-Cambrian rifting by the Ouachita orogeny

collision. However, the Llano uplift did not experience a long structural inversion. Many of the deformed areas in the Ancestral Rocky Mountains are cored by mafic rocks. These mafic rocks are relatively weak and are susceptible to uplift and deformation when subjected to compressional forces associated with such a convergent tectonic event. This process may have affected the deep crust of the Llano uplift.

Several structural features and stratigraphic processes played minor roles in the evolution of the Llano uplift. The Llano uplift area was subjected to differential subsidence during the Cambrian time where sandstone and limestone were deposited in a seaway extending northeastward (Cheney and Goss, 1952). The uplift area was eroded to a hilly area with a topographic relief similar to the current Llano uplift's topography in the Middle-Late Cambrian time (Long, 2004). Marine sedimentation dominated the area and the igneous and metamorphic rocks were covered with sediments during the remainder of the Paleozoic (Preston et al., 1996; Hunt, 2008). By the Devonian, the northwest part of Llano area was subjected to uplift and erosion which is indicated by the noticeable loss of the thickness of the Ellenburger Formation. Many of the grabens in the area of Llano may have formed due to uneven subsidence during the formation of the basins, whereas the horsts may have been formed by deep pressure associated with the Ouachita orogeny near the end of Middle Pennsylvanian (Cheney and Goss, 1952). Central Texas was subjected to westward tilting due to the epeirogeny of the Ouachita orogenic belt during the latest Pennsylvanian, Permian and possibly Triassic time. In the Jurassic, the direction of the tilting reversed to be eastward tilting which is indicated by the drainage pattern (Cheney and Goss, 1952).

The Concho arch extends from the Texas Panhandle in the north to the western Llano area in the south (Fig. II.1). The arch was active during the Early Pennsylvanian time (Preston et al., 1996), and it resulted in 200 m of uplift of the Llano area (Ewing, 2004). The Fort Worth basin was subjected to subsidence in the Early Pennsylvanian. The subsidence process was followed by westward tilting of the west Texas basin in the Permian and Mesozoic times resulting in the formation of the Bend arch (Fig. II.1). The Bend arch is a broad feature plunging northward from the Llano uplift (Ewing, 1991, 2004). Both subsidence and tilting processes kept the Llano uplift and Bend arch as high topographic features. The east-west extending Ozona arch developed in Late Pennsylvanian-Permian time. The arch is interpreted to be a forebulge associated with the subsiding Val Verde basin. The Llano uplift is located at the eastern end of the arch. The Ozona arch dips into the Val Verde basin to the south. The Maverick basin and northeastern Mexico subsided during the deposition of the Edwards Group of Late Cretaceous age. The Llano uplift area was exposed, and might have played a role as a sediment source in the Late Cretaceous (Preston et al., 1996; Ewing, 2004).

Minor NE-SW normal faults with downthrows to the south and southeast developed in Late Paleozoic in response to increasing vertical loads exerted by the Ouachita thrust sheets. These faults were close and parallel to the southern continental margin (Johnson, 2004). Consequently, the areas to the south and southeast (known later as the Gulf Coastal Plain) experienced subsidence while central Texas remained a high topographic area. Moreover, the southern and eastern margins of North America were dominated by extension and volcanism in the Triassic time as part of the rifting of the continental margin and the formation of the Gulf of Mexico and the North Atlantic

Ocean in the Jurassic (Ewing, 1991). Mickus et al. (2009) detected a large-amplitude magnetic anomaly corresponding to the Texas continent-ocean boundary. They related this high magnetic anomaly to a deeply buried volcanic rifted margin associated with the opening of the Gulf of Mexico. They also reported uplift in central Texas during the Late Triassic based on sedimentary patterns.

The Llano uplift experienced stability during Mesozoic and Cenozoic while the Gulf Coast, East Texas and Rio Grande experienced subsidence. The epeirogenic continental emergence in the Cenozoic promoted the erosion of the relatively thin Mesozoic rocks and uplifted the Precambrian and Early Paleozoic rocks overlain by the Early Cretaceous limestones and shales (Cheney and Goss, 1952). The Llano uplift may have achieved its current form during the Miocene period. The Balcones fault zone acted as a line of flexure or boundary between the Edwards Plateau and the subsiding Gulf Coast basin (Young, 1972; Preston et al., 1996). The Edwards Plateau on which the Llano uplift lies was uplifted by the Balcones and associated faults (Barnes and Bell, 1977). This fault zone consists of a series of down-to-the-southeast normal faults with locally more than 500 m of cumulative displacement. An earlier movement along the fault occurred by the end of the Lower Cretaceous, and the major activity of the fault occurred in the Oligocene or Miocene (Weeks, 1945). Finally, the Precambrian rocks of the Llano uplift were exposed due to the incision of the Colorado River which removed the Cretaceous sedimentary cover (Ewing, 2004).

Data and methodology

Gravity and magnetic methods are commonly used to measure geophysical information in mineral and oil exploration as well as in deep crustal studies. Gravity and magnetic surveys are less expensive than reflection seismology, and can be carried out at larger regional scale (Naidu and Mathew, 1998). The density, magnetic susceptibility and natural magnetization change considerably from one rock type to another. Valuable information about the geology and structures of the subsurface can be provided by knowledge of the distribution of such properties in the subsurface.

The gravity method aims to locate and describe subsurface causative bodies and/or structures from their gravity effects caused by variations in densities (Lowrie, 2007). The magnitude of the gravitational field is directly proportional to the mass, and hence the density of the subsurface materials. Anomalies in the Earth's gravitational field result from lateral variations in the densities of the subsurface materials. The anomalies are affected also by the depths to the anomalous bodies and their lateral extent.

The magnetic anomalies result from variations in the Earth's magnetic field. The uneven distribution of the magnetic minerals in the rocks of the upper part of the Earth's crust is responsible for the variations. The pattern and distribution of the magnetic anomalies can provide some information about the locations of the magnetite-bearing rocks and depth to the basement surface (Lowrie, 2007). The shape and size of a magnetic anomaly depend on the shape of the causative body. The magnetic anomaly also depends on the inclination and declination of the body's magnetization as well as its orientation with respect to the magnetic north (Nabighian et al., 2005).

The interpretation of the anomalies of the total magnetic intensity maps is complicated by the fact that these anomalies are dipolar. The magnetic inclination and the presence of remnant magnetization add more complexity to the interpretation process because the body and its edges do not coincide with the mapped feature (Salem et al., 2007). The anomalies of the total magnetic intensity maps can be transformed to anomalies that would be measured if the field was vertical using the reduction to the pole (RTP) technique. The RTP technique makes the shape of a magnetic anomaly more closely related to the spatial location of the source structure, and hence easier to interpret. The RTP technique locates the anomaly maxima over the body center (Baranov and Naudy, 1964; Salem et al., 2007) as long as a strong component of remanent magnetization is not present (e.g., Shurbet et al., 1976).

In this study, gravity and magnetic data are represented by the complete Bouguer gravity anomaly and total magnetic intensity (TMI) grids downloaded from the Pan American Center for Earth and Environmental Studies (PACES) website (research.utep.edu/paces). The complete Bouguer gravity map was constructed using a 5000 m grid, while the TMI was constructed using a grid size of 2000 m and then transformed to a reduced-to-pole total magnetic intensity (RTP) grid. The complete Bouguer gravity and the RTP grids were subjected to a variety of processing techniques such as regional-residual separation, band-pass filtering and vertical derivatives techniques to obtain improved maps for optimizing the interpretation process. The next few paragraphs introduce a little about the different techniques applied to the gravity and magnetic data.

Regional-residual separation

Any Bouguer gravity map shows superposed anomalies from different sources. The regional anomalies have long wavelengths, and they originate due to deeply buried large geologic bodies or structures. The regional anomalies are valuable for studying the large tectonic features such as subduction zones, oceanic ridges and orogenic belts. The residual anomalies have relatively short wavelengths, and they originate due to shallow targets that may have geological interest (Lowrie, 2007). Upward continuation transforms the potential field measured on one surface to the field that would be measured on another surface farther from the source. The field can be computed at different successive levels if there is no disturbing body within the range of continuation (Nettleton, 1971). The technique functions as a low-pass filter that enhances the regional anomalies and attenuates the residual ones (Blakely, 1996).

The isolation of residual anomalies represents the main priority for exploration geophysicists. Residual anomalies are good indicators for hydrocarbon accumulation traps, mineral deposits and other small, shallow targets of geological interest. The size and depth of a buried geological mass can be indicated by the wavelength of its anomaly. The large, deep bodies produce long-wavelength, low amplitude anomalies while the small, shallow ones have short-wavelength, sharp amplitude anomalies (Lowrie, 2007). A residual gravity grid can be constructed by removing the regional gravitational effect and showing its residue due to the local structure (Griffin, 1949). In the current study, the residual gravity and magnetic grids were calculated by subtracting the upward continuation grids to different heights from the complete Bouguer gravity and the RTP grids.

Band-pass filtering

A band-pass filter isolates gravity or magnetic anomaly with wavelengths between preselected upper and lower cutoff limits. We define the upper and lower cutoff wavelengths depending on the lateral extension (size) of the geological feature of interest. The function of the band-pass filter is either to pass or reject a certain range of wavelengths. In the current study, we applied both band-pass and rejection band-pass filter with different cutoff wavelengths.

Directional filtering

Directional spectral analysis and filtering are applied to the magnetic and gravity maps to determine linear anomalies corresponding to subsurface faults, dykes and tectonic features (Thorarisson et al., 1988; Naidu and Mathew, 1998). The directional filtering removes undesired features with orientations such as pipeline and fence line anomalies in magnetic maps. The process can be carried out by the application of a cosine tapered, pass or rejection filter to the data in the Fourier domain (Sykes and Das, 2000).

Interpretation of Gravity and magnetic data

In order to look at the geophysical signature (expression) of the Llano uplift in regional context, a series of regional maps were prepared. First, the regional complete Bouguer gravity map of the study area shows the Llano uplift as a unique circular feature with a very high gravity anomaly relative to its surroundings (Fig. II.5). The gravity signature suggests that the Llano uplift might be a distinct terrane with a distinct

tectonic origin. In addition, the very high NE-SW trend to the east and northeast of the Llano uplift is related to the buried igneous and metamorphic rocks of the Ouachita interior zone (OIZ). The trend wraps around the Llano area and becomes east-west south of the Llano area. However, there are low gravity anomalies related to the Fort Worth, Kerr, Val Verde and the possible San Antonio basin interpreted by Keller (1989) using gravity data.

The regional upward continuation map to a height of 40 km and its residual (residual gravity after upward continuation to a height of 40 km) are shown in Figure 6. The Llano uplift still appears as roughly circular, local feature with high gravity although the upward continuation functions as a low-pass filter that attenuates the local, small features (Fig. II.6A). The residual gravity enhances the short wavelength, positive gravity anomalies (G1, G2, G3 and G4) (Fig. II.6B). The gravity lows related to the Fort Worth, Kerr, Val Verde, and the possible San Antonio basins are also enhanced. A regional RTP map of the area was generated but does not show enough detail in the Llano uplift area to be useful (Fig. A1). The map shows a very high NE-SW magnetic trend coinciding with the rifted volcanic margin of the Texas Gulf Coast detected by Mickus et al. (2009).

In addition to these regional maps, we generated local maps to focus more on the area of Llano uplift. The careful examination of the complete Bouguer gravity map of the Llano uplift area shows a number of short wavelength, very high gravity anomalies superimposed on a relatively broad, circular, high gravity anomaly (Fig. II.7A). Based on the gravity signature, the actual areal extension of the Llano uplift looks much larger than what the outcropping geology shows (Fig. II.7B). The Llano

area can be divided into two parts; the northern uplift where the Precambrian rocks are exposed, and the southern uplift where the Precambrian rocks are buried. The short wavelength, very high anomalies (G1 and G2) at the northern half coincide with the exposures of the Precambrian rocks. These anomalies could be related to the exposed metamorphic rocks as well as shallow buried metamafic rocks. The southern half of the uplift shows two very high anomalies (G3 and G4) coinciding with outcrops of Cretaceous rocks. These two very high gravity anomalies are most likely related to shallow buried metamafic rocks. The broad, circular, high gravity anomaly may be related to a deeper large body of approximately 150 km diameter situated in the middle crust. As interpreted by Mosher et al. (2008), this large source could be mafic underplating.

The RTP map of the Llano uplift area shows NW-SE high magnetic trends coinciding with the metamorphic exposures (Fig. II.8A). These high magnetic trends follow the axis of the folded exposed schist and gneiss rocks in the form of parallel anticlines and synclines (Fig. II.8B). The high magnetic anomalies are mostly related to the orientation of the magnetic mineral grains of the schist and gneiss. The buried metabasalts and metagabbros appear to have a minimal contribution to these high anomalies. These metabasalts and metagabbros may lack strong orientation of the magnetic mineral grains, or their magnetic properties were altered by the igneous activity associated with the intrusion of the younger granitic rocks. There are also many NW-SE high magnetic trends occurring in the area of large gravity high. Magnetic lows also occur to the northeast and northwest of the Llano uplift.

The upward continued gravity map to a height of 40 km shows a broad, circular, high gravity anomaly coinciding with the Llano uplift area (Fig. II.9A). The broad, circular high gravity anomaly of the Llano uplift may be related to a deep, large geological body or structural feature situated in the middle crust. The residual gravity map after upward continuation to 40 km enhances the short wavelength, very high anomalies (G1, G2, G3 and G4) (Fig. II.9B). The gravity lows related to the Fort Worth, Kerr, Val Verde, and the possible San Antonio basins are also enhanced. Two selected profiles (A-B and C-D) to construct density models across the area are shown in Figure 9B.

Moreover, a number of upward continuation maps to different heights and their residuals were constructed. The upward continuation maps to heights of 10 and 12 km show the first clear occurrence of the short wavelength anomalies (Fig. A2). These anomalies are related to the shallow buried metabasalt and metagabbro rocks that intruded the metamorphic rocks of the uppermost crust. The maps of the upward continuation to different heights show a strong decrease in the gravity values from east to west (Figs. A2 and A3). The high gravity of the eastern Llano uplift can be explained by the presence of thick metamorphic rocks with higher densities or the presence of mafic intrusions. About 7 km of the Packsaddle Schist and 3.8 km of the Valley Spring Gneiss exist in the southeastern part of the uplift (McGehee, 1979; Garrison, 1981). The southeastern part of Llano uplift also exposes the mafic Coal Creek serpentine which is absent in the western Llano uplift. The low gravity of the western Llano uplift may result from crustal thickening of the western part of the area. The thicker crust of the western Llano uplift resulted from continent-continent collision while the eastern Llano

uplift represents an arc-continent collision (Garrison, 1981; Mosher et al., 2008).

However, the residual gravity maps after upward continuation to different heights look similar to each other and do not add more detailed information (Figs. A4 and A5).

The maps of the band-pass filter with 1-50 and 1-100 km wavelengths passed look over-filtered while the maps with 1-150 and 1-200 km wavelengths passed show positive gravity at the eastern and southern parts of the Llano uplift as well as negative gravity at the western part (Fig. A6). The maps with 1-300 and 1-400 km wavelengths passed show the broad, high gravity anomaly overlain by the short wavelength anomalies (Fig. A6). The map with 1-50 km wavelength rejected looks similar to the upward continuation map to a height of 10 km since it shows the short wavelength anomalies corresponding to the shallow sources (Fig. A7). The map with 1-200 km wavelength rejected looks similar to the upward continuation map to a height of 40 km, which shows the broad, circular anomaly corresponding to the deep source. The broad gravity anomaly has a lateral extension of about 150 km diameter (Fig. A7).

We applied rejection directional band-pass and cosine filters to the complete Bouguer gravity and RTP maps to enhance anomalies with linear trends related to tectonic or structural events of geological interest. We preferred to use a rejection band-pass filter to mask or exclude a certain azimuthal range of the signal instead of passing this range to avoid overfiltering the data. The complete Bouguer gravity and RTP maps with a rejection band-pass directional filter with cutoffs at 0° and 90° show NW-SE anomalies (Fig. II.10A and B). These anomalies enhance the NW-SE compressional tectonic features related to the N-S\NE-SW directed Grenville orogeny that dominated the Llano uplift and west Texas areas in the Mesoproterozoic. However, the maps with

a rejection band-pass directional filter with cutoffs at the 90°-180° show NE-SW anomalies related to the Late Paleozoic Ouachita orogeny and/or the Early Cambrian continental rifting (Fig. II.10C and D). In addition, we applied a rejection directional cosine filter with 45° and 135° centered azimuth ranges rejected to the Bouguer gravity and RTP maps, and obtained similar results (Fig. II.11).

Modeling

The modeling process is used as the final step in the interpretation of the geophysical data. All the results obtained from different geophysical techniques and all the available geological information from the literature should be used to construct and constrain the model (Williams and Finn, 1985). We constructed two density models along the profiles A-B and C-D extending NE-SW and NW-SE across the residual gravity map after upward continuation to a height of 40 km (Fig. II.9B).

The first model A-B extends northeast-southwest across the entire Llano uplift area (Fig. II.12). The model shows two local, very high anomalies at the left and center of the model, as well as two low gravity anomalies at both ends of the model superimposed on a relatively broad gravity high. The high anomaly to the left coincides with metamorphic rock exposures, while the one at the center coincides with large thickness of buried metamorphic rocks and/or mafic intrusion. The low gravity anomalies coincide with the granite exposures and the sedimentary rock outcrops. The source of the broad gravity high lies in the middle crust and has a diameter of about 150 km.

The second model CD extends northwest-southeast across the exposed Precambrian rocks of the northern Llano uplift (Fig. II.13). A high gravity anomaly is centered on the model and coincides with the exposed metamorphic rocks. A negative anomaly lies to the left of the very high anomaly and coincides with a thin sedimentary cover where the granitic intrusions are shallow. Two high gravity anomalies exist close to both ends of the model and coincide with sedimentary covers underlain by metamorphic rocks. At the boundaries of the models, the gravity signature decreases outward due to thick sedimentary covers underlain by granitic rocks.

Discussion and conclusion

Our results are generally consistent with the model proposed by Mosher et al. (2008). Although Grenville continental collision resulted in crustal thickening involving sedimentary and upper crustal units whose composition suggests they would be associated with gravity and magnetic lows, the Llano uplift area is dominated by high gravity and magnetic anomalies. The anomalously high gravity and magnetic signatures can be interpreted and related to a variety of geologic sources. First, the short wavelength, positive gravity anomalies can be related to intrusion of metamafic rocks into the uppermost crust rocks. Metabasalts and metagabbros of an island arc or ocean floor origin intruded the Packsaddle Schist and Spring Valley Gneiss in the southeastern Llano uplift (Garrison, 1981). Similarly, metamafic rocks intruded the upper crust in the northern and northwestern parts of the Llano uplift (Walker, 1992). The high gravity anomalies can also be explained by the emplacement and obduction of ophiolitic material in the eastern Llano uplift during the subduction of Laurentia beneath the

southern continent in the Mesoproterozoic. Second, the broad, circular high gravity anomaly could be related to a deeply buried, dense source in the middle crust. Basaltic magma derived from the mantle invaded or underplated the newly thickened continental crust (Huppert and Sparks, 1988; Barker and Reed, 2010). This resulted in denser material below the crust in the uplift area which gives rise to the unexpected high gravity anomaly. This can be explained also by the intensive erosion that acted on the Precambrian rocks after the uplift process and removed several kilometers from the top of these exposed rocks (Barker and Reed, 2010).

However, the high anomalous gravity occurs as a local circular feature in the Llano uplift area. This suggests that the crust in the area of Llano uplift may belong to a distinct terrane that is different in its origin and composition from the surrounding continental crust of Laurentia. The terrane was accreted to the southern margin of Laurentia and welded together by granitic plutonism prior to the continental collision between the Laurentia and southern continent during the Grenville orogeny. According to Whitmeyer and Karlstrom (2007), volcanic arcs and oceanic terrane have been accreted along the southern continental margin, and they contributed to build the lithosphere of the southern North America continent. Many of the provinces that were accreted along the southern continental margin during the continental growth were composed of several small scale blocks or terranes. An island arc terrane (Coal Creek Domain) had been involved in the earlier arc-continent collision and later in the continental collision during the western Grenville orogeny in the Mesoproterozoic (Mosher, 1998; Mosher et al., 2008). The high magnetic anomalies are mostly related to the exposed schist and gneiss rocks. These magnetic anomalies follow the axis of the

folded schist and gneiss rocks, and they have short wavelength anomalies. These NW-SE folds originated due to the S-N/SW-NE compressional forces associated with the southern Grenville orogeny.

The current Llano uplift shape developed due to many successive tectonic and structural events as well as stratigraphic processes throughout its long geological history. The story began with the initial tectonic uplift due to the arc-continent collision where the arc was thrust above the southern margin of Laurentia. The major phase of uplift was due to the continental collision between Laurentia and the arc as a package in one side and the southern continent on the other side during the Grenville orogeny in the Mesoproterozoic. The continental collision resulted in crustal thickening and uplift of the area of Llano uplift by about 6 to 7 km (Garrison, 1981). Intensive deep erosion removed about 10 km from the exposed igneous and metamorphic rocks (Barker and Reed 2010), and the Llano uplift was eroded to a hilly area with a topographic relief similar to the current Llano uplift's topography by the Late Cambrian (Long, 2004). The Cambrian extensional structures might be reactivated as NE-SW normal faults with downthrows to the south and southeast by the vertical load exerted by the thrust sheets of the Ouachita frontal zone. These faults acted close and parallel to the attenuated southern continental margin. Consequently, the areas to the south and southeast (known later as the Gulf Coastal Plain) experienced subsidence while central Texas remained a high topographic area. Moreover, extensional tectonism dominated the area in the Triassic and ended with rifting and opening of the Gulf of Mexico during the Jurassic (Ewing, 1991). The subsidence of the Gulf Coastal Plain began in the Jurassic and was reactivated by the Cretaceous and Miocene down-to-the south

movements along the Balcones fault zone. The subsiding process kept Llano uplift and central Texas high relative to the subsiding Gulf Coastal Plain (Weeks 1945; Ewing, 2004). However, the Ouachita orogeny related northwest directed compressional forces might play a role in the deformation and uplift of the Llano area. The Llano uplift might be developed in response to the southwestward spreading deformation of the Ouachita orogeny in similar analogue to the Arbuckle uplift and the Ancestral Rocky Mountains. The stress component of the Ouachita deformation reactivated the movements along pre-existed faults and uplifted the cored mafic rocks to a higher level. In addition, the formation and subsidence of a number of foreland basins (Fort Worth, San Antonio, Kerr and Val Verde) around the Llano area contributed to keep the Llano uplift high relative to its neighbors. Moreover, the actions of several structural arches that intersected at the Llano uplift area might play minor roles in the modification of the Llano uplift during the period extending from the Middle Ordovician to the Cretaceous (Ewing, 2004). Finally, the Colorado River and its tributaries incised the area and removed the Cretaceous and the Paleozoic sedimentary cover and the Precambrian rocks exposed.

Our integrated analysis suggests an interpretation of the final step in the evolution of the crust of the Llano uplift. The gravity models show the source of the broad, circular gravity high to be a mid-crustal bump (Fig. II.14). Underplating of the thickened Laurentia by basaltic magma during the final stages of the continental collision is responsible for producing the bump in the middle crust.

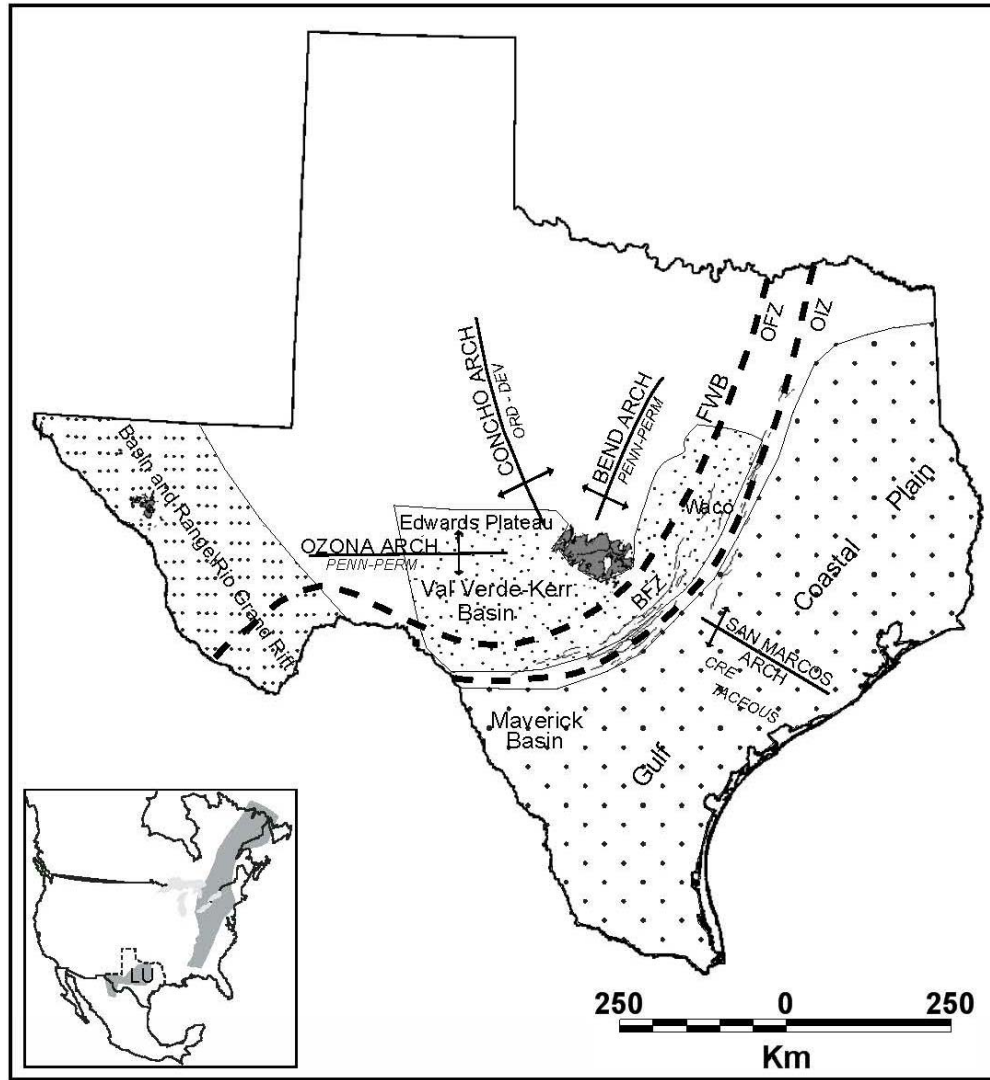


Figure II.1: Index map showing the Precambrian rocks exposures in Llano uplift (LU), and west Texas in gray color. Inset shows the exposures of the Grenville orogenic belt in Canada, United States and Mexico. The Ouachita frontal zone (OFZ) and Ouachita interior zone (OIZ) are shown in bold dashed lines. Balcones fault zone (BFZ) lies to the south and southeast Llano uplift area. FWB refers to the Fort Worth basin. A number of structural arches intersecting at Llano area as well as basins are shown. Modified after Ewing, 2004; Barker and Reed, 2010.

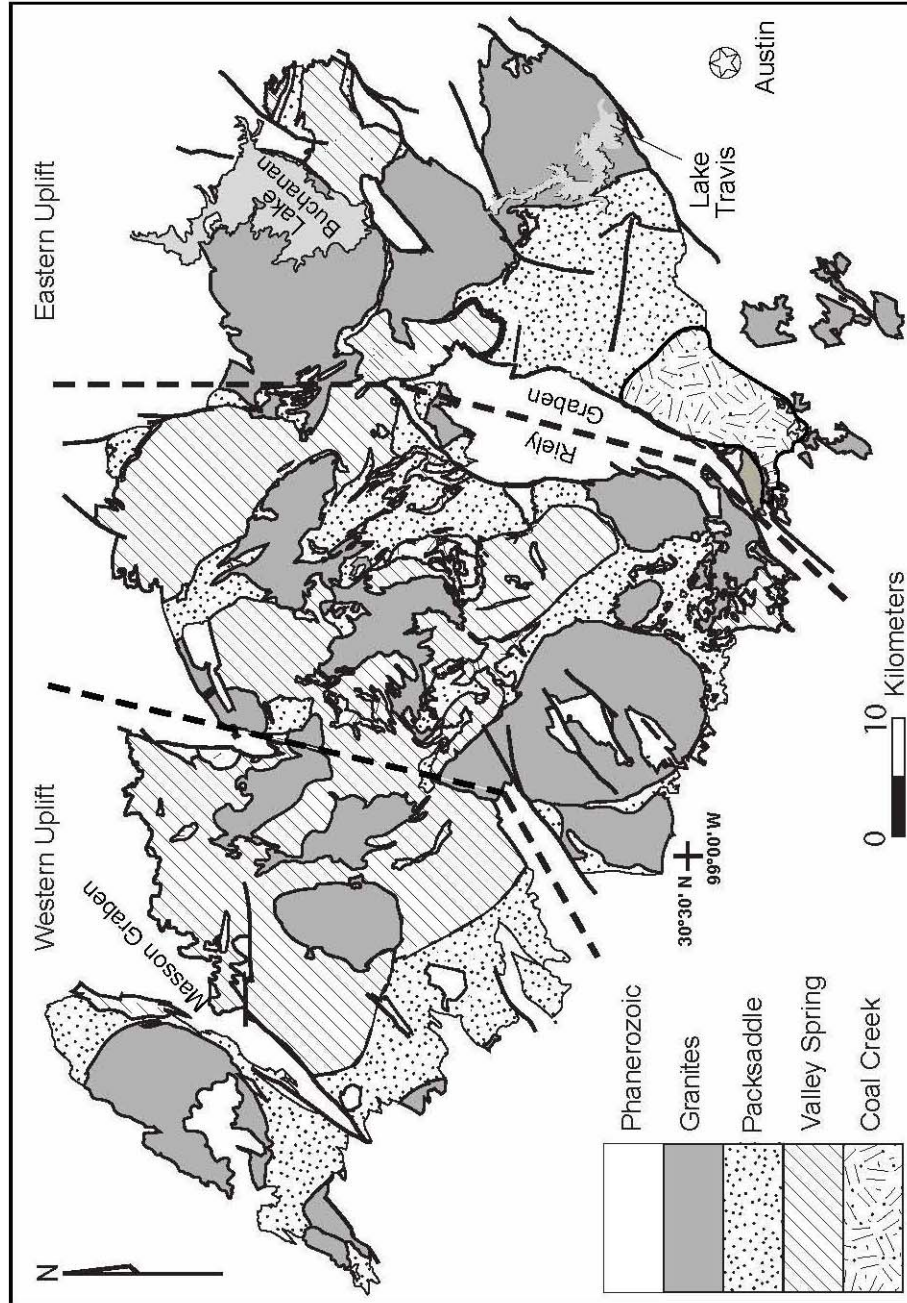


Figure II.2: Geologic map of the Llano uplift showing the Precambrian rocks exposures and major faults. The uplift is divided into three main parts by a set of major faults. The boundaries of the eastern and western portions of the uplift are shown by the dashed lines, Levine and Mosher, 2010.

Era	System	Group	Formation	Members/Units	Description
Paleozoic	Pennsylvanian	Bend	Smithwick	Undivided	Shale
			Marble Falls Limestone	Upper	Fine-grained limestone interbedded with shale
				Lower	Massive limestone
	Ordovician	Ellenburger	Honeycut	Undivided	Karistified limestone and dolomite
			Gorman		
			Tanyard		
	Cambrian	Moore Hollow	Wilberns	San Saba	Limestone and dolomite
				Point Peak	Siltstone, limestone and shale
				Morgan Creek	Limestone with interbeds of silty limestone
			Welge Sandstone	Marine sandstone	
			Riley	Lion Mountain	Sandstone, sandy lime and limestone
				Cap Mountain	Mainly limestone and sandstone
				Hickory Sandstone	Mixture of terrestrial and marine sandstone, siltstone and mudstone
Post-tectonic		Coarse-grained granite and medium to fine-grained granite			
Precambrian	Proterozoic	Granites	Syn-tectonic		Foliated granitic rocks
			Packsaddle		Schists, marbles, and amphibolites
		Metamorphic Rocks	Valley Spring		Gneiss, granite, rhyolite and arkose protoliths
			Coal Creek		Dioritic to tonalitic gneiss and serpentine

Figure II.3: The stratigraphy of the Llano uplift area, modified from Preston et al., 1996; Mosher, 1998; Standen and Ruggiero, 2007; Mosher et al., 2008.

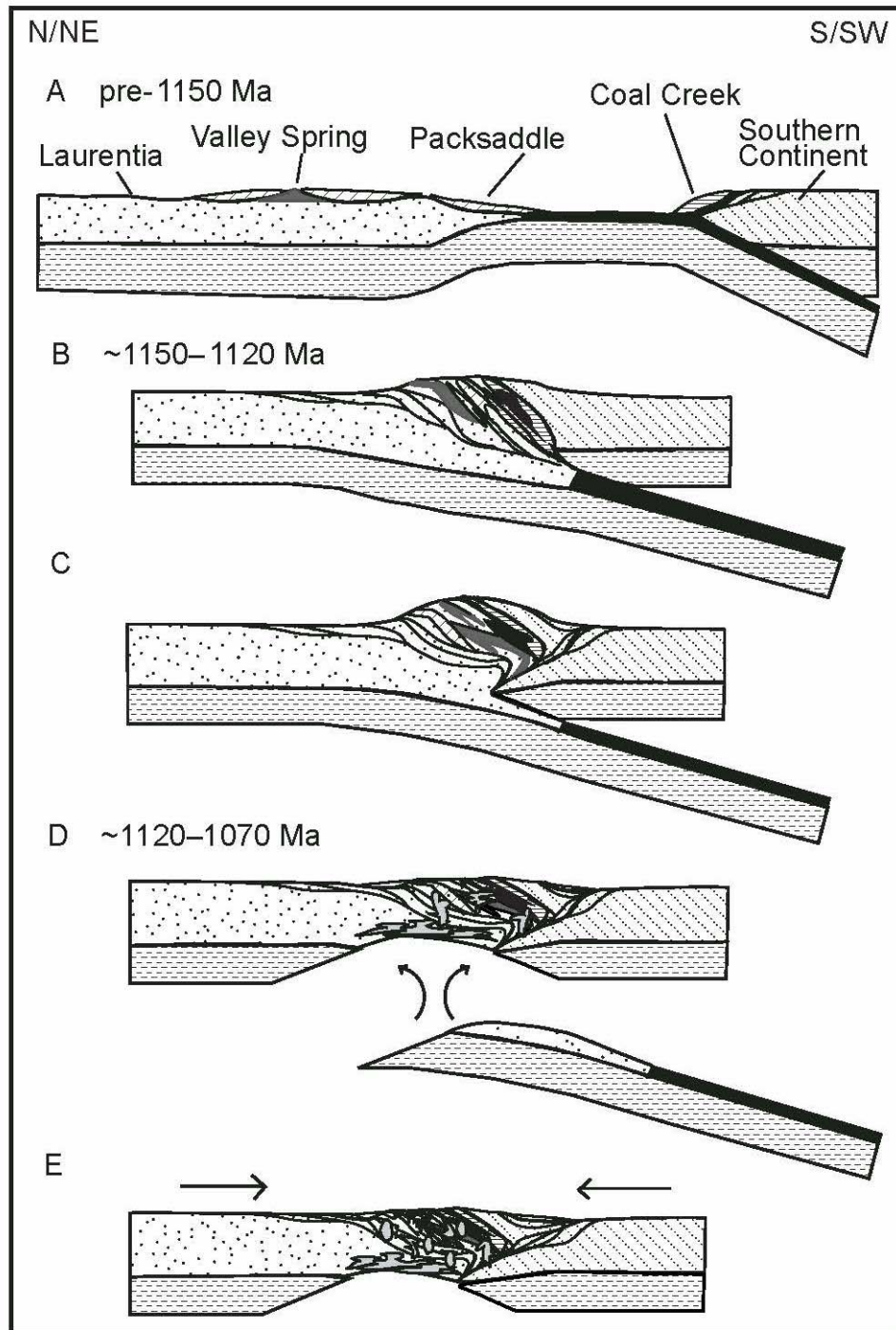


Figure II.4: Tectonic model for the western Grenville orogeny showing the evolution of Llano uplift, redrawn from Mosher et al., 2008.

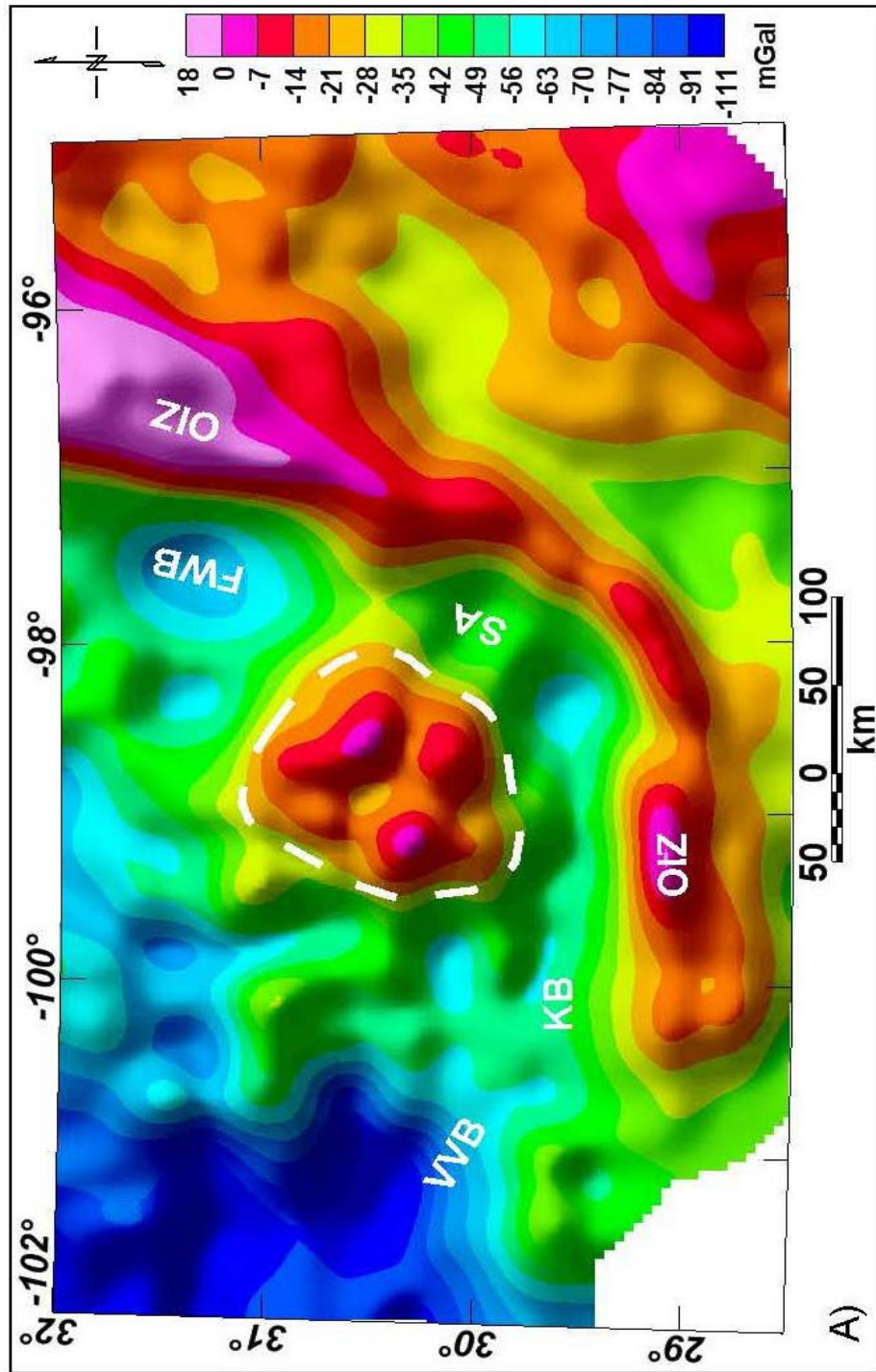


Figure II.5: Regional complete Bouguer gravity map showing the Llano uplift as a circular feature with high gravity relative to its surrounding. The high gravity trend (OIZ) is related to the Ouachita interior zone. The gravity lows (FVB, SA, KB and VVB) are related to the Fort Worth, San Antonio, Kerr, and Val Verde basins.

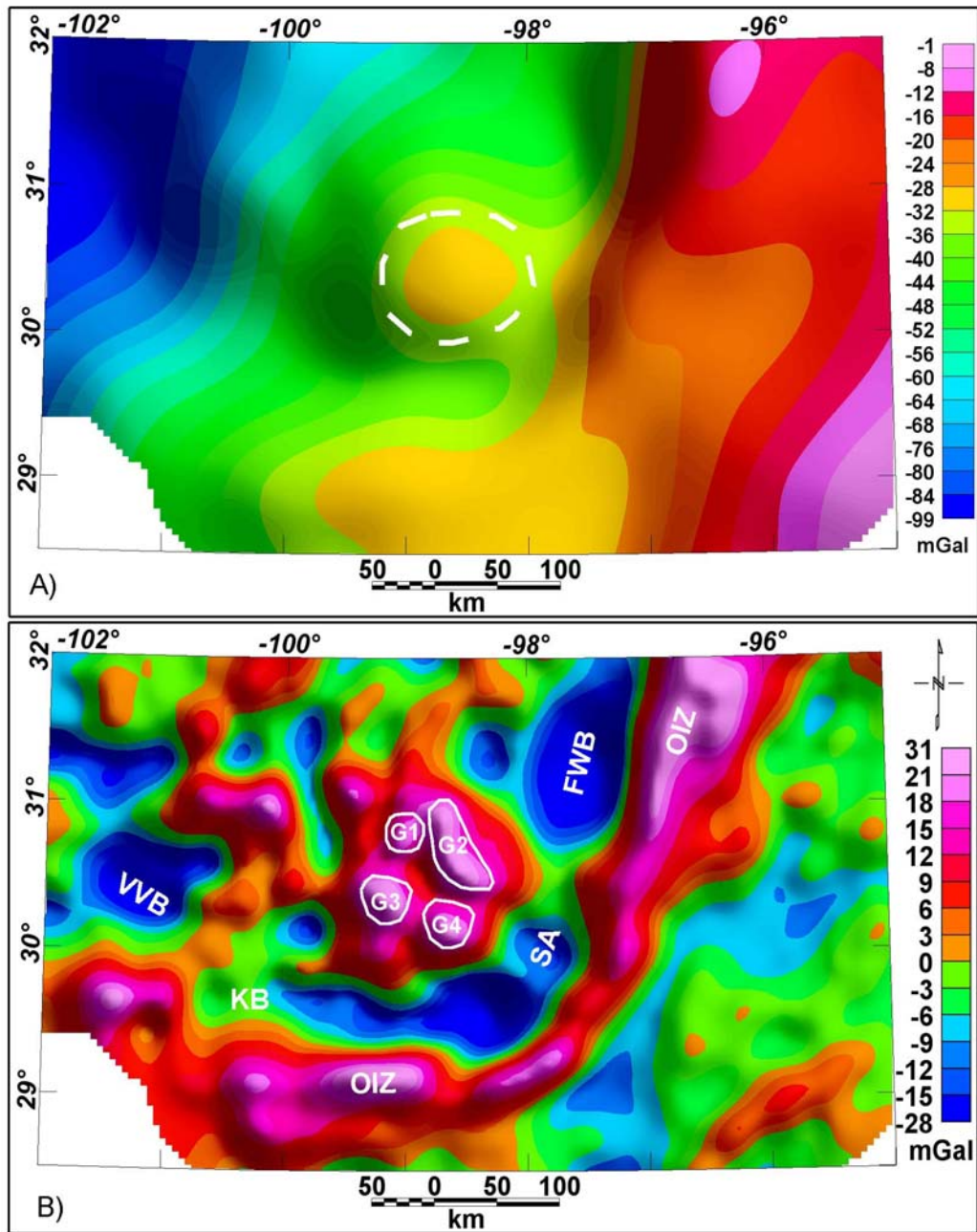


Figure II.6: (A) Regional upward continuation of the gravity data to a height of 40 km. The Llano uplift shows up as a circular feature with high gravity. (B) The residual gravity after upwrd continuation to height of 40 km enhancing the short wavelength anomalies (G1,G2,G3 and G4). The gravity lows (FWB, SA, KB and VVB) show up clearer than those in Figure (5).

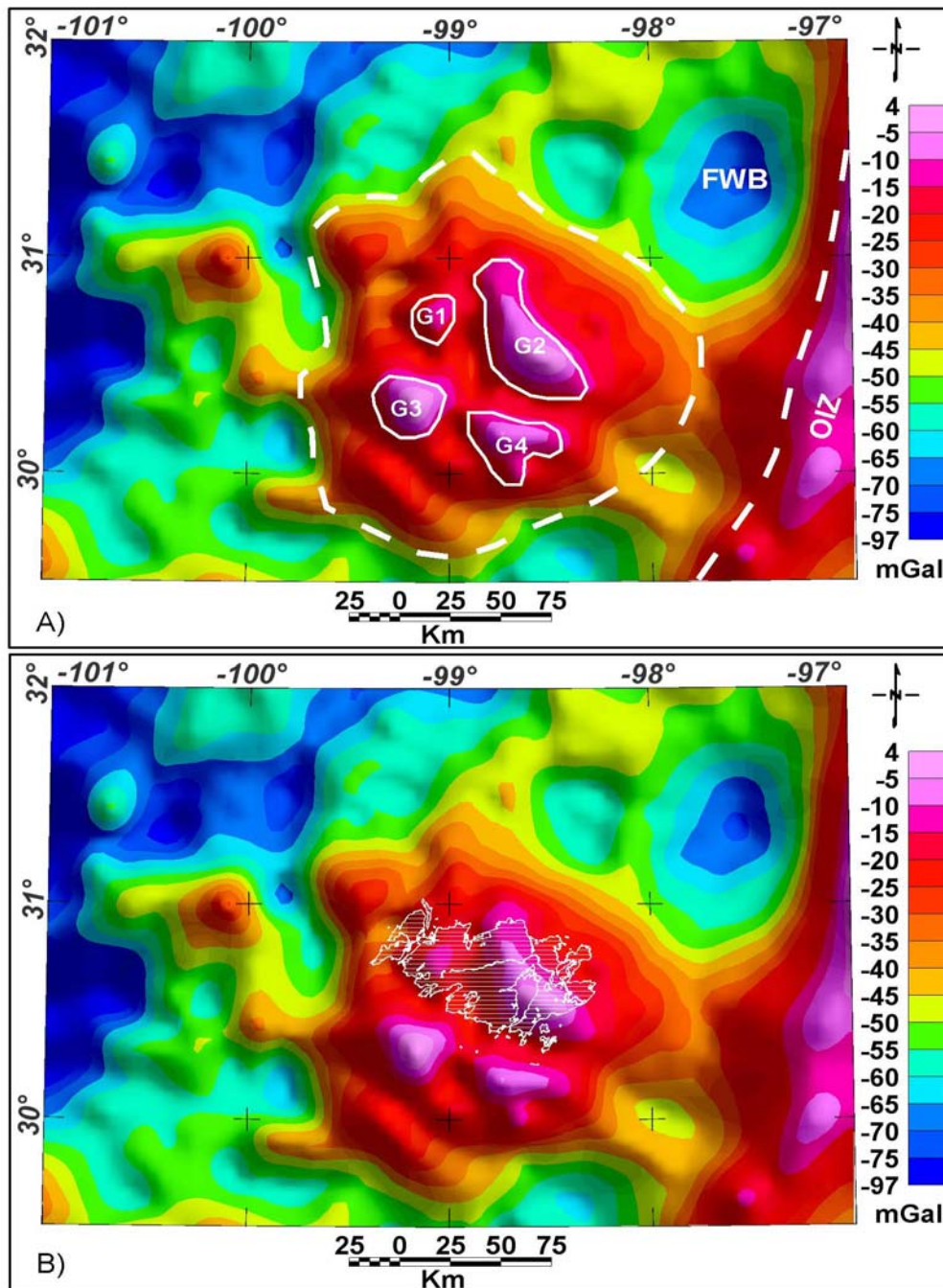


Figure II.7: (A) The complete Bouguer gravity map of Llano uplift area showing short wavelength, very high gravity anomalies (G1,G2,G3 and G4) superposed on a relatively broad high anomaly. The NE-SW high gravity trend at the east is related to the Ouachita interior zone (OIZ). (B) shows the exposures of the Precambrian rocks overlying the complete Bouguer gravity map.

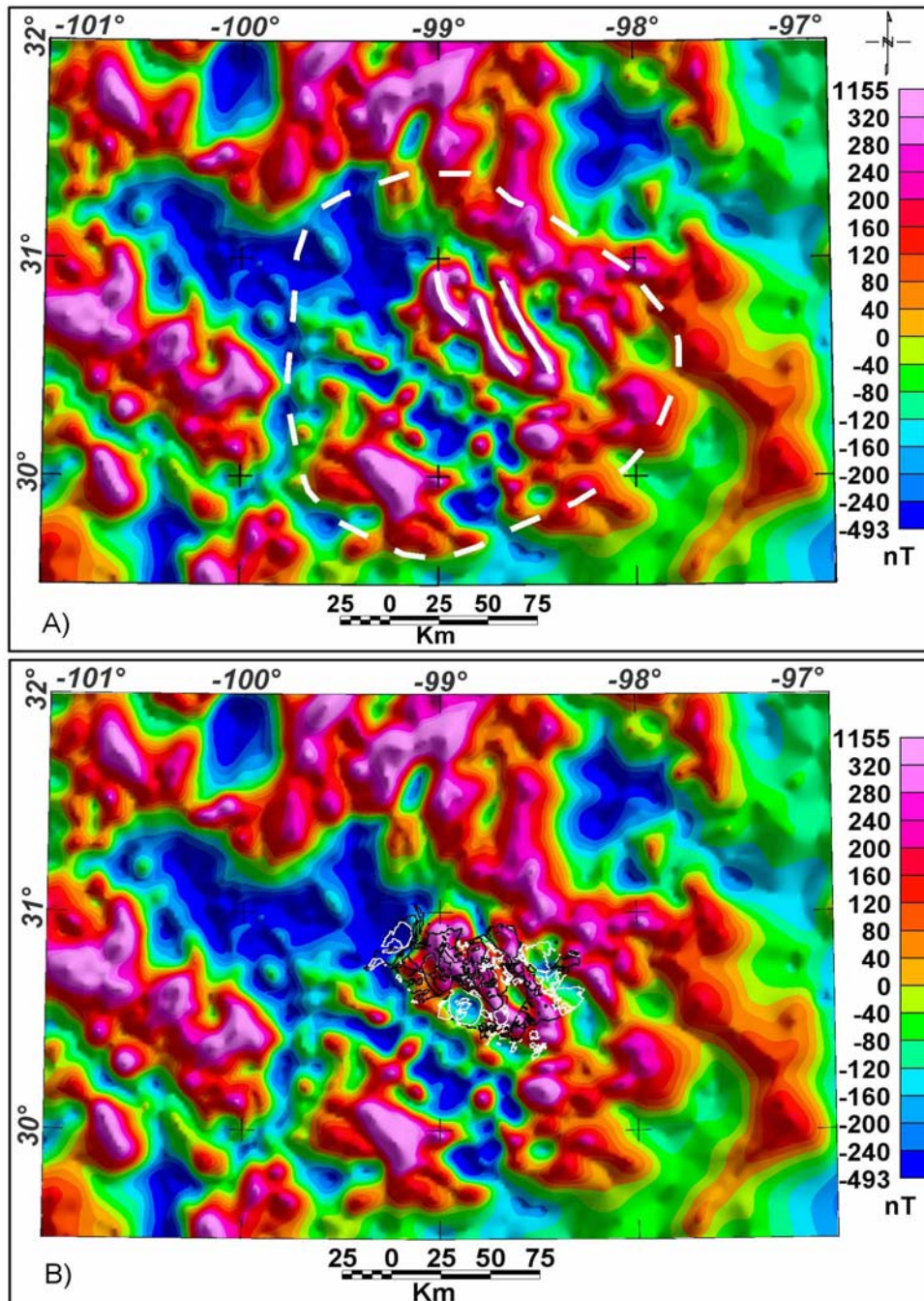


Figure II.8: (A) The RTP map of Llano uplift showing three NW-SE high Magnetic trends, see the white lines. (B) The RTP map with the exposures of the granite shown in white outlines and the metamorphic rocks shown in black outlines. The NW-SE high magnetic trends coincide with the metamorphic rocks exposures.

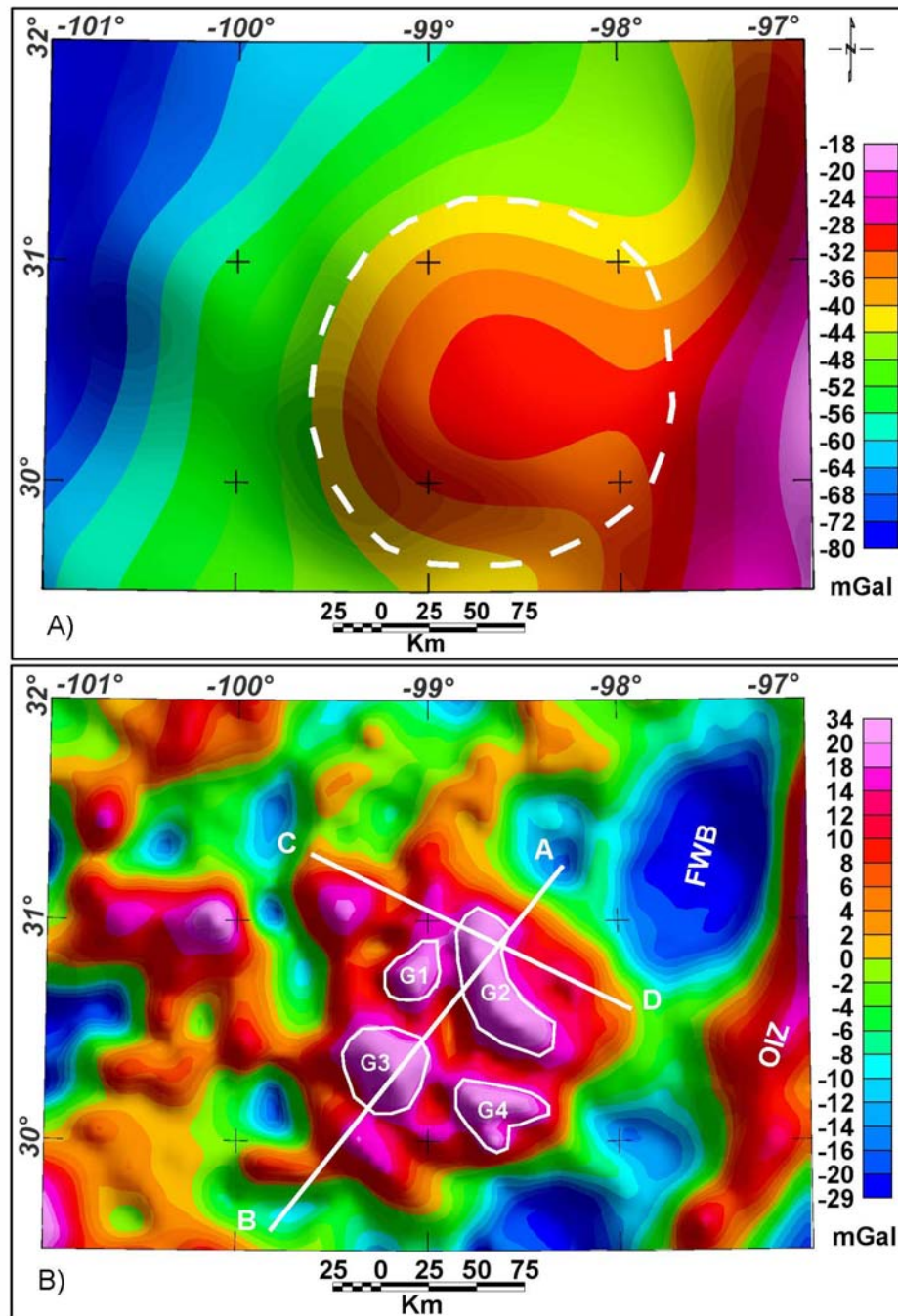


Figure II.9: (A) Upward continuation of the gravity data to a height of 40 km showing a circular high gravity anomaly in white dashed circle. (B) The residual gravity after upward continuation to height of 40 km enhancing the short wavelength anomalies (G1,G2,G3 and G4). A-B and C-D are two profiles to construct density models.

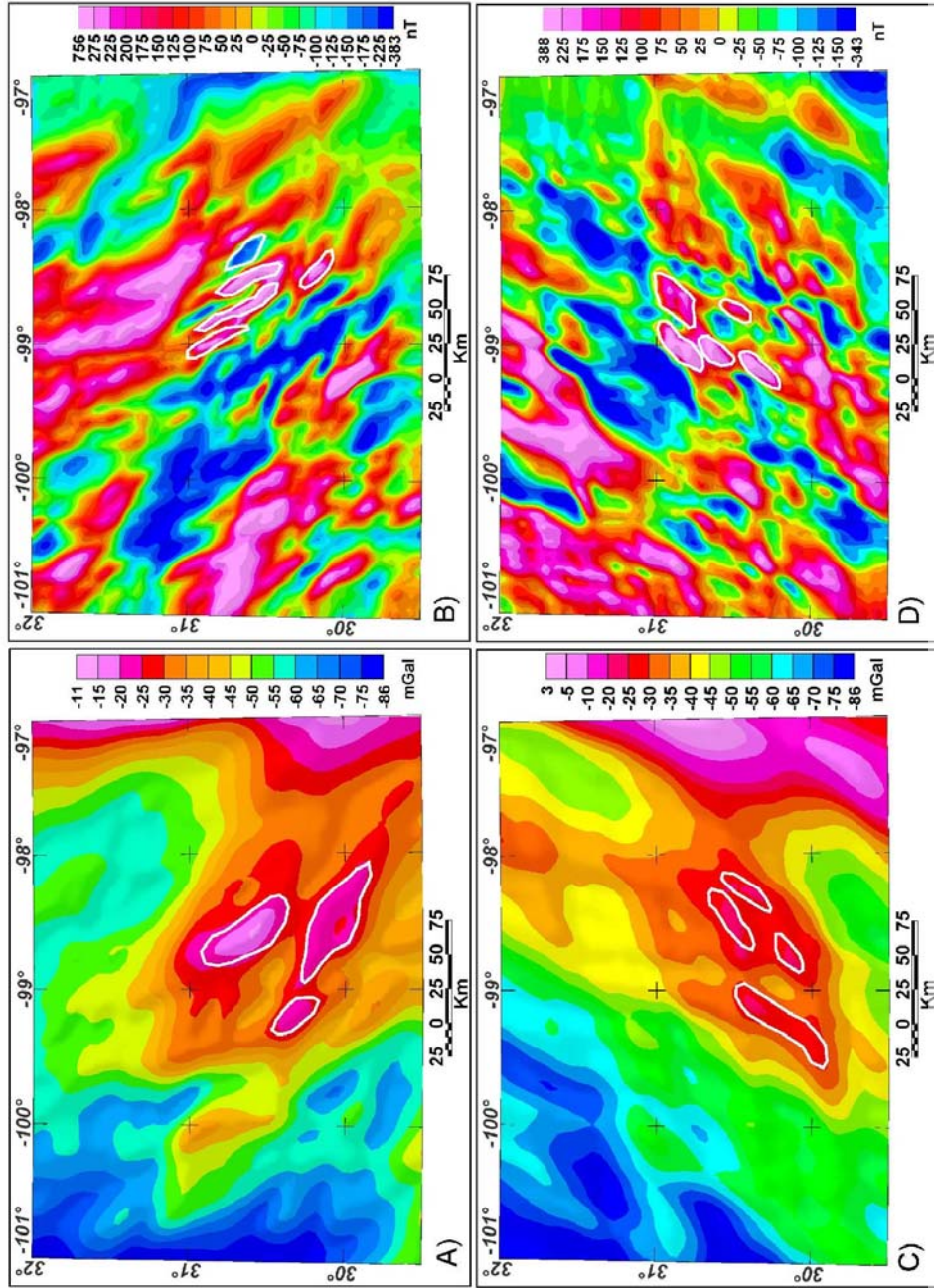


Figure II.10: (A) The complete Bouguer gravity and (B) the RTP maps with rejection directional bandpass filter with 0-90 degree azimuth rejected showing NW-SE anomalies related to the western Grenville orogeny. (C) and (D) are the same maps in (A and B) with 90-180 degree azimuth rejected enhancing the Cambrian rifting and Ouachita orogeny related NE-SW tectonic features.

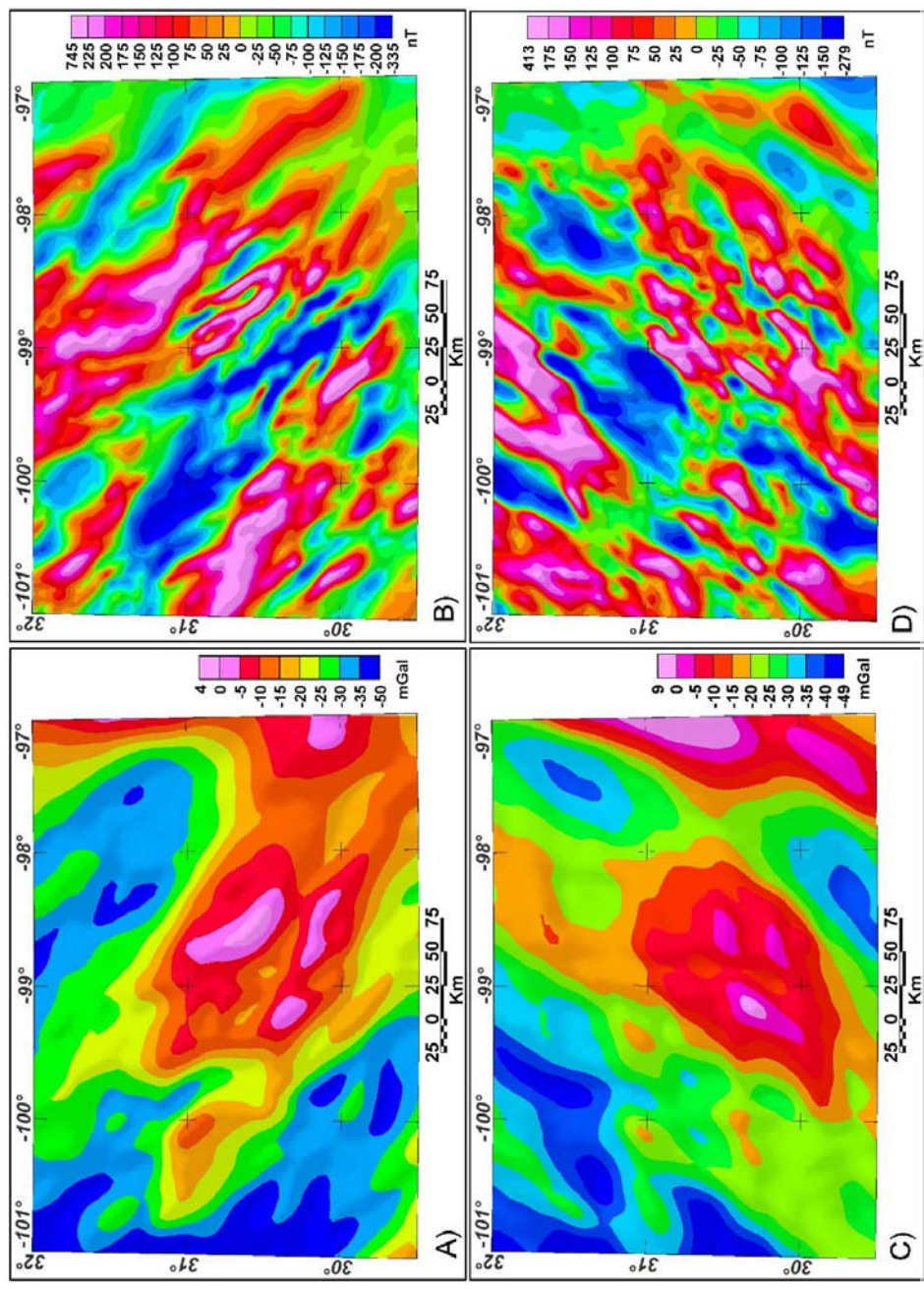


Figure II.11: (A) The complete Bouguer gravity and (B) the RTP maps with rejection directional cosine filter with 45 degree centered azimuth rejected showing NW-SE anomalies related to the western Grenville orogeny. (C) and (D) are the same maps in (A and B) with 135 degree centered azimuth rejected enhancing the Cambrian rifting and Ouachita orogeny related NE-SW tectonic features.

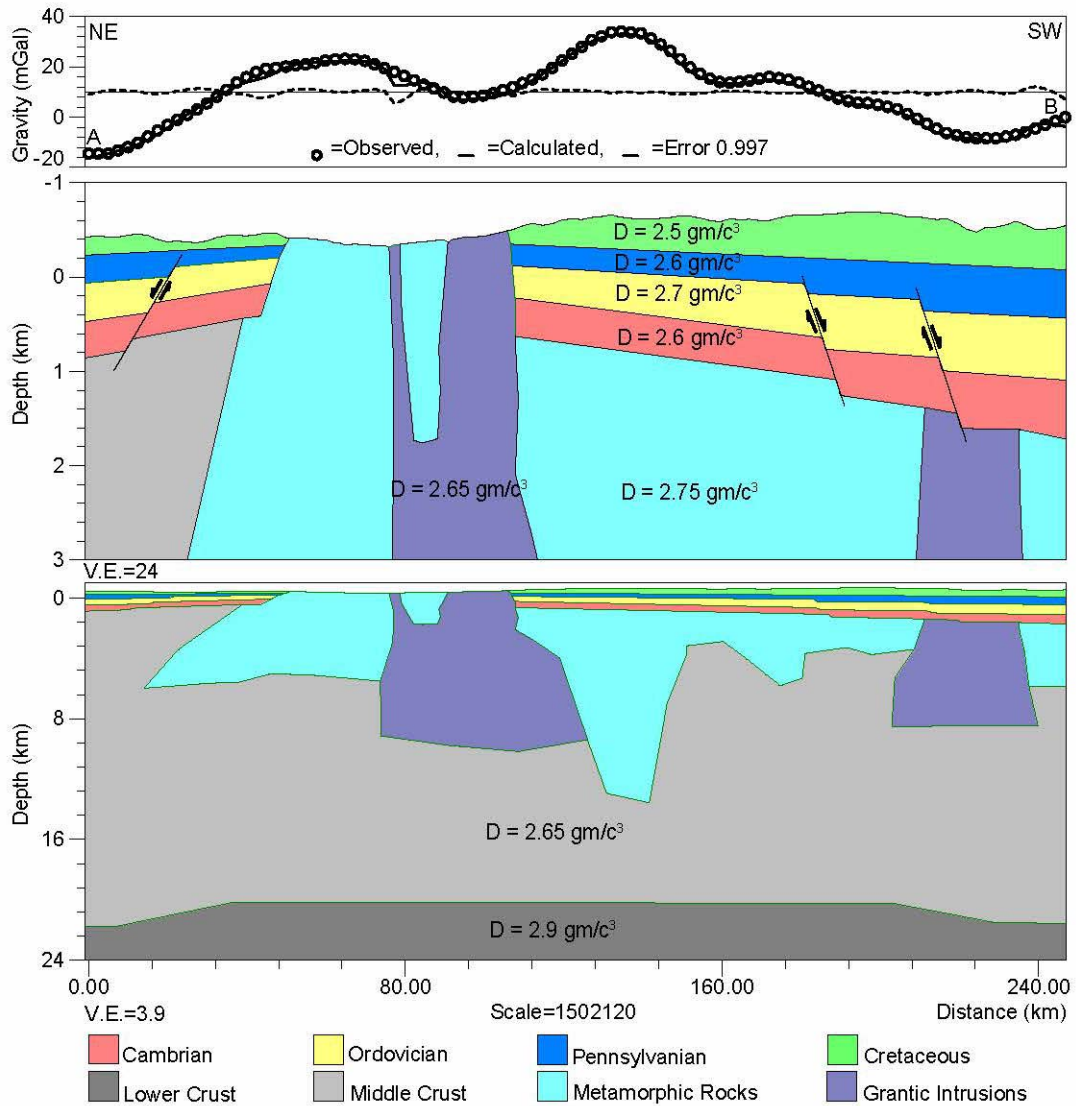


Figure II.12: Gravity model A-B showing two local, high anomalies at the left and center of the model. The one to the left coincides with metamorphic exposures and the one at the center coincides with sedimentary cover underlain by thicker metamorphic block. The medium gravity between the previous two high ones coincides with exposed granitic exposure. The low gravity anomaly at the left end of the model coincides with sedimentary cover underlain by upper crust rocks. The low gravity anomaly at the right end of the model the sedimentary cover and granitic intrusion. The source of the broad gravity high lies at the middle crust and has a diameter of about 150 km. The model reflects extensional faulting dominating the basement and Early Paleozoic rocks.

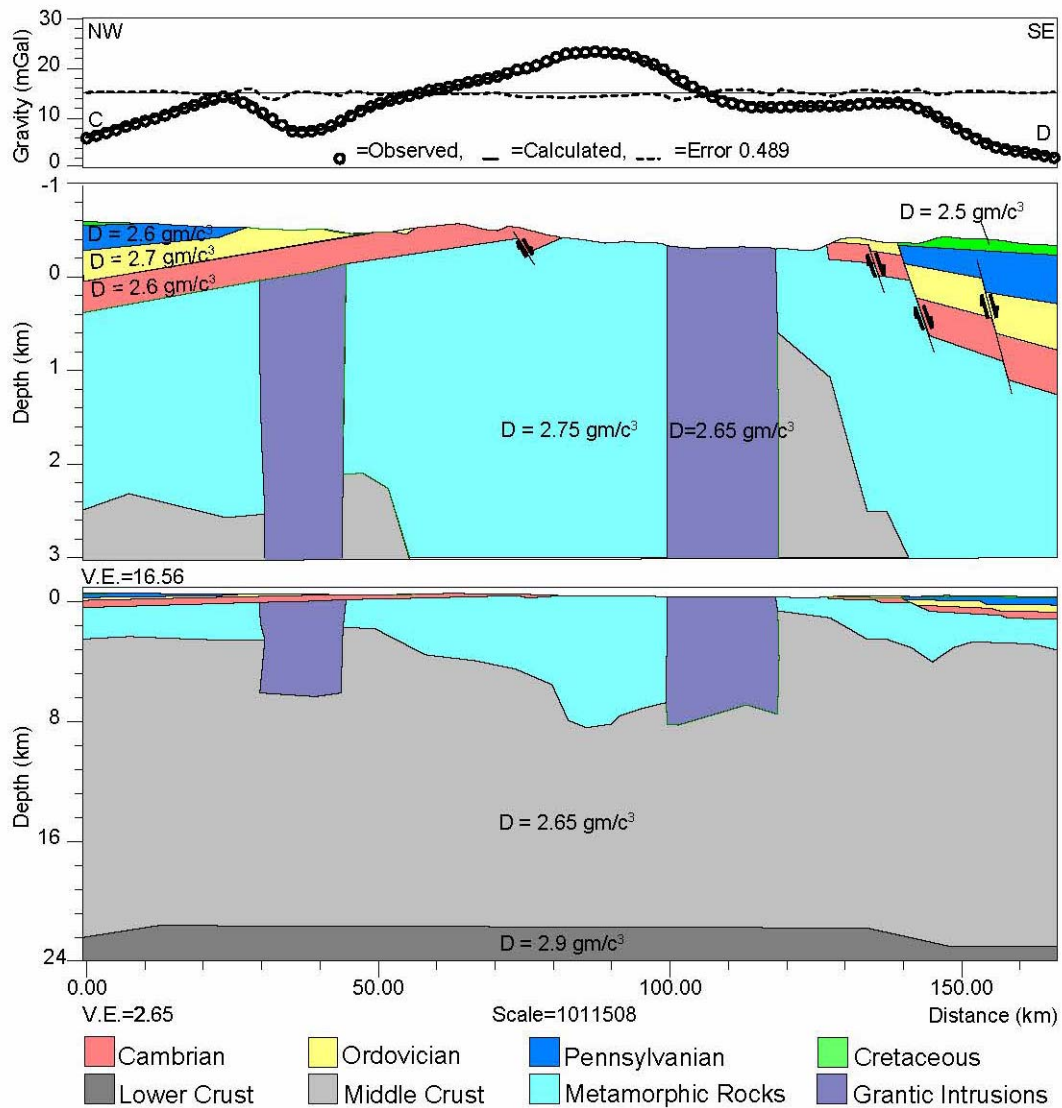


Figure II.13: Density model C-D showing a very high gravity anomaly at the center of the model coinciding with the exposed metamorphic rocks. A negative anomaly lies to the left of the very high anomaly and coincides with a thin sedimentary cover where the granitic intrusions are shallow. There are two high gravity anomalies close to both ends of the model and coinciding with sedimentary covers underlain by metamorphic rocks.

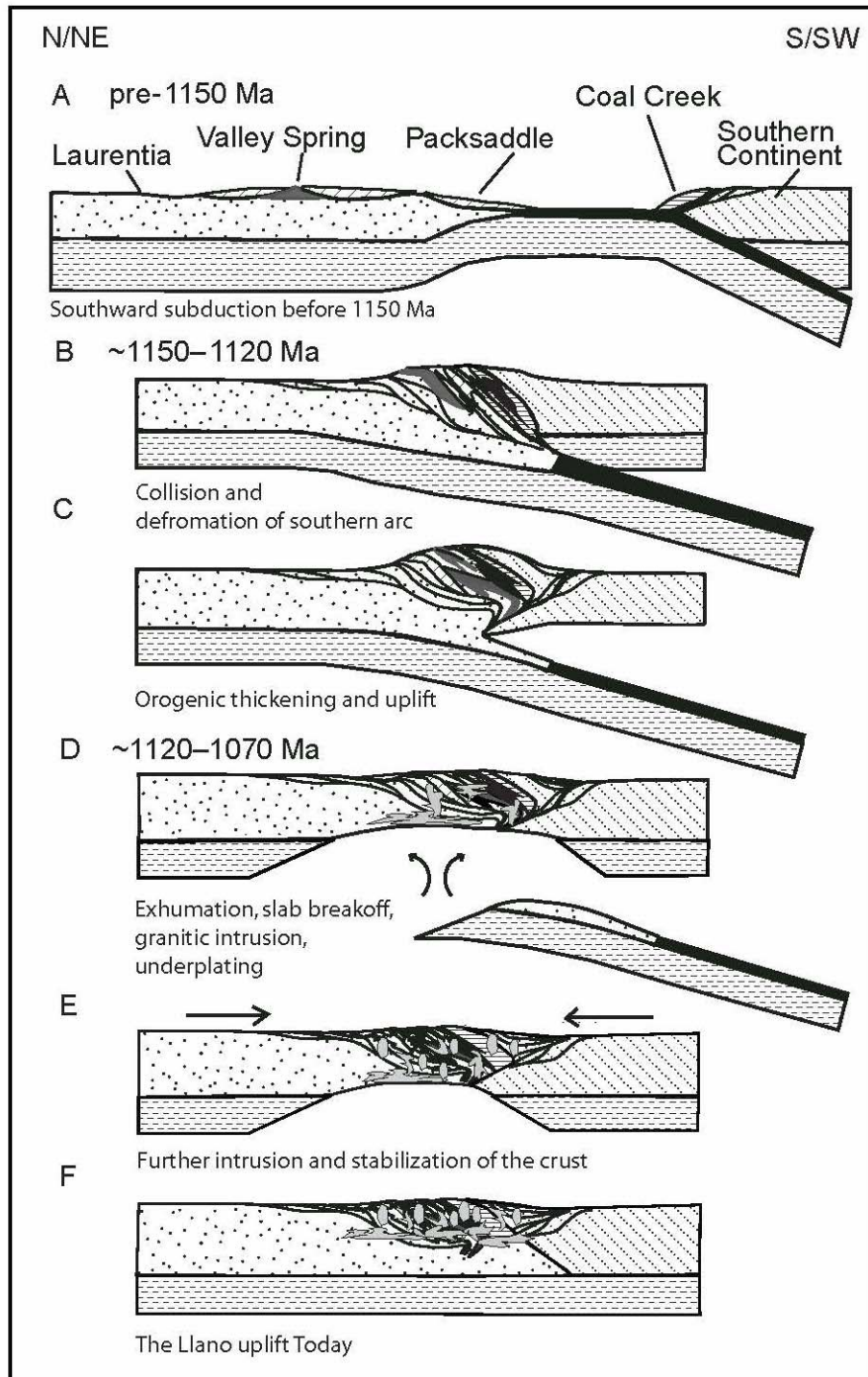


Figure II.14: Modified tectonic model for the western Grenville orogeny showing the evolution of Llano uplift, after Mosher et al., 2008.

REFERENCES

- Baranov, V., and Naudy, H., 1964, Numerical calculation of the formula of reduction to the magnetic pole: *Geophysics*, v. 29, p. 67–79.
- Barker, D. S., and Reed, R. M., 2010, Proterozoic granites of the Llano uplift, Texas: A collision-related suite containing rapakivi and topaz granites. *Geological Society of America Bulletin*; v. 122; no. 1-2; p. 253-264.
- Barnes, V. E., 1988, The Precambrian of central Texas, *in* Hayward, O. T., (ed.), Centennial field guide, Volume 4: Boulder, Colorado, Geological Society of America, South-Central Section, p. 361–368.
- Barnes, V. E., and Bell, W. C., 1977, The Moore Hollow Group of central Texas. The University of Texas at Austin, Bureau of Economic Geology, Report of Investigations no. 88, 169 p.
- Blakely, R. J., 1996, Potential theory in gravity and magnetic applications: Cambridge University Press, 441p.
- Braile, L. W., Hinze, W. J., Frese, R. R. B., and Keller, G. R., (1989), Seismic properties of the crust and uppermost mantle of the conterminous United States and adjacent Canada, *in* Pakiser, L. C., and Mooney, W. D., (eds.), Geophysical framework of the continental United States: Geological Society of America Memoir 172, p. 655-680.
- Carrell, C. L., 2000, Structural influences on the North Hickory Aquifer, San Saba County, Texas. Master's thesis, Baylor University, 72 p.
- Cheney, M. G., and Goss, L. F., 1952, Tectonics of Central Texas. *American Association of Petroleum Geologists Bulletin*, v. 36, no. 12; p. 2237-2265.
- Cloud, P. E., and Barnes, V. E., 1948, The Ellenburger Group of central Texas. University of Texas, Bureau of Economic Geology Publication no. 4621, 473 p.

- Dickinson, W. R., 1974, Plate tectonics and sedimentation, *in* Dickinson, W. R. (ed.), Tectonics and sedimentation: Tulsa, Oklahoma, Society of Economic Paleontologists Mineralogists, Special Publication, v. 22, p. 1-27.
- Ewing T. E., 1991, The tectonic framework of Texas: Text to accompany " The Tectonic Map of Texas". University of Texas at Austin, Bureau of Economic Geology, 36 p.
- Ewing, T. E., 2004, Phanerozoic development of the Llano Uplift, *in* Hoh, A. and Hunt, B. (eds.), Tectonic history of southern Laurentia: A look at Mesoproterozoic, Late-Paleozoic, and Cenozoic structures in central Texas: Austin Geological Society Field Trip Guidebook 24, Texas, p. 25-37.
- Freeman, T., and Wilde, G. L., 1964, Age and stratigraphic implications of major faults in the Llano region, central Texas: American Association of Petroleum Geologists Bulletin, v. 48, no. 5; p. 714-718.
- Frezon, S. E., and Dixon, G. H., 1975, Texas Panhandle and Oklahoma: U.S. Geological Survey Professional Paper 853, p. 177-196.
- Garrison, J. R., 1981, Metabasalts and metagabbros from the Llano uplift, Texas: Petrologic and geochemical characterization with emphasis on tectonic setting. Contributions to Mineralogy and Petrology v. 78; p. 459-475.
- Griffin, W. R., 1949, Residual gravity in theory and practice. Geophysics, v. 14, no. 1, p. 39-56.
- Houseknecht, D. W. and S. M. Matthews, 1985, Thermal maturity of Carboniferous strata, Ouachita Mountains: American Association of Petroleum Geologists Bulletin, v. 69, p. 335-345.
- Houseknecht, D. W., 1987, The Atoka formation of the Arkoma basin: Tectonic, sedimentology, thermal maturity, sandstone petrology: Tulsa Geological Society Short Course Notes, 72 p.

- Hunt, B. B., 2008, Crystalline basement aquifer, Llano uplift, central Texas: An overlooked minor aquifer of Texas: Gulf Coast Association of Geological Societies Transactions, v. 58, p. 433-449.
- Huppert, H. E., and Sparks, R. S. J., 1988, The generation of granitic magmas by intrusion of basalt into continental crust: *Journal of Petrology*, v. 29, p. 599–624.
- Johnson, B., 2004, The Llano uplift and associated Pennsylvanian-age faults: An overview and field example of faults exposed at Hoover Point in the Backbone Ridge Graben, *in* Hoh, A. and Hunt, B. (eds.), Tectonic history of southern Laurentia: A look at Mesoproterozoic, late-Paleozoic, and Cenozoic structures in central Texas. Austin Geological Society Field Trip Guidebook, 24, p. 62-71.
- Keller, G. R., 1989, Geophysical evidence for the presence of a Paleozoic San Antonio basin, *in* Ewing, T. E., (ed.): South Texas Geol. Soc. Fieldtrip Guidebook, p. 50-54.
- Keller, G. R., Lidiak, E. G., Hinze, W. J., and Braile, L. W., 1983, The role of rifting in the tectonic development of the midcontinent, USA: *Tectonophysics*, v. 94, p. 391-412.
- Kluth, C. F., and Coney, P. J., 1981, Plate tectonics of the Ancestral Rocky Mountains. *Geology*, v. 9, p. 10-15.
- Krause, S. J., 1996, Stratigraphic framework, facies analysis, and depositional history of the Middle to Late Cambrian Riley Formation, central Texas. Master's thesis, University of Texas at Austin, 172 p.
- Kruger, J. M., and Keller, G. R., 1986, Interpretation of crustal structure from regional gravity anomalies, Ouachita Mountains area and adjacent Gulf Coastal Plain: *American Association of Petroleum Geologists Bulletin*, v. 70, no. 6, p. 667-689.
- Long, L. E., 2004, Middle to late Cambrian nonconformity in the Llano uplift, *in* Hoh, A. and Hunt, B. (eds.), Tectonic history of southern Laurentia: A look at Mesoproterozoic, late-Paleozoic, and Cenozoic structures in central Texas. Austin Geological Society Field Trip Guidebook 24, p. 59-61.

- Lowrie, W., 2007, *Fundamentals of geophysics*, second edition. Cambridge University Press, New York, 381 p.
- McGehee, R. V., 1979, Precambrian rocks of the southeastern Llano region, Texas: University of Texas Bureau of Economic Geology Geological Circular, no. 79-3, 36, p.
- Mickus, K., Stern, R. J., Keller, G. R., and Anthony, E. Y., 2009, Potential field evidence for a volcanic rifted margin along the Texas Gulf Coast. *Geological Society of America Bulletin*; v. 37; no. 5; p. 387-390.
- Mosher, S., 1998, Tectonic evolution of the southern Laurentian Grenville orogenic belt. *Geological Society of America Bulletin*; v. 110; no. 11; p. 1357–1375.
- Mosher, S., Levine, J. S. F., and Carlson, W. D., 2008, Mesoproterozoic plate tectonics: A collisional model for the Grenville-aged orogenic belt in the Llano uplift, central Texas. *Geological Society of America Bulletin*, v. 36; no. 1; p. 55–58.
- Nabighian, M. N., Grauch, V. J. S., Hansen, R. O., LaFehr, T. R., Li, Y., Peirce, J. W., Phillips, J. D. and Rude, M. E., 2005, The historical development of the magnetic method in exploration. *Society of Exploration Geophysics, Geophysics, 75th Anniversary*, v. 70, no. 6; P. 33ND–61ND.
- Naidu, P. S., and Mathew, M. P., 1998, *Analysis of geophysical potential fields*. Elsevier Pub., Netherlands, 298 p.
- Nettleton, L. L., 1971, *Elementary gravity and magnetics for geologists and seismologists*. Society of Exploration Geophysicists, Geophysical monograph series, no. 1; 121p.
- Preston, R. D., Pavilcek, D. J., Bluntzer, R. L., and Derton, J., 1996, The Paleozoic and related aquifers of central Texas. Texas Water Development Board, Report 346, 85 p.
- Reese, J. F., Mosher, S., Connelly, J., and Roback, R., 2000, Mesoproterozoic chronostratigraphy of the southeastern Llano uplift, central Texas: *Geological Society of America Bulletin*, v. 112, p. 278–291.

- Roback, R. C., 1996, Characterization and tectonic evolution of a Mesoproterozoic island arc in the southern Grenville orogen, Llano uplift, central Texas. *Tectonophysics*, v. 265, nos. 1-2, p. 29-52.
- Salem, A., Williams, S., Fairhead, J., Dhananjay, R., and Smith, R., 2007, Tilt-depth method: A simple depth estimation method using first order magnetic derivatives. *The Leading Edge*, v. 26, no. p. 12, 1502–1505.
- Shurbet, D. H., Keller, G. R., and Freiss, J. P., 1976, Remanent magnetization from comparison of gravity and magnetic anomalies: *Geophysics*, v. 41, p. 56-66.
- Standen, A. P. G. and Ruggiero, R. P. G., 2007, Llano uplift aquifers structure and stratigraphy, Texas Water Development Board, report, 78 p.
- Sykes, M. P., and Das, U. C., 2000, Directional filtering for linear feature enhancement in geophysical maps, *Geophysics*, v. 65, no. 6; p. 1758-1768.
- Thorarisson, F., Magnusson, S. G., and Bjornsson, A., 1988, Directional spectral analysis and filtering of geophysical maps. *Geophysics*, v. 53, no. 12; p. 1587-1591.
- Viele, G. W., and Thomas, W. A., 1989, Tectonic synthesis of the Ouachita orogenic belt, *in* Hatcher, R. D., Thomas, W. A., and Viele, G. W., (eds.), *The Appalachian-Ouachita Orogen in the United States: Geological Society of America, The Geology of North America*, v. F-2, p. 695-728.
- Walker N., 1992, Middle Proterozoic evolution of Llano uplift, Texas: Evidence from U-Pb zircon geochronometry. *Geological Society of America Bulletin*, v. 104, p. 494-504.
- Weeks, A. W., 1945, Balcones, Luling and Mexia fault zones in Texas: *American Association of Petroleum Geologists Bulletin*, v. 29, p. 1733-1737.
- Whitmeyer, S. L., and Karlstrom, K. E., 2007, Tectonic model for the Proterozoic growth of North America, *Geological Society of America, Geosphere*, v. 3; no. 4; p. 220-259.

Williams, D. L., and Finn, C., 1985, Analysis of gravity data in volcanic terrain and gravity anomalies and subvolcanic intrusions in the Cascade Range, U. S. A., and at other selected volcanoes, *in* Hinze, W. J., Kane, M. F., O'Hara, N. W., Reford, M. S., Tanner, J., and Weber, C., (eds.), The utility of regional gravity and magnetic anomaly maps, Tulsa, Oklahoma, Society of Exploration Geophysicists, p. 361-374.

Young, K., 1972, Mesozoic history, Llano region, *in* Barnes, V. E., Bell, W. C., Clabaugh, S. E., and Cloud, P. E., (eds.), Geology of the Llano region and Austin area, field excursion: The University of Texas at Austin, Bureau of Economic Geology Guidebook 13, 77 p.

APPENDIX

This appendix contains the regional reduced-to-pole total magnetic intensity map of the study area. It also contains the upward continuation maps of the gravity data to different heights as well as the residual gravity maps after upward continuation to different heights. In addition, maps with band-pass filter with different cutoff limits and maps with rejection band-pass filter are shown.

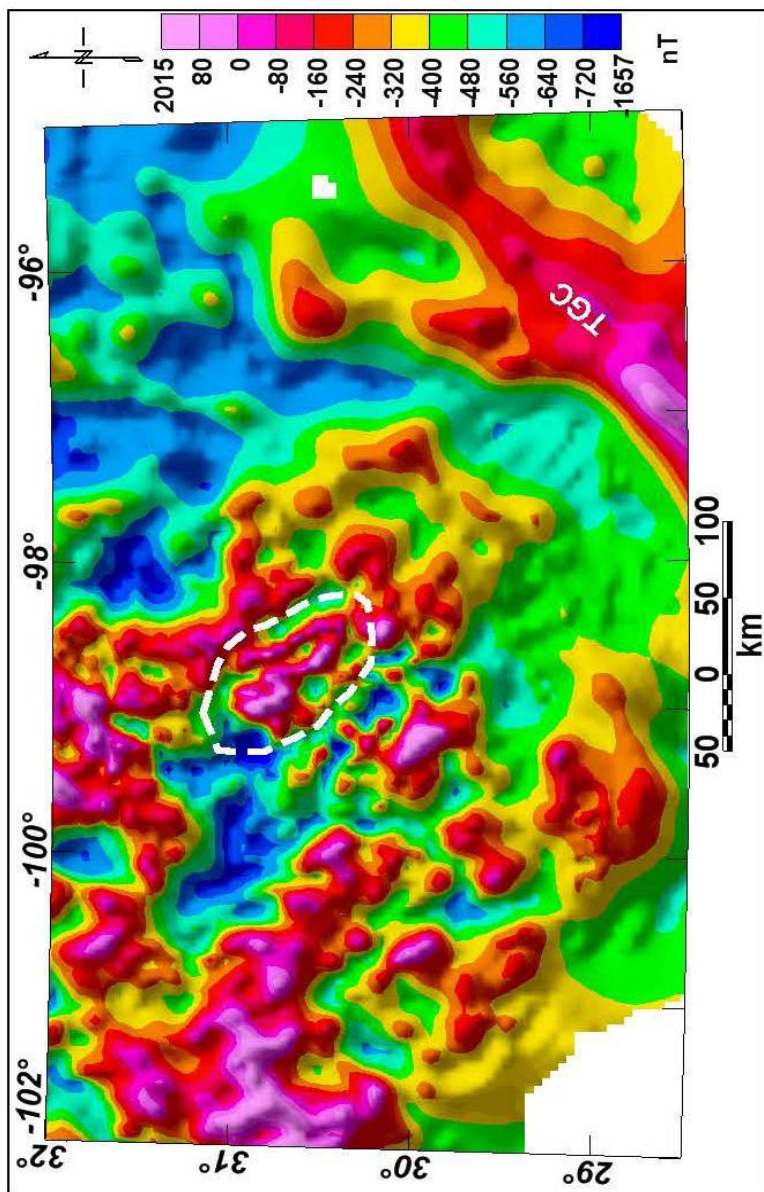


Figure A1: Regional RTP map showing NW-SE high magnetic trends in the Llano uplift area. A NE-SW high amplitude magnetic anomaly at the southeastern corner coinciding with Texas Gulf Coast (TGC).

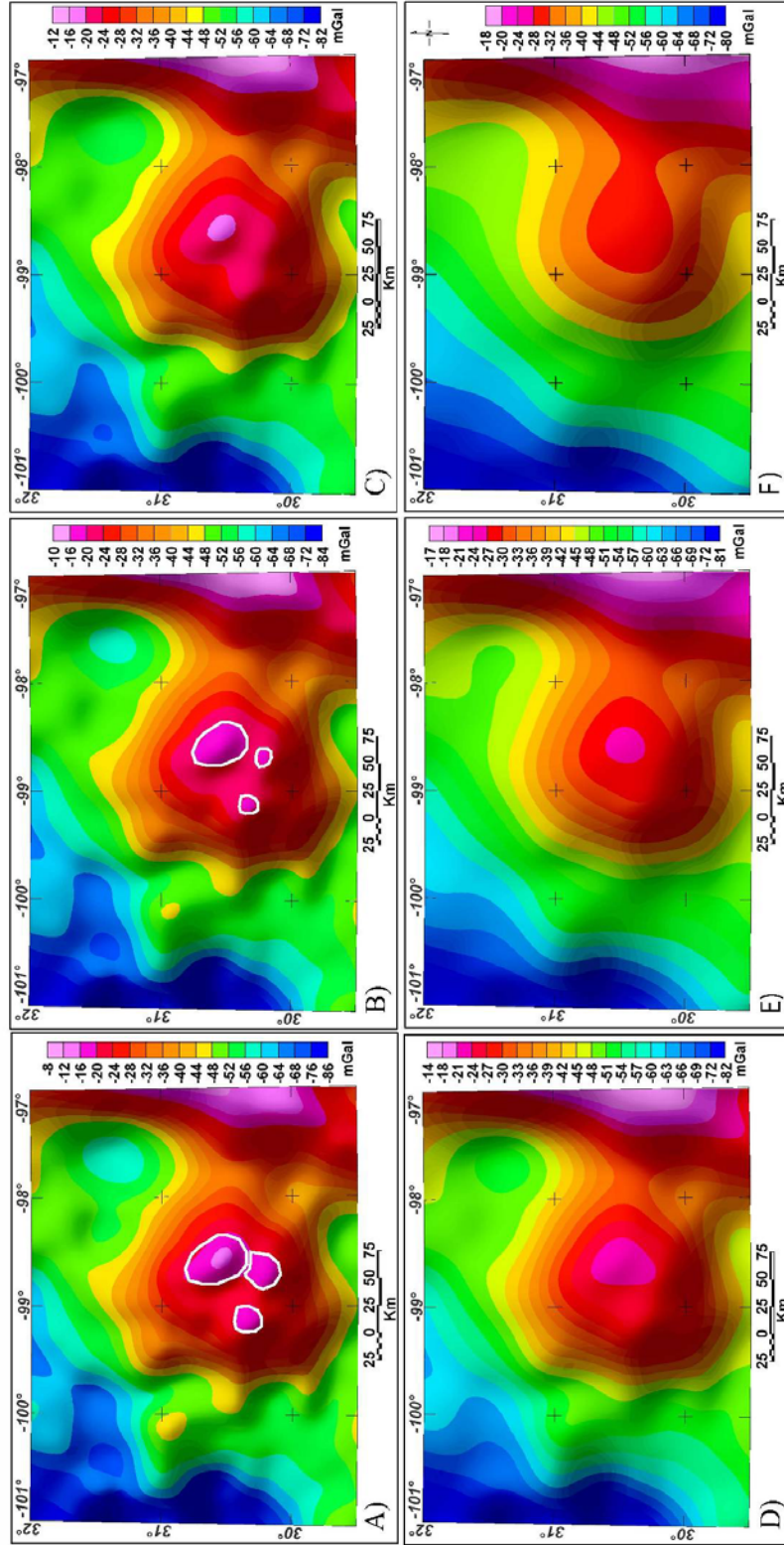


Figure A2: Upward continuation maps of the Bouguer gravity to heights of (A) 10 km, (B) 12 km, (C) 15 km, (D) 20 km, (E) 30 km and (F) 40 km. These maps show general decreasing of the gravity from the east to the west. The maps of the upward continuation to heights of 10 and 12 km (A) suggest the occurrence of the possible sources of the small, shallow high gravity anomalies, see white dashed circles.

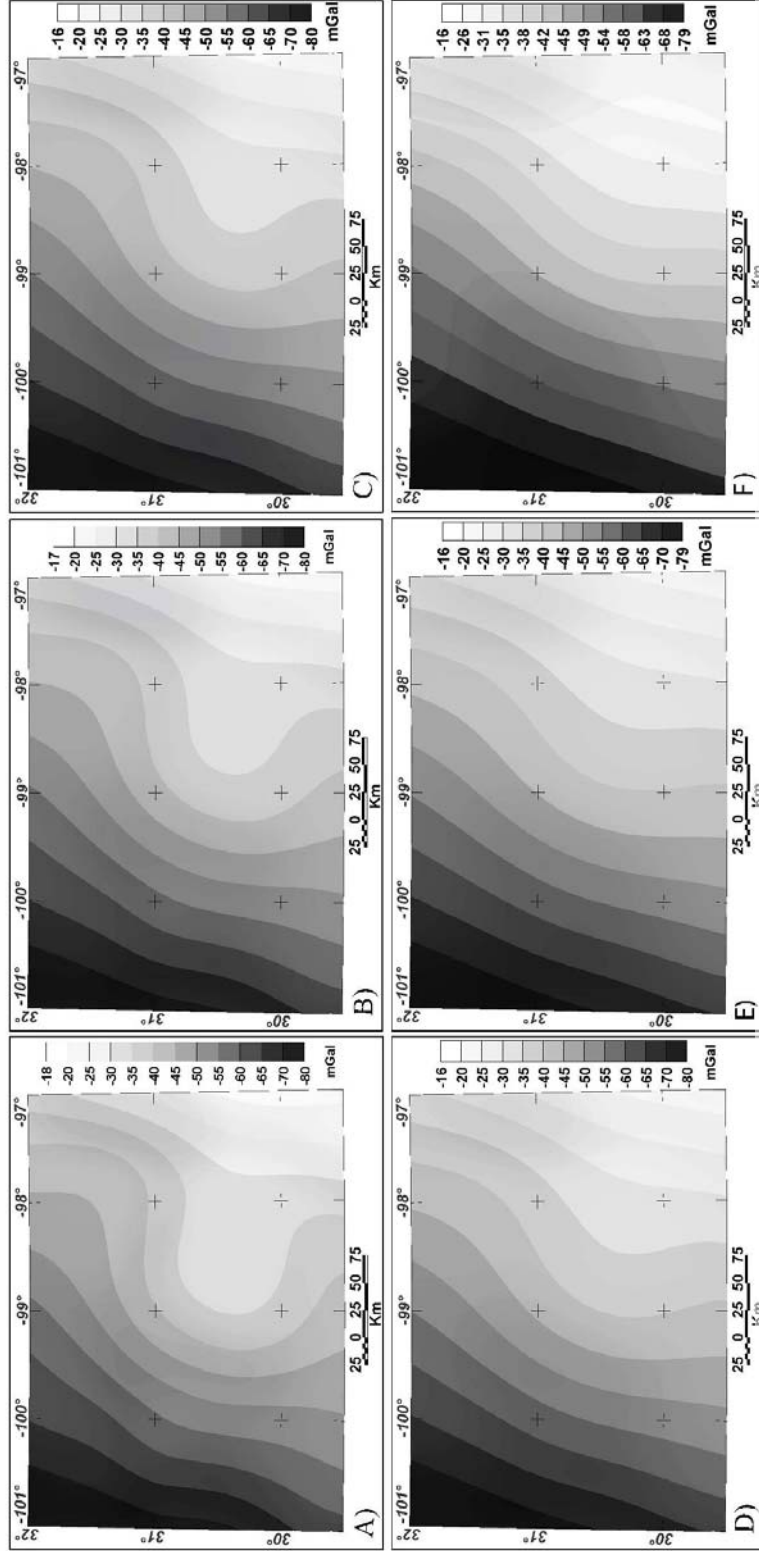


Figure A3: Upward continuation maps of the Bouguer gravity to heights of (A) 100 km, (B) 80 km, (C) 60 km, (D) 50 km, (E) 70 km and (F) 90 km shown in gray scales. These maps show decreasing of the gravity from the east to the west. The map with upward continuation to 50 km suggests the occurrence of possible deep source.

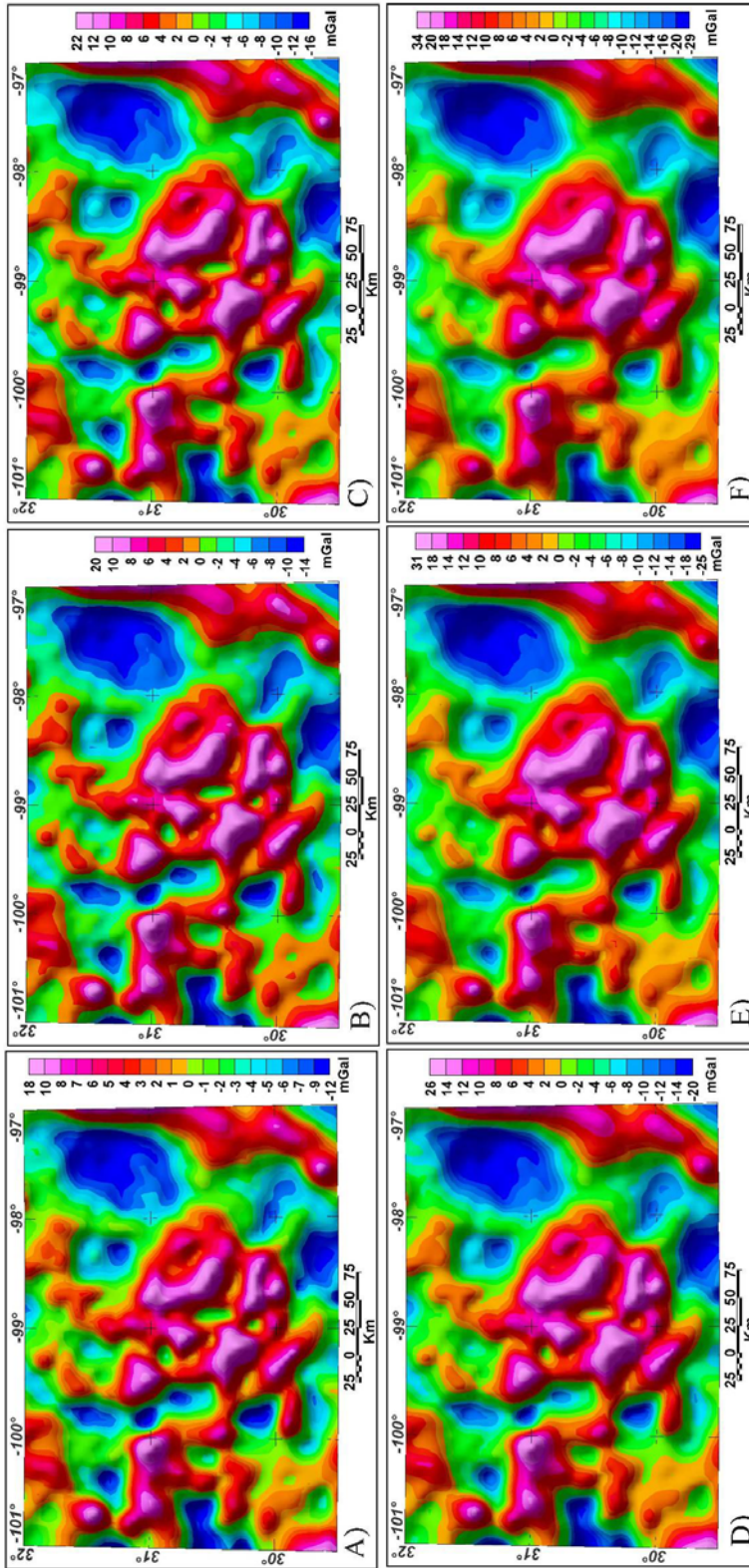


Figure A4: Residual gravity maps after upward continuation to heights of (A) 10 km, (B) 12 km, (C) 15 km, (D) 20 km, (E) 30 km and (F) 40 km. These maps enhance the short wavelength anomalies and make them clearer than those in Figures 5 and 7.

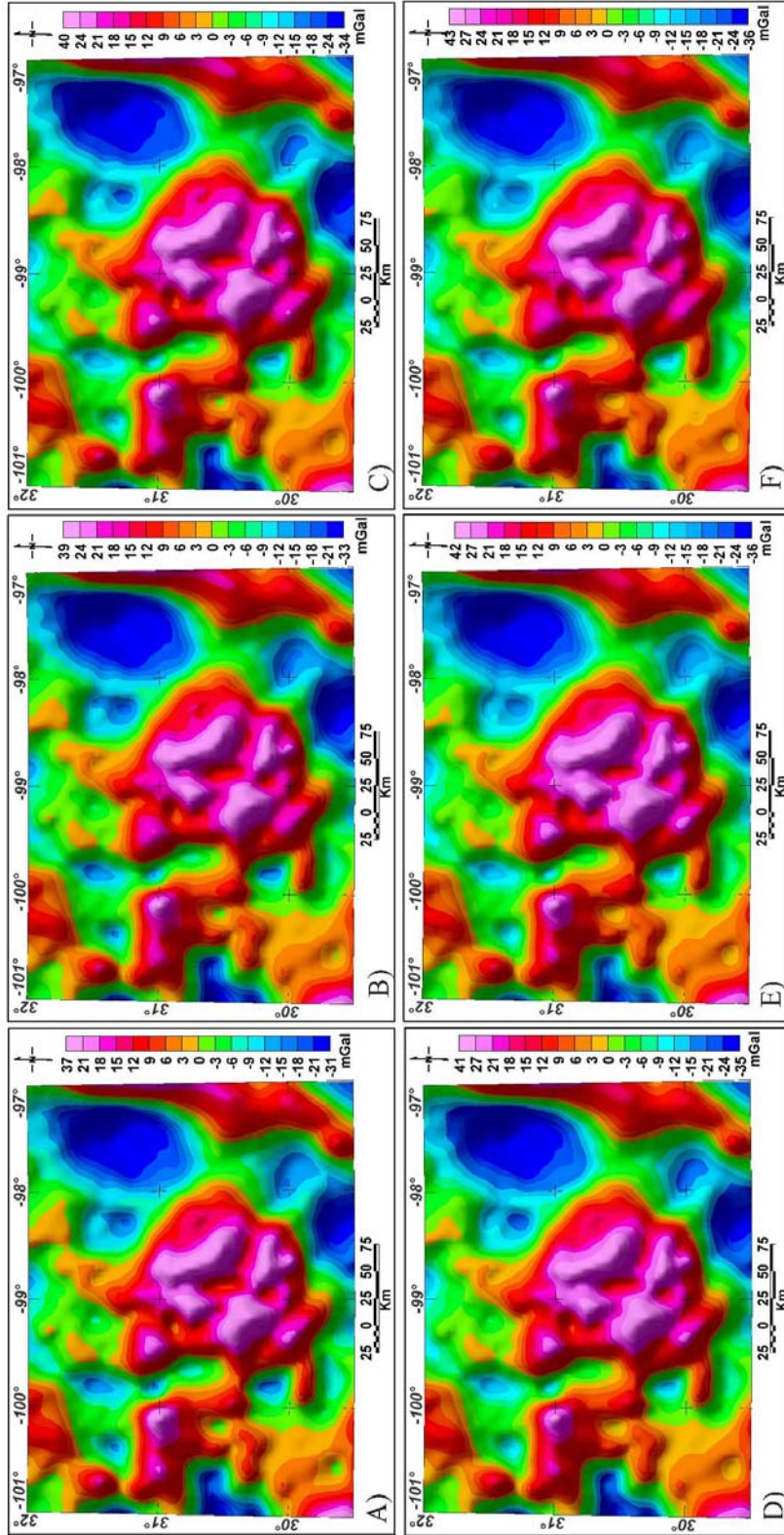


Figure A5: Residual gravity maps after upward continuation to heights of (A) 50 km, (B) 60 km, (C) 70 km, (D) 80 km, (E) 90 km and (F) 100 km.

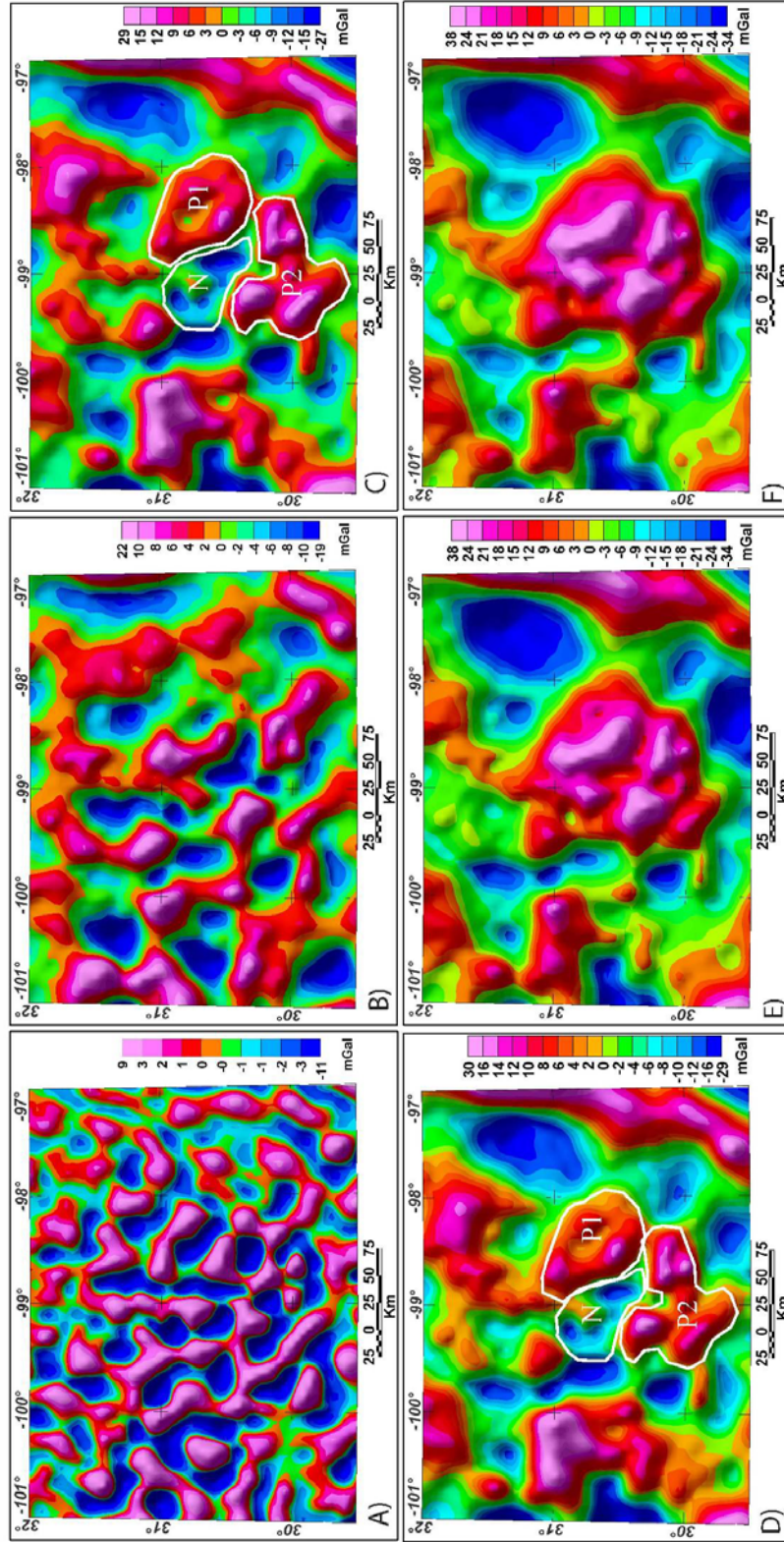


Figure A6: Band-pass filter maps with cutoffs of (A) 1-50 km, (B) 1-100, (C) 1-150, (D) 1-200, (E) 1-300 and (F) 1-400 km passed. The first two maps with wavelengths of (A) 1-50 and (B) 1-100 km passed look over-filtered, while the maps with wavelengths of (C) 1-150 and (D) 1-200 km passed show positive anomalies (P1 and P2) in the eastern and southern parts as well as negative anomaly (N) in the western part.

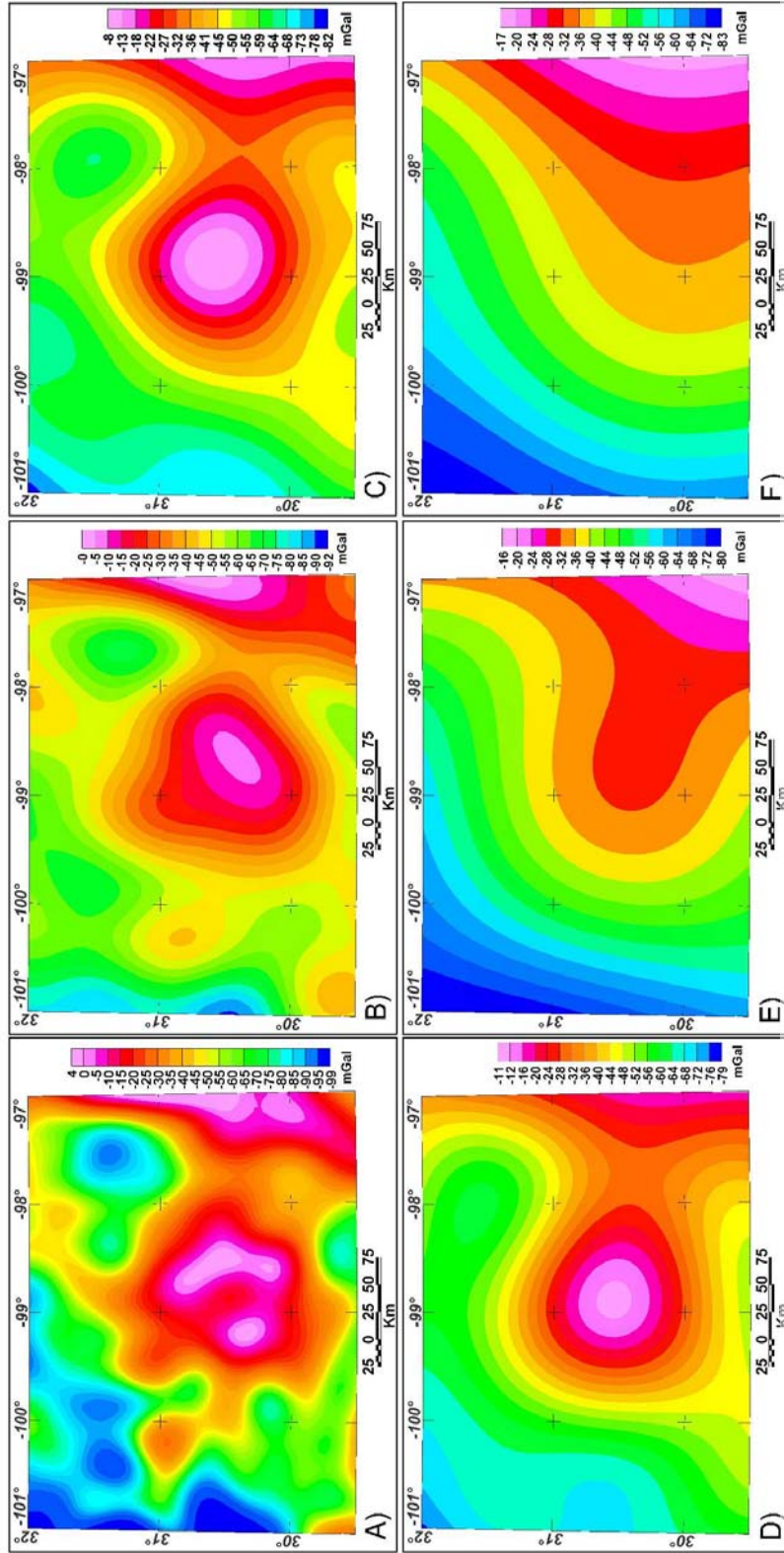


Figure A7: Rejection band-pass filter maps with cutoffs of (A) 1-50 km, (B) 1-100, (C) 1-150, (D) 1-200, (E) 1-300 and (F) 1-400 km rejected. The first map (A) shows short wavelength, very high gravity anomalies corresponding to the shallow buried sources. The maps (A, B, C, D) show a circular anomaly with about 150 km diameter corresponding to the deep buried source.

CHAPTER III: MAPPING THE EXTENSION OF THE MEERS FAULT IN SOUTHWESTERN OKLAHOMA, USING INTEGRATED GEOPHYSICAL AND GEOLOGICAL DATA

Abstract

The Meers fault is the southernmost member of the Frontal Wichita fault zone that separates the igneous rocks of the Wichita uplift to the south and the Anadarko basin to the north. A large gravity dataset of about 14780 gravity station and magnetic data of Oklahoma have been used to complete this study. The interpretation of the gravity and magnetic data suggests a newly interpreted extension of the Meers fault in the subsurface in both southeast and northwest directions. The residual gravity and magnetic maps and the edge detector techniques show gravity and magnetic contrasts on both sides of the Meers fault trace and indicate the limits of its extension. Profiles of gravity readings from a new data base constructed for this study as well as seismic reflection lines beyond both the southeastern and northwestern end of the surface expression of Holocene Meers fault scarp support the new interpreted extension of the fault.

Introduction

The Meers fault is the southernmost element of the complex and massive (10-15 km of throw) frontal fault zone that forms the boundary between the uplifted igneous rocks of the Wichita Mountains, and the Anadarko basin, which is the deepest intra-continental basin in the United States (e.g., Luza, 1989; Jones-Cecil, 1995; Cetin, 1998)

(Figs. III.1 and 2). The fault is the only known Quaternary fault scarp east of Colorado (Crone and Luza, 1990). The clear fault scarp is straight and strikes approximately N60°W for 26 km based on a recent analysis of high-resolution aerial photography as part of this study (Fig. III.3). At the surface, the fault scarp offsets the Permian Post Oak Conglomerate and Hennessy Shale, as well as, Quaternary alluvium (Madole, 1988; Crone and Luza, 1990; Cetin, 1997, 1998).

The most recent movement occurred in the Late Holocene and a number of efforts to date this movement have been undertaken. Crone and Luza (1990) stated the last movement occurred between 1,200 and 1,300 yr ago. Based on the ¹⁴C age dating of soil humus and charcoal, the most recent movement occurred on the fault between 1400 and 1100 yr B.P. in Late Holocene (Madole, 1988). According to Cetin (1997, 1998), the most recent movement occurred about 1,100 yr ago. Based on radiocarbon dating of soil humus and charcoal collected from trenches across the fault scarp, Kelson and Swan (1990) identified two Holocene events: the more recent event occurring 1050 yr ago, and the older one occurring between 2900 and 3400 yr ago.

Motion on the Meers fault represents continued activity on one of the largest structural features in North America. The Wichita uplift and the Anadarko basin, which are separated by the Meers fault and related, subparallel fault strands (Fig. III.1), indicate significant intraplate deformation along the trend of the Southern Oklahoma aulacogen, which is a classic example of a failed and massively inverted rift (e.g., Keller and Stephenson, 2007). The mechanisms of intraplate deformation are not nearly as well understood as the processes occurring at plate boundaries. The Wichita uplift,

the Anadarko basin, and the associated fault zones represent an area in the intracontinental United States with long history of intraplate deformation.

Oklahoma has a well-documented history of seismicity (Luza, 1989) with more than 600 events being located in 2010, including a 4.7 M_b event in October that was felt from Kansas City to Dallas. Although Meers fault is considered to be an active feature, there is no historical record of earthquakes associated with it. The most recent movement in the Late Holocene resulted in 5 m vertical and possibly more left-lateral strike slip displacement on the fault (Ramelli and Slemmons, 1986; Madole, 1988; Luza, 1989; Kelson and Swan, 1990). The Quaternary soils along the fault area were ruptured and folded during this event (Cetin, 1997, 1998).

Mapping the lateral and vertical extent of the Meers fault is important from several perspectives. First, the Meers fault represents a significant seismic hazard to the central United States and detailed mapping and follow-up paleoseismic studies can add information to quantitative seismic risk assessments. Secondly, studies on the Meers fault will increase our knowledge of intra-plate deformation and intra-continental seismicity in analogous areas. The fault is not well mapped in detail beyond the area of the trenching studies conducted in the 1980's and 1990's. The full length of the scarp and the full extent of the fault are unclear due to insufficient study.

In this study, a large gravity dataset compiled from datasets provided by the Pan-American Center for Earth and Environmental Studies (PACES) and the United States Geological Survey (USGS) to investigate the relationship between the Frontal Wichita fault zone, which the Meers fault is the southern member, and the associated intraplate deformation in the Wichita uplift-Anadarko basin province. The total

magnetic intensity map of Oklahoma downloaded from the USGS website is also employed to conduct this study. In addition, we collected two gravity profiles with closed space station separation beyond the southeastern end of the 26 km long clear Holocene scarp to examine the gravity surface signature across the fault. Moreover, three seismic reflection lines; two to the northwest end of the Meers fault scarp, and the third to the southeastern end, were provided by Geokinetics to facilitate our investigation of the subsurface extension of the fault.

Previous geological and geophysical work

Harlton (1951) named the Meers fault as “Thomas fault”, and described it to be downthrown on the south with 2,500 ft vertical displacement, but later in (1963), he stated that the fault is reverse and downthrown on the north. Moreover, he recognized a major structural dislocation between younger rocks of the Slick Hills to the north and the Middle Cambrian rocks of the Wichita Mountains to the south. The scarp of the Meers fault trends N60°W and forms a straight and very clear scarp about ~26 km long, and as discussed below, there have been many efforts discussing its possible total length. A major goal of this study is refining our knowledge of its structure and extent. At the surface, the fault scarp offsets Post Oak Conglomerate and Hennessy Shale of Permian, as well as the alluvium deposits of the Quaternary (Madole, 1988; Cetin, 1998; Jones-Cecil, 1995). The maximum vertical displacement is about 5 m at the center of the fault scarp (Ramelli et al., 1987).

The straightness of the clear Holocene fault scarp implies that the fault is nearly vertical at the surface. Based on trenching studies by Crone and Luza (1990) and

Kelson and Swan (1990), the reactivated part of the Meers fault is nearly vertical in the upper 2 m. In addition, interpretation of shallow seismic-reflection data showed the fault to be nearly vertical to depths of 200–300 m (Miller et al., 1990). Using the Consortium for Continental Reflection Profiling (COCORP) deep seismic-reflection profiles beyond the northwest end of the Meers fault scarp, Brewer (1982) and Brewer et al. (1983) reported 30°–40° southwest dip to the Meers fault. However, reprocessing of the same COCORP data by Lemiszki and Brown (1988) indicated that the Meers fault has a southwest dip of 70° or greater. Based on aeromagnetic models, Jones-Cecil and Crone (1989) stated that the fault has near-vertical dip to at least 6 km depth. The interpretation of ground magnetic data by Jones-Cecil (1995) and Jones-Cecil et al. (1995) indicated that the dip of the fault is vertical down to at least 0.5 km depth.

Harlton (1963) extended the fault for 83-109 km using subsurface data where he assigned the northwest end at Texas state boundary and the southeast end at the Criner uplift. Ramelli and Slemmons (1986) used low sun-angle aerial photograph to extend the Holocene scarp toward the southeast to be 37 km length. Based on deflection of stream alignments and soil studies, Cetin (1991) reported that the Holocene fault scarp can be extended additional 30 km to the northwest where it bifurcates and follows a new N80W trend. The geophysical maps show that the fault might have a length of about 70 km (Slemmons et al., 1985). The examination of new high resolution aerial photography indicates a clear length of 24 km (Fig. III.3).

Geological Setting

The extension of the southern margin of the North America continent during the Early Paleozoic break-up of the supercontinent Rodinia resulted in formation of two rifts that trend at high angles to the Cambrian continental margin of the central U.S. In the Late Paleozoic, the rift in the southern Oklahoma region was inverted during tectonism associated with the Ouachita orogeny to form the Southern Oklahoma aulacogen. The only location where the Cambrian rift-related rocks are uplifted and exposed is southern Oklahoma. The most extensive exposures of the Cambrian igneous rocks in the midcontinent exist in the Wichita Mountains (McConnell and Gilbert, 1990). The Southern Oklahoma aulacogen (SOA) dominated the area occupying south-central and southwestern Oklahoma from the Late Precambrian-Early Cambrian to Pennsylvanian (Fig. III.1). The SOA was an elongated, deep west-northwest trending trough that extended into the craton from the southern margin of North America (Ham et al., 1964; Ham and Wilson, 1967). According to Gilbert (1982), the early history of the aulacogen was characterized by rifting, deep-seated faulting, and bimodal magmatism. The crustal thinning associated with the extension was compensated by addition of magma derived from the mantle (McConnell and Gilbert, 1990). Large gabbroic bodies of the Raggedy Mountains Gabbro Group intruded the upper crust, and its extrusive equivalent Navajoe Mountain Basalt-Spilitite Group erupted onto the surface in Late Precambrian or Early Cambrian (Fig. III.2). This magmatism was followed, first by erosion, and later by eruption of the Carlton Rhyolite Group and intrusion of its equivalent Wichita Granite Group in Middle Cambrian time (Gilbert, 1982). The igneous activity ended with intrusion of a variety of igneous intrusions such as dikes

and sills throughout the entire area (Burke et al., 1969; Vidrine and Fernandez, 1986). The rift phase of the aulacogen formed as a result of a major continental breakup in Late Precambrian-Early Cambrian (Keller et al., 1983). Subsidence and basin filling dominated the aulacogen from Late Cambrian to Late Mississippian time where the Anadarko basin was filled with as much as 6 km of mostly carbonate sediments (Ham et al., 1964). Cambrian and Ordovician rocks of this sequence are exposed in the Slick Hills northeast of the Meers (Gilbert, 1982) (Fig. III2). Keller and Stephenson (2007) reviewed previous geophysical studies of the Southern Oklahoma aulacogen and revisited the classic comparison of the SOA to the Dnieper-Donets aulacogen on central Europe.

The Ouachita orogenic belt developed as the result of the collision between North America and South America plates during the Mississippian and Pennsylvanian periods (Viele and Thomas, 1989). The Wichita uplift is an extensive basement-involved uplift located within the foreland of the Ouachita orogen. Regional cross sections show basement-involved thrusts and folds in the Wichita uplift-Anadarko basin province (McConnell, 1989a). By the end of the Ouachita orogeny, the Late Precambrian-Early Cambrian extension faults were inverted as high angle thrust faults, and the entire area was intensely uplifted and deformed. The Amarillo-Wichita uplift was developed and exposed due to the uplift of the igneous core of the aulacogen, and the adjacent Anadarko basin formed by downwarping of the crust beneath the basin (Gilbert, 1982; Donovan, 1986; Johnson, 1989). Syn-tectonic sedimentation occurred in the aulacogen area during Early Pennsylvanian into Permian time (Ham and Wilson, 1967), and the Arbuckle and Wichita uplifts became important sources of sediments to

the foredeep (Viele and Thomas, 1989). Consequently, the Anadarko basin, the deepest basin in North America was filled with more than 11 km of sedimentary rocks (Ham and Wilson, 1967).

A west-northwest network of faults developed across the area extending from south central Oklahoma to Texas Panhandle during the Late Paleozoic deformation. The orientation and the location of these faults could be controlled by pre-existing zones of crustal weakness associated with the initial rifting of the aulacogen area (Crone and Luza, 1990). Harlton (1951) named these faults the Frontal Wichita fault system (FWFS) (Fig. III.1). The Mountain View fault represents the northern boundary of the Frontal Wichita fault system, and the Meers fault may represent the southern boundary. Deformed Lower Paleozoic sedimentary rocks crop out in the Slick Hills and represent part of the Frontal Wichita fault system that separates the Wichita uplift from the Anadarko basin. The Meers fault separates the deformed Lower Paleozoic Arbuckle Group carbonate rocks of the Slick Hills from the Wichita uplift igneous rocks (McConnell, 1989a). This fault system represents the structural boundary between the Wichita-Amarillo uplift to the southwest and the Anadarko basin to the northeast. The FWFS is dominated by reverse faults with moderate to steep dips and greater than 9 km of combined net vertical displacement (Ham et al., 1964). The FWFS has cumulative throw with more than 12 km between the Wichita Uplift and the Anadarko basin (Ham and Wilson, 1967). Based on the orientation and the pattern of faults and folds along this fault system, Donovan et al. (1983) suggested that the faults of the FWFS were produced in part by strike-slip faulting. McConnell (1989b) used the palinspastic restoration of isopach pattern to suggest oblique slip on the Frontal Wichita fault zone.

These oblique slip has a left-slip component of about 14.5-33.8 km and reverse slip of about 10.8 km.

The Meers fault has a net throw of about 6.4 km, and is responsible in part for the structural offset between the Cambrian-Ordovician rocks and the Wichita Mountains (Harlton, 1951, 1963). The Meers fault defines the northeastern boundary of the SOA, and it was reactivated during the Pennsylvanian (Johnson, 1989), and during the Tertiary (Crone and Luza, 1990). Although, the fault is not associated with historical seismicity, it could be responsible for hazardous earthquakes due to the documented recent movements that are as young as 1,300 yr. The Late Holocene activity suggests that the tectonic setting of the Meers fault is similar to those of the active seismic zones in the southeastern United States, and reinforces the assumption of that the deformation in the southeastern United States occurs along zones of crustal weakness (Kelson and Swan, 1990).

Geologic history and characteristics of the Meers fault

The Meers fault may have developed as a rift fault during the formation of the Southern Oklahoma aulacogen in the Late Proterozoic-Cambrian periods (Ham et al., 1964) (Figs. III.1 and 2). The major activity along the fault occurred as oblique-slip movement (approximately equal amounts of strike-slip and reverse movement) during the Late Mississippian-Pennsylvanian. The movement consisted of left lateral strike-slip and dip-slip of about 2 km of vertical displacement down to the north. Rocks of Cambrian-Mississippian age were faulted and folded during this major tectonic event, and Permian sediments were deposited on these deformed rocks (Madole, 1988). The

igneous rocks of the Wichita Mountains were juxtaposed against the Early Paleozoic carbonates of the Slick Hills (Jones-Cecil, 1995; Jones-Cecil et al., 1995).

The nature of the vertical movement along the Meers fault reversed between the major activity in the Pennsylvanian and the subsequent relatively minor reactivations. The first reactivation was in Permian time with a minor reversal in the sense of vertical motion to be up-to-the-north (Donovan et al., 1989). The Holocene reactivation represents the latest activity, and it includes two movements; the most recent one occurred 1050-1300 yr ago, and the older one occurred between 2900 and 3400 yr ago (e.g., Kelson and Swan, 1990). Similar to the Permian reactivation, the Holocene reactivation was characterized by left-lateral and up to the north movement, and resulted in a nearly straight fault scarp about 26 km in length (Crone and Luza, 1990; Kelson and Swan, 1990). The Meers fault trends N60°W along most of its length but trends more northerly at its northwest end where it divides and intersects the Mountain View fault (Jones-Cecil et al., 1995).

Gravity and magnetic data

Data acquisition and processing

The gravity data used for the current study are a combination of three different gravity datasets. These datasets include gravity data provided by the Pan-American Center for Earth and Environmental Studies (PACES; www.research.utep.edu/paces), gravity data provided by the United States Geological Survey (USGS), and the most recently collected gravity data were part of this study. The PACES compilation process and the reduction procedures were discussed by Hinze et al. (2005) and Keller et al.

(2006). The PACES compilation includes approximately 12991 gravity stations and the USGS gravity dataset includes about 1747 stations.

We re-reduced the USGS data using the spreadsheet by Holom and Oldow (2007) that is based on the equations presented in Hinze et al. (2005) to obtain simple Bouguer anomaly (SBA) values at every station. The gravity data during this study include 42 stations collected beyond the accepted southeastern end of the Meers fault scarp. The observed gravity data were collected along two parallel profiles 2 miles apart with a 0.5 mile station separation. The observed gravity values were obtained by tying with base station number BLWPO at the Federal Building (U.S. Courthouse) in Lawton, Oklahoma, which has an observed gravity of 979622.830 mGal. Terrain corrections were calculated for both the USGS and the new datasets using the Oasis Montaj 7.2 software package to obtain complete Bouguer anomaly (CBA) values. The terrain corrections assumed a density of 2.67 g/cm^3 , and employed a regional terrain grid to calculate terrain corrections out to a distance of 167 km. Finally, all the CBA values for the three datasets were merged and gridded at 2 km to construct the complete Bouguer anomaly map for the current study.

The magnetic data of the current study are represented by the total magnetic intensity map of Oklahoma downloaded from the United States Geological Survey (USGS) website. The total magnetic intensity (TMI) grid was constructed with a 1 km grid size, and transformed into the reduced-to-pole total magnetic intensity (RTP) grid. The complete Bouguer anomaly and RTP grids were subjected to a variety of filtering techniques to enhance certain anomalies and trends.

The complete Bouguer gravity map of the area exhibits a large northwest-trending gravity high related to the deep-seated igneous rocks of the Wichita Uplift whose outcrops are shown in horizontal striped white lines (Fig. III.4A). The carbonate rocks of the Slick Hills (striped blue diagonal lines) that lie north of the Meers fault are also associated with a relatively high gravity anomaly since their densities are close to those of the Wichita Uplift igneous rocks. Further to the north, the Anadarko basin, the deepest basin in North America, shows a relatively low gravity anomaly, but this anomaly is not as low as would be expected given the 12 km thick sedimentary fill. As discussed by Robbins and Keller (1992), the modest low gravity anomaly could be related to mafic layered bodies that floor the Anadarko basin and the high density, thick Lower Paleozoic carbonate rocks. The low gravity anomaly to the southwest of the uplift is related to the Hardeman basin. The gravity expression of the Meers fault is subdued due to the low density contrast between the igneous rocks and the carbonate rocks (e.g., Robbins et al., 1989; Robbins and Keller, 1992). The complete Bouguer gravity map also shows the location of nine ground gravity profiles. Seven profiles were extracted from the compiled gravity dataset, and the most recently collected two profiles lie to the southeast (Fig. III.4B).

The reduced-to-pole total magnetic intensity map shows more detail in the Wichita Uplift area than the gravity maps since the uplift mostly consists of a variety of igneous rocks with highly variable magnetic susceptibilities (Fig. III.5A). The nonmagnetic carbonate rocks of the Slick Hills are juxtaposed against the highly magnetic igneous rocks of the Wichita Uplift across the Meers fault (e.g., Jones-Cecil, 1995). Figure III.5b shows the clear scarp of the fault and its new interpreted extension

from this study. The magnetic expression suggests the fault can be extended further to the northwest and southeast directions (dashed lines). We projected the nine gravity profiles on this map to test if we can trace the fault expression clearly, and compare the results to the seismic reflection lines discussed below.

Data filtering and enhancement

As a common step before the interpretation process, observed geophysical data is subjected to filtering and enhancement techniques. This step aims to prepare the data for integration with other techniques, enhance anomalies of geological interest, and obtain initial information on the location of the sources of anomalies (Nabighian et al., 2005).

Regional-residual separation

The regional gravity and magnetic anomalies were calculated using the upward continuation technique, which when subtracted from the original anomaly data, functions as a low-pass filter. The complete Bouguer gravity and RTP anomaly grids were upward continued to a height of 5 km then subtracted from the complete Bouguer and RTP grids to construct the residual anomaly grids. The residual gravity map shows a complex gravity high in the area of the Wichita Uplift related to the igneous rocks (Fig. III.6A). A NW-SE trending low gravity anomaly is located to the northeast of and parallels the Wichita uplift. This low gravity trend coincides with the southeastern part of Anadarko basin and the Ardmore basin. The Hardeman basin to the southwest appears more clearly than it does in the complete Bouguer anomaly map. The magnetic

residual map after upward continuation to a height of 5 km shows a clear magnetic contrast to the southeast and northwest ends of the Holocene fault scarp suggesting that the fault can be extended further in both to the NE and SW (dashed line) (Fig. III.6B).

Edge detector techniques

The total horizontal derivative (THD) is commonly used to delineate edges of features such as faults or igneous bodies. Prior to the application of the total horizontal derivative, the total magnetic intensity needs to be corrected for the inclination of the Earth's magnetic field (Lahti and Karinen 2010). The total horizontal derivative peaks over the edges and is zero over the body (Miller and Singh, 1994).

The THD of the residual gravity data shows gravity maxima that coincide with the fault scarp (Fig. 7A). The gravity maxima continue to the southeast and to the northwest where it splays or branches indicating that the fault can be extended further in both directions. Moreover, the THD of the magnetic data shows sharper and more defined maxima that coincide with the surface rupture of the Holocene Meers scarp, and it suggests that the fault can be extended in both to the northwest and the southeast (Fig. III.7B) in agreement with the extension based on the magnetic anomalies. The gravity or magnetic maxima appear to be centered on the edges of dike-like bodies trending parallel to the fault trace. Purucker (1986) identified shallow mafic dike-like bodies that extend for a distance longer than half the fault length. Jones-Cecil (1995) and Jones-Cecil et al. (1995) recognized a dike-like body along about 12 km of the Holocene rupture of the Meers fault.

The tilt derivative (TDR) of the potential field is defined as the ratio of the first vertical derivative to the total horizontal derivative of the field. The tilt derivative is positive over the source, close to zero at the edge, and it is negative outside the source region. The method has a unique advantage over the other edge detectors in that it responds equally to shallow and to deep sources (Miller and Singh, 1994). The horizontal derivative of the TDR (HD_TDR) generates well-defined and sharp maxima centered over the edges of bodies.

The map of the TDR of the gravity data shows close to zero gravity values that coincide with the fault scarp and its interpreted extensions to the southeast and northwest (Fig. III.8A). The horizontal derivative of the TDR of the gravity data displays clearer gravity maxima that coincide with the fault scarp, and supports my interpreted extensions to the southeast and northwest where it splays (Fig. III.8B). Similarly, the TDR of the magnetic data shows close to zero magnetic values that coincide with the fault scarp, and also support the southeast and northwest extensions (Fig. III.9A). The horizontal derivative of the TDR of the magnetic data displays sharper magnetic maxima that coincide with the fault trace (Fig. III.9B). This sequence of maps shows a very consistent geophysical signature demonstrating that the fault can be traced further to both the northwest and southeast. The fault trend seems to be controlled by NW-SE linear bodies such as altered zones along the fault and possibly dikes.

Gravity profiles

Nine gravity profiles were constructed across and beyond the ends of the Meers fault scarp (Figs. III.4B and III.5B). Two of these profiles consist of the most recently collected gravity data beyond the southeastern end of the clear scarp. The remaining seven profiles were extracted from the merged gravity dataset and constructed across and beyond the northwestern end of the scarp. The complete Bouguer gravity readings in mGal were plotted against the distance in km, and a linear trend was removed from the profiles in order to enhance the local anomalies that might be associated with the trace of the Meers fault. The difference between the original profile gravity readings and the calculated ones using the linear trend was plotted against the distance (Figs. III.10-III.18).

Profile AA', the northwestern most one, shows decreasing in gravity readings from south to north but it is located beyond the clear magnetic contrast shown by the fault trace (Fig. III.10). Profile BB' shows a clear change in the anomaly values near the middle of the profile where the proposed extension of the Meers fault intersects the profile (Fig. III.11). The plot of the gravity difference exaggerates this change and shows it as a trough of 8 mGal. Similarly, profile CC' shows a small jump, which shows up clearly at 14 km where the profile intersects interpreted extension of the fault (Fig. III.12).

Profile DD', which crosses the fault scarp at approximately 18 km, shows a small jump in the gravity signature, and it is only modestly clearer in the residual profile (Fig. III.13). Similarly, profile EE' crosses the fault scarp at approximately 20 km, and it appears as a small inflection in the profile (Fig. III.14A). This inflection is exaggerated

in the residual profile and is expressed as a sharp drop in the gravity values at 20 km (Fig. III.14B). Profile FF' crosses the fault scarp at its southeastern end, and it shows a clear signal at a distance of 18 km along the profile (Fig. III.15). Profile GG' mostly is from a detailed line in the USGS database and is the first one beyond the southeastern end of the clear fault scarp. It intersects the possible extension of the fault at a distance of 2-3 km, but obvious anomaly exists. However, the residual anomaly after removal of the linear trend shows a clear anomaly of ~1.4 mGal (Fig. III.16).

The two profiles of recently collected data (HH' and II') have the advantage of close station spacing, 2-3 microGal precision gravity measurements, and high precision GPS determinations of elevation (10 cm). Profile HH' shows a clear decrease (~5 mGal) in the gravity readings from the south to the north with a deflection point at a distance of approximately 16-17 km where the profile intersects with the interpreted fault extension (Fig. III.17). Like profile HH', profile II' shows a clear gravity change (~7 mGal) at 12 km where the profile intersects the possible extension of the fault (Fig. III.18). The gravity signature along the three profiles beyond the southeastern end of the Meers fault scarp show a clear south to north drop in gravity values across the interpreted location of the fault. The 5 mGal anomalies on the two new detailed profiles suggest an increase in throw in the reverse movement as the fault approaches the Wichita Thrust Front.

Seismic data

Seismic reflection data are a major element of this study and consist of three seismic reflection lines that actually are vertical slices through a large merged 3-D data

volume that extends along the Wichita Thrust Front and was originally produced by Petroleum Geo-Services (PGS). Two of the profiles lie beyond the northwest end of the mapped Meers fault scarp and were provided by PGS, and the third lies beyond its southeastern end (Fig. III.19) and was provided by Geokinetics. The surveys that were merged to create this 3-D data volume are high resolution with high trace density and were recorded with wide azimuths.

Seismic line A is located beyond the northwestern end of the Meers fault scarp, and it shows the interpreted relatively high-angle reverse faults with their planes dipping southward. However, these seismic sections are highly vertically exaggerated, and the actual dips are approximately 45° . The second fault from the left appears to have been reactivated during the Late Paleozoic tectonism since it offsets the Late Paleozoic strata (white arrow, Fig. III.20). Seismic line B is located SE of line A, and reveals a number of clear high-angle vertical reverse faults (Fig. III.21). The Meers fault was interpreted to be the second one from the left since it intersects the southern third of the seismic lines and correlates spatially with the projection of the fault suggested by the magnetic and gravity data. Seismic line C is located beyond the southeastern end of the Meers fault scarp (Fig. III.22) and shows a nearly vertical disruption in the reflections in a position that suggests the presence of the extension of the Meers.

Since the Mountain View fault is a major fault of the Wichita Thrust Front, it can be traced to larger depth than Meers fault as interpreted by the COCORP seismic data (Brewer et al., 1983). COCORP seismic line 2-2A extends from the Anadarko basin to the Wichita uplift crossing the potentially Meers fault. Brewer et al. (1983) used these old 2-D data that have far less resolution than the modern 3-D data to

interpret the near surface Meers fault at station number 750 (Fig. III.23). However, the magnetic expression of the Meers fault suggests that the fault extension ends just east the COCORP seismic line 2-2A. There is weak evidence of a fault similar to the ones shown on the PGS lines, and this possible fault is shown on Figure III.23.

Figure III.24 shows the RTP map with the 26 km clear Meers fault scarp (black segment) and the locations of the nine gravity profiles as well as the three seismic lines. The interpreted northwestern extension of the Meers fault appears to have merged with the Wichita Thrust Front on seismic line A (red line) but intersects seismic line B (blue line) at the position indicated by the white circle, Fig. III.24). Similarly, the interpreted southeastern extension of the Meers fault appears to intersect seismic line C (green line) at the location indicated by the black circle, Fig. III.24). Comparing the projection of the seismic line C on the index map (Fig. III.1) and on Figure III.22 supports this interpretation.

Conclusions

The Meers fault scarp and its subsurface extension separate rocks with magnetic properties that vary clearly more than densities. The strong magnetic contrast on both sides of the Meers fault is mostly due to the Late Paleozoic movement, which juxtaposed Early Cambrian igneous rocks against Cambrian-Ordovician carbonate rocks. The Meers fault defines the southern boundary of the deformed rocks of the Slick Hills, which represent northward thrusting of a large block over the southern Anadarko basin. The fault may also define the northeastern boundary of dikes-like bodies trending northwest-southeast parallel to the Southern Oklahoma aulacogen axis. Reactivations of

the Meers fault, including the Holocene movements, are of relatively small magnitude. However, the 3-D seismic profiles presented here provide impressive images of the structural complexity of the Wichita Thrust Front, and suggest that the Meers fault is a deep-seated high-angle thrust fault. Based on the magnetic signature of the Meers fault as revealed by the reduced-to-pole total magnetic intensity and the residual magnetic maps as well as magnetic edge detector techniques, the Meers fault can be extended about 21 km southeastward further beyond the clearly defined scarp. The most recently collected gravity profiles and seismic reflection data support and reinforce this interpretation. Similarly, the fault extension can be traced northwestward for about 51 km where it splays and strikes more northerly. On both ends, the fault appears to merge with the Wichita Thrust Front. Thus, its extent is limited laterally to ~95 km. While it is likely that the Holocene movement extended beyond the clearly defined scarp, we believe that the entire length of the fault should be considered as a potential seismic hazard. The seismic reflection profiles show that it is related to a complex series of large reverse faults that form the northern margin of the Wichita uplift.

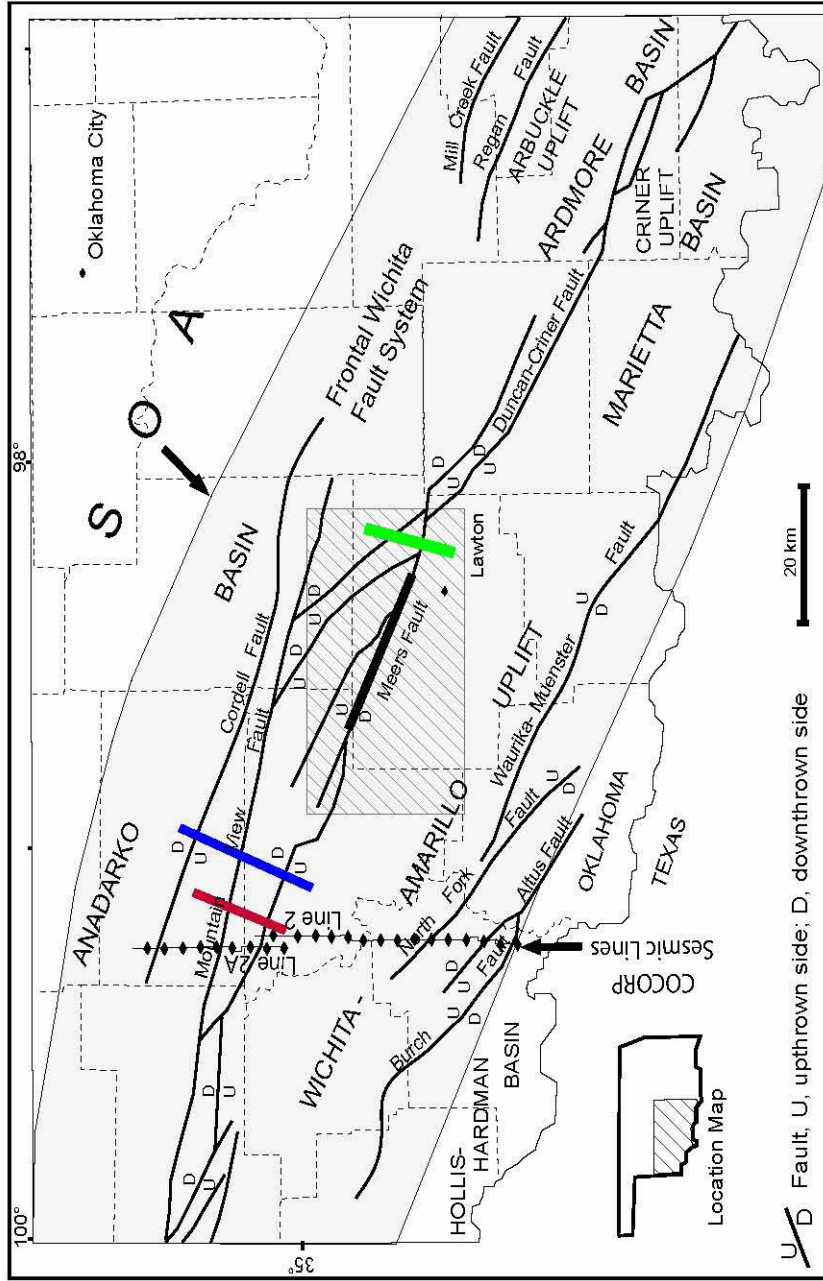


Figure III.1: Index map of southwestern Oklahoma showing the Frontal Wichita Fault System that separates the Anadarko basin from the Wichita Uplift. The clear Holocene scarp of the Meers fault is shown as heavy black segment. The Consortium for Continental Reflection Profiling (COCORP) seismic reflection lines 2 and 2A are shown. Seismic lines A, B and C provided by Geokinetics are shown as red, blue and green segments, respectively. The gray area shows the approximate areal extent of the Southern Oklahoma Aulacogen (SOA), and the stripped rectangle shows the boundary of Figure 2, redrawn from Harlton, (1951, 1963); Ham et al., (1964).

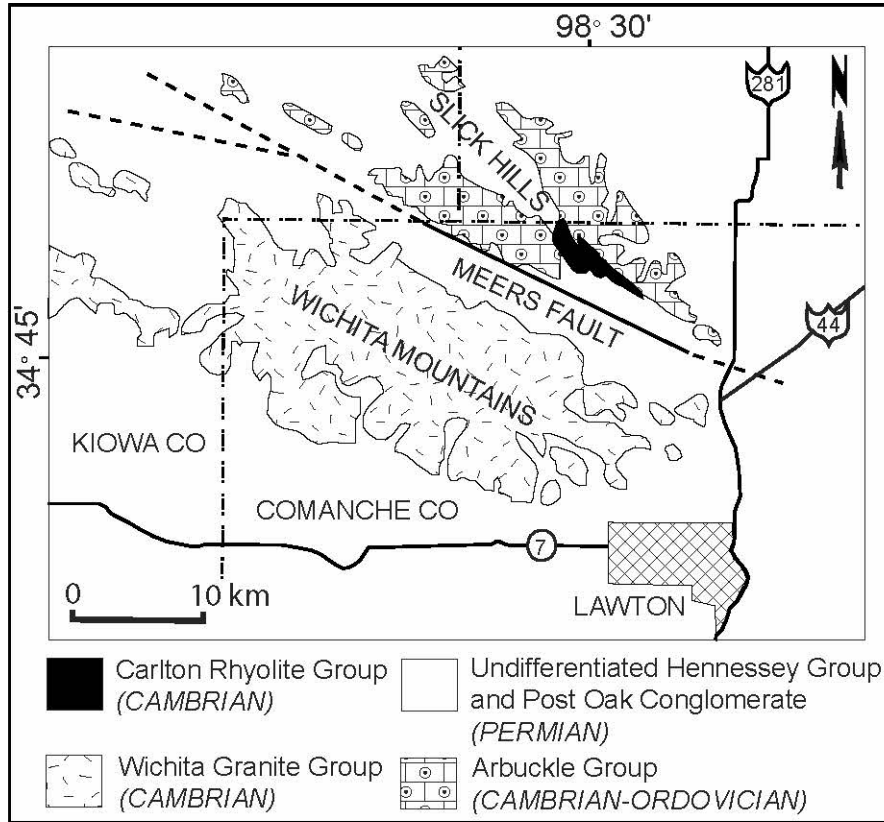


Figure III.2A: Geologic map of the area of the Meers fault scarp. The dashed lines show the possible extensions beyond the fault scarp, redrawn from Cetin, 1998.

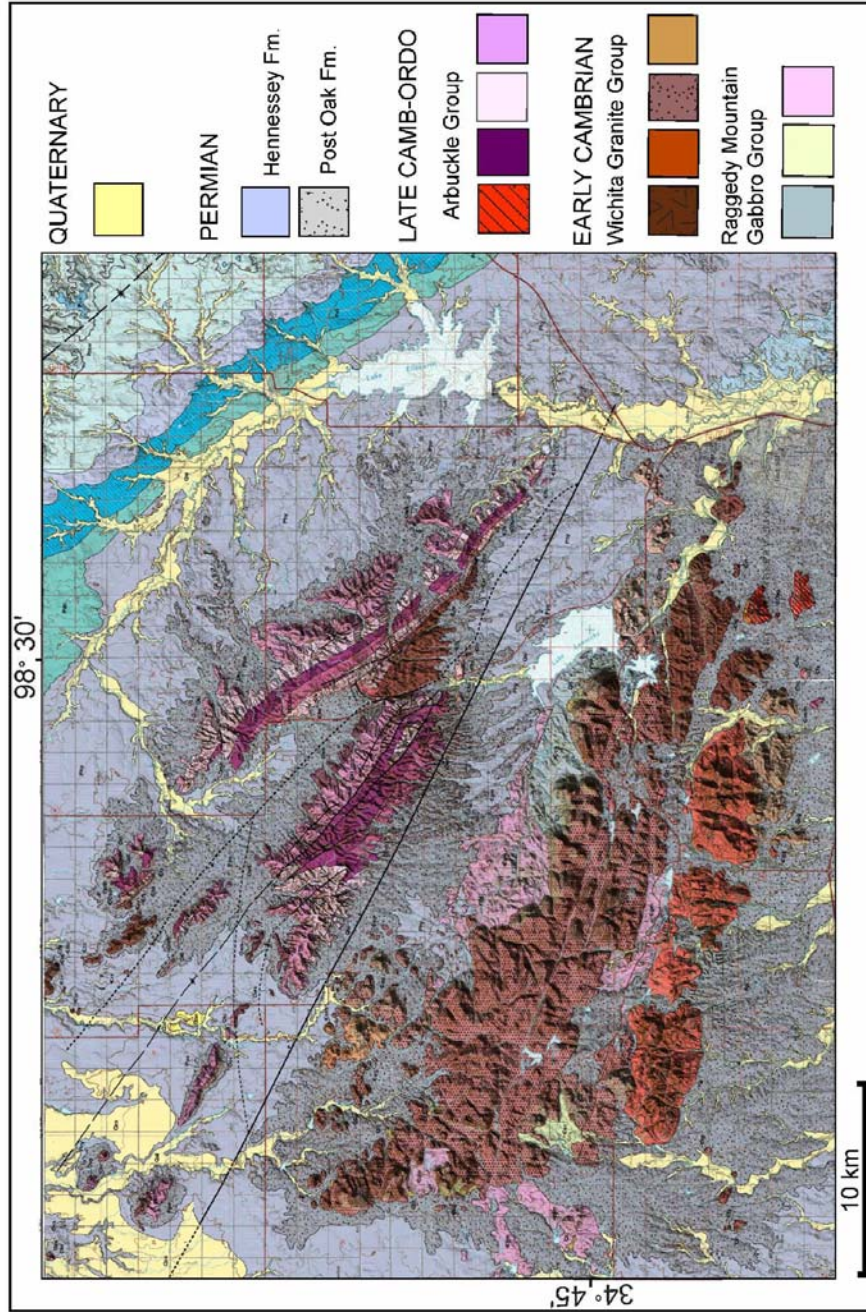


Figure III.2B: Geologic map of Lawton area showing the Meers fault separating the Wichita igneous rocks to the south and the Slick Hill carbonate rocks to the north. The Meers fault cuts through Post Oak Conglomerate and Henessy Shale formations of the Permian as well as Quaternary alluvium, redrawn from Stanley et al., (2005).



Figure III.3: Aerial photograph of southwestern Oklahoma showing the Meers fault scarp extending northwest-southeast for a distance 24-26km.

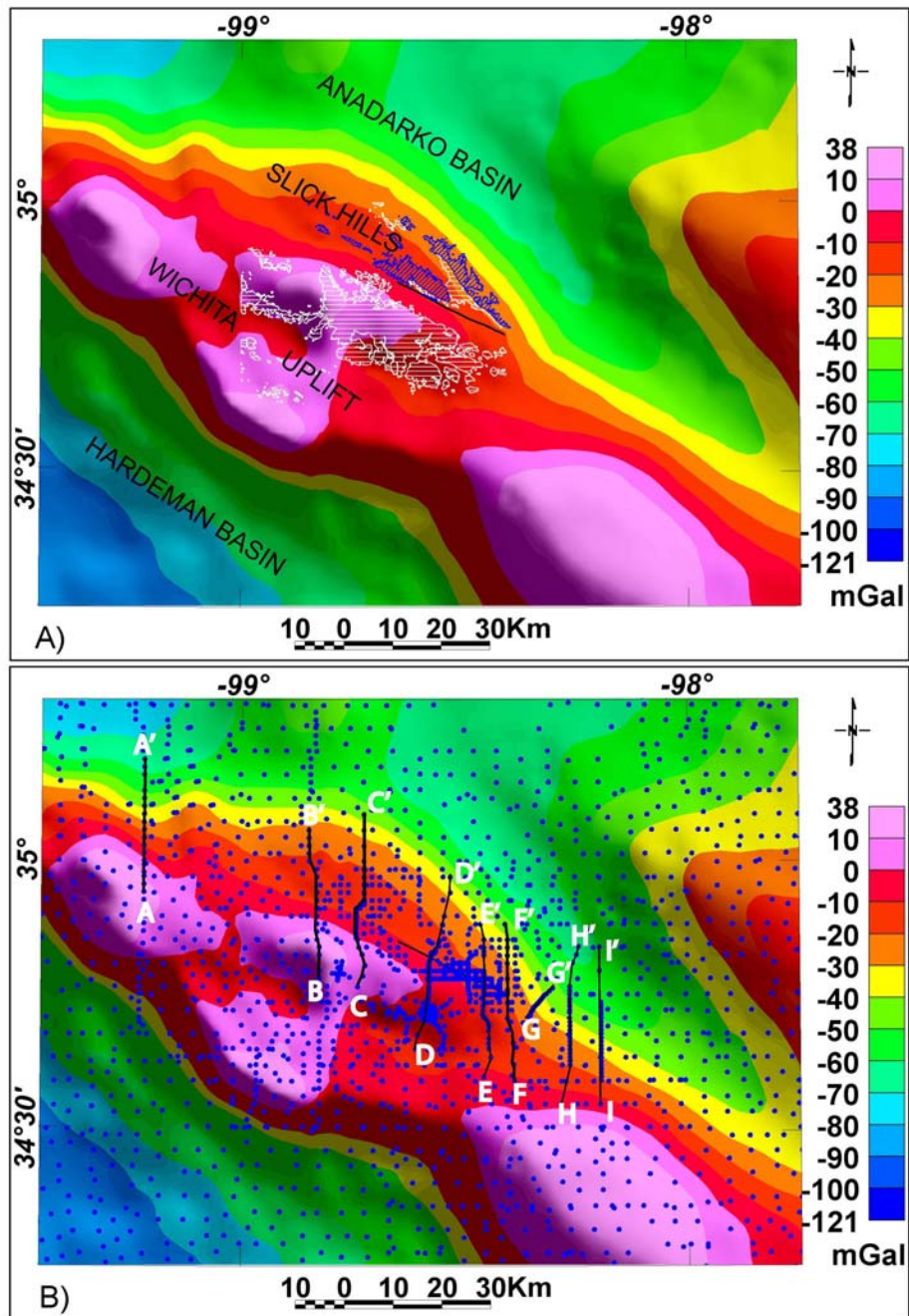


Figure III.4: (A) Complete Bouguer gravity map of the study area showing NW-SE. High gravity anomaly related to the Wichita Uplift. The Meers fault scarp (black segment) separates the high gravity signature of the Wichita Uplift igneous rocks (stripped horizontal white lines) to the south and the moderately high gravity of the Slick Hills carbonate rocks (stripped diagonal blue lines) to the north. (B) The map in (A) showing the distribution of gravity stations and the locations of nine ground gravity profiles.

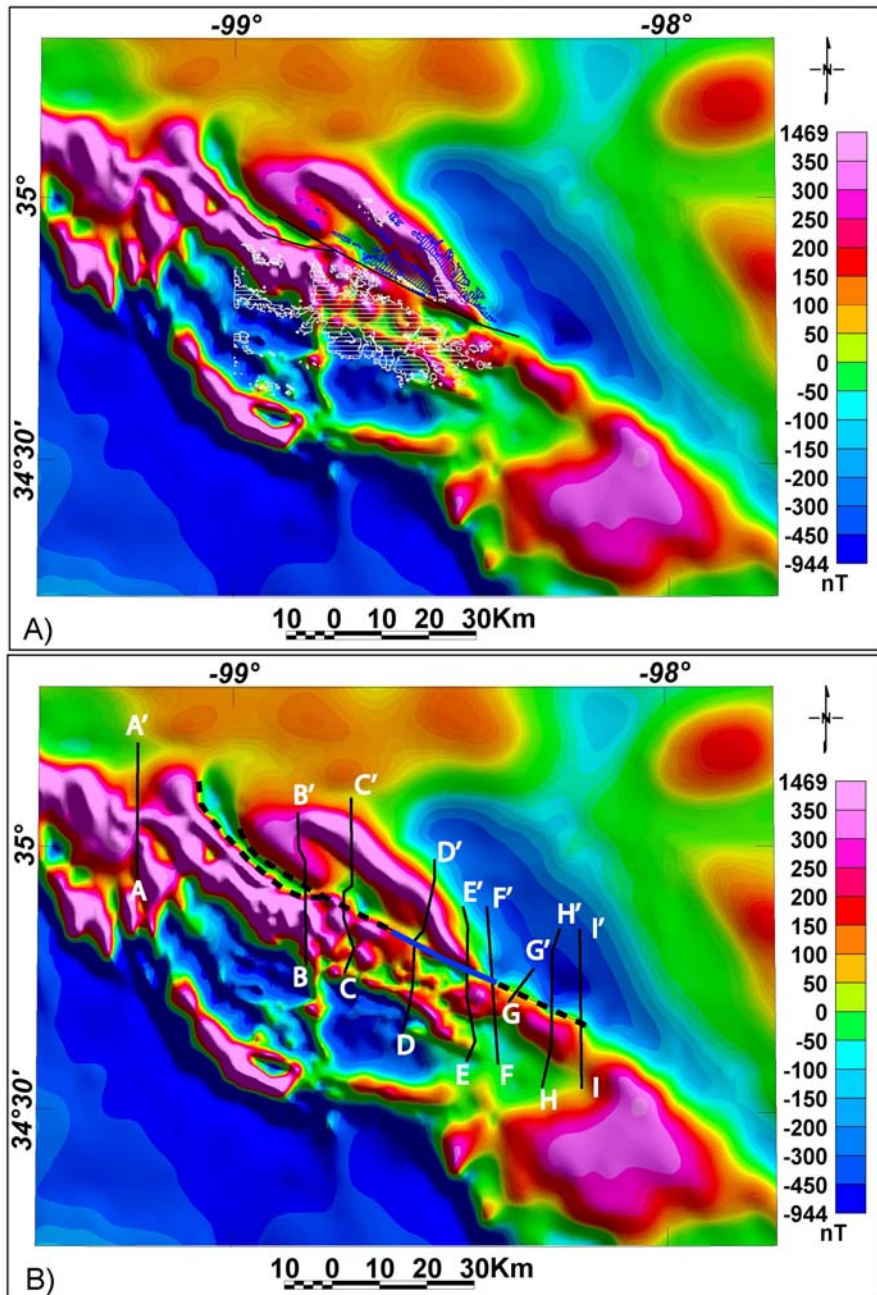


Figure III.5: (A) The reduced-to-pole total magnetic intensity (RTP) Map showing the Meers fault trace as determined by earlier workers (e.g., Ramelli and Slemmons (1986); Cetin, 1991; Jones Cecil, 1995). (B) The RTP map showing the locations of nine ground gravity profiles. Meers fault scarp (blue segment) and its new interpreted extensions (dashed black lines).

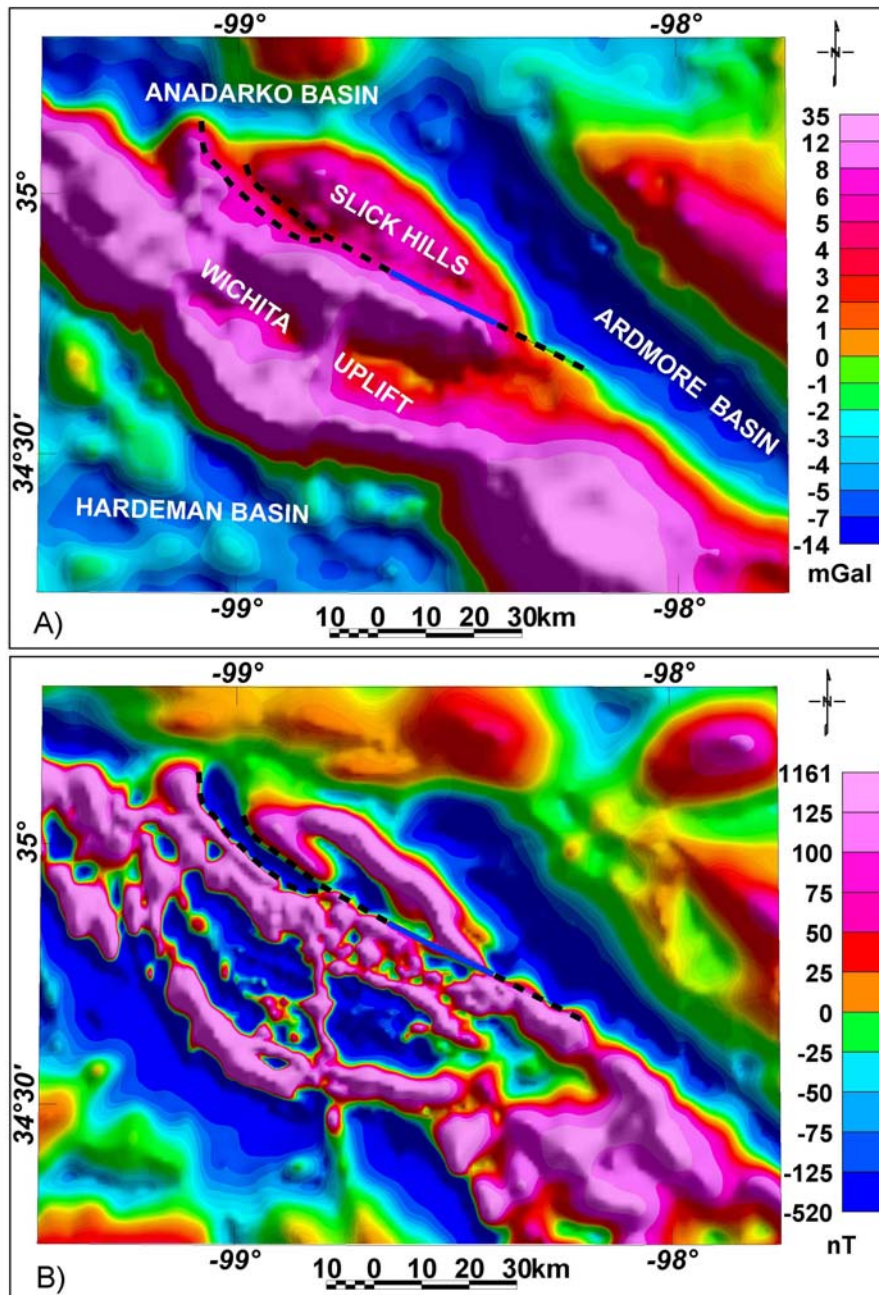


Figure III.6: (A) Residual gravity map after upward continuation to a height of 5 km showing the Meers fault scarp (blue line), and the new interpreted fault extension dashed black line). (B) Residual magnetic map after upward continuation to a height of 5 km showing clearer magnetic contrast across the Meers fault scarp and its extensions.

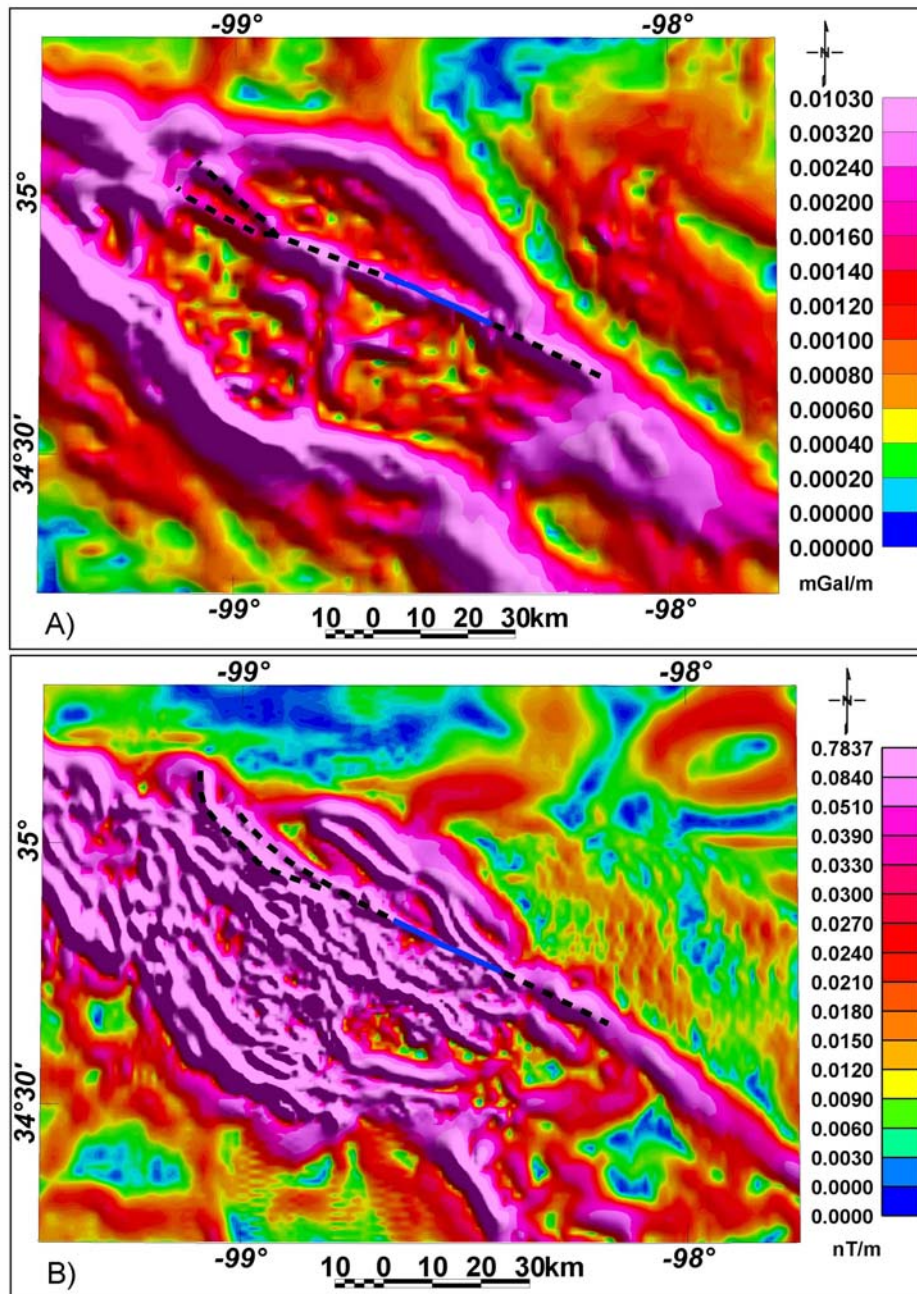


Figure III.7: (A) The total horizontal derivative (THD) of the gravity data showing maxima above the edge of dike-like bodies which control the fault trend. (B) The THD of the magnetic data showing sharper and more clear maxima than gravity shows.

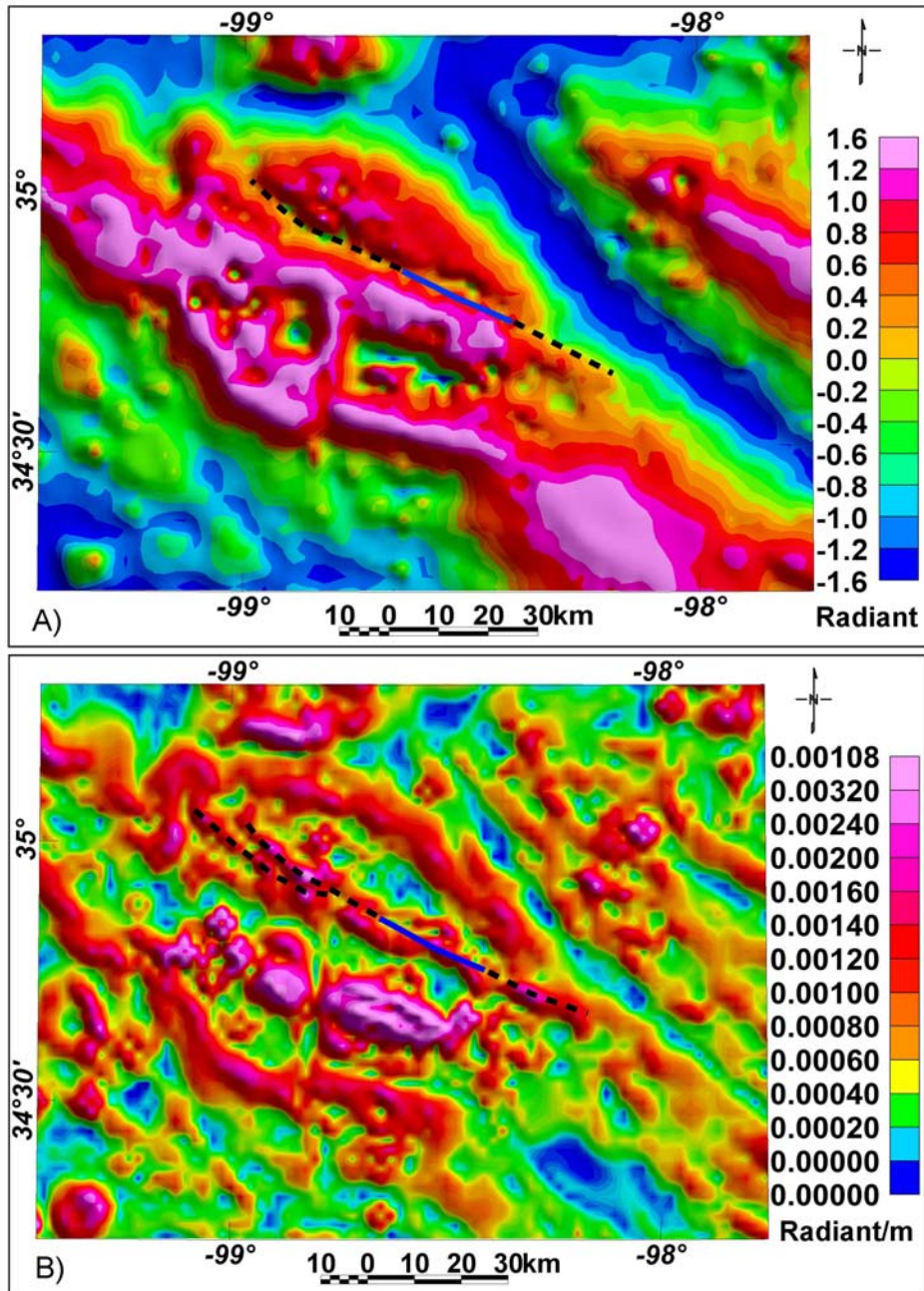


Figure III.8: (A) The tilt derivative of the gravity data showing close to zero gravity that coincides with the fault scarp and it can be extended in both southeast and northwest. (B) The horizontal derivative of the tilt derivative of the gravity data shows peak gravity that coincides with the fault scarp and it can be extended to southeast and northwest where it branches.

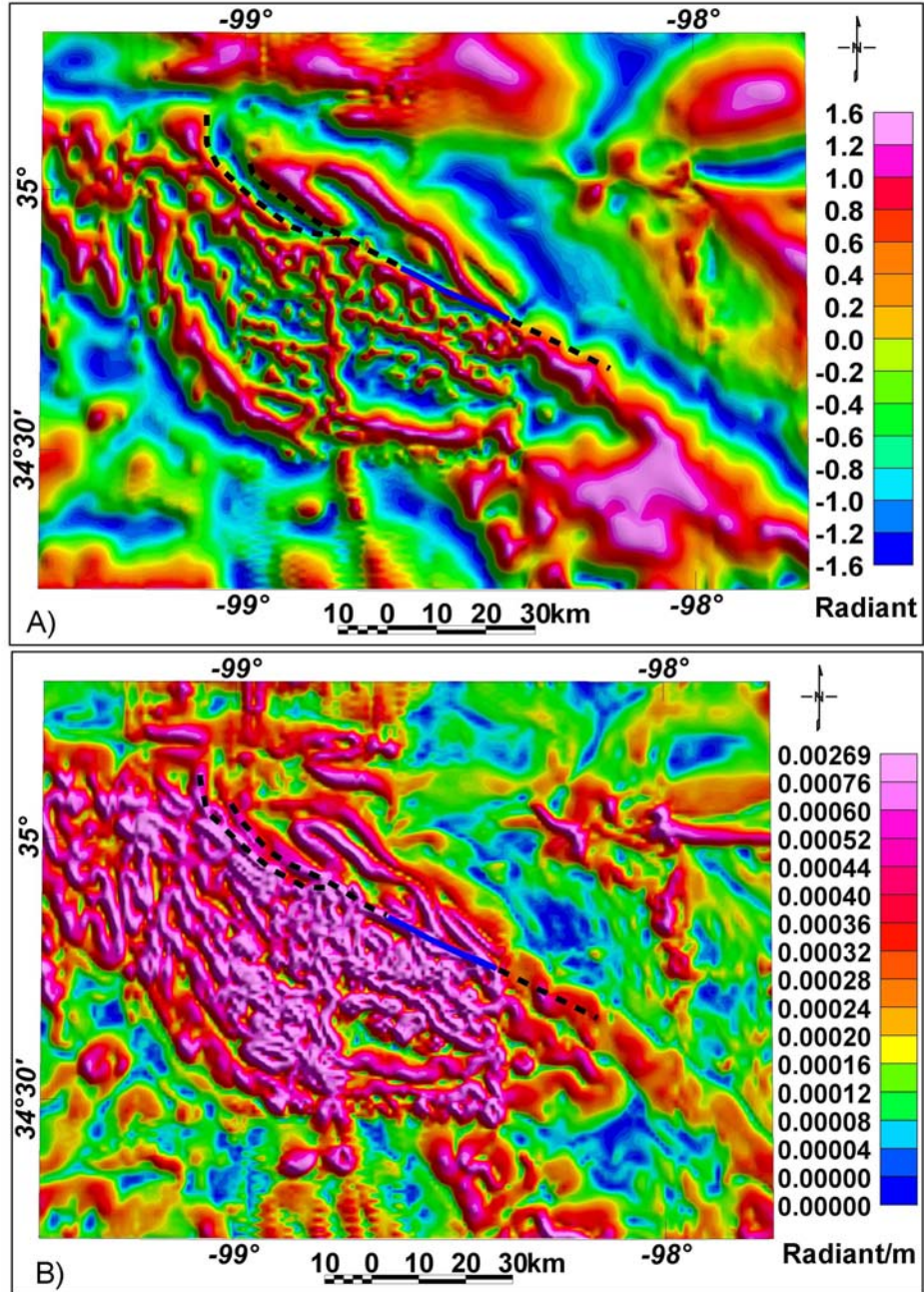


Figure III.9: (A) The tilt derivative of the magnetic data and (B) the horizontal derivative of the tilt derivative of the magnetic data show similar function as the tilt derivative of the gravity data but with sharper magnetic signature.

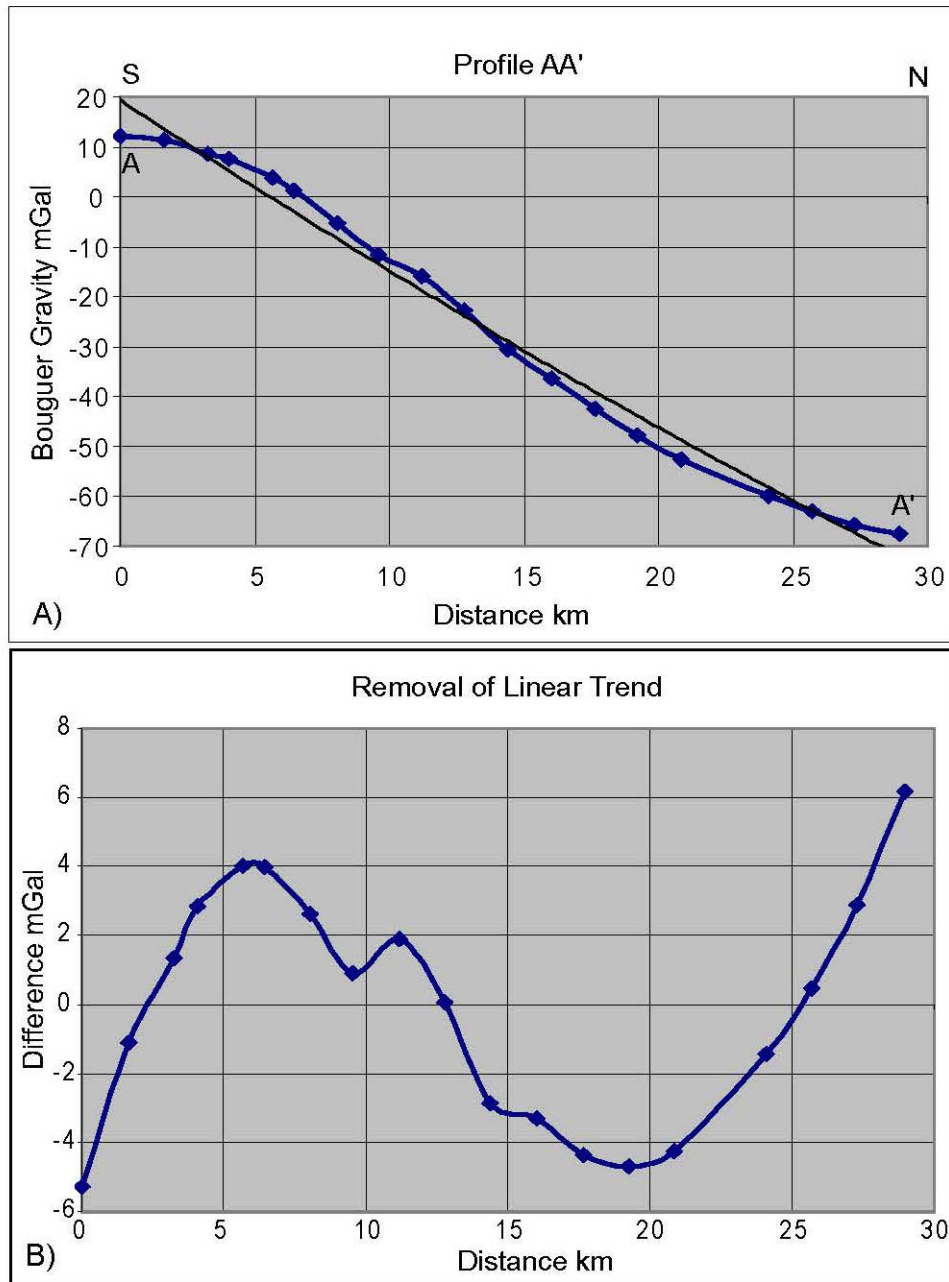


Figure III.10: (A) Ground gravity profile AA' beyond the northwestern end of the Meers fault scarp. (B) The removal of a linear trend of the gravity readings of the profile.

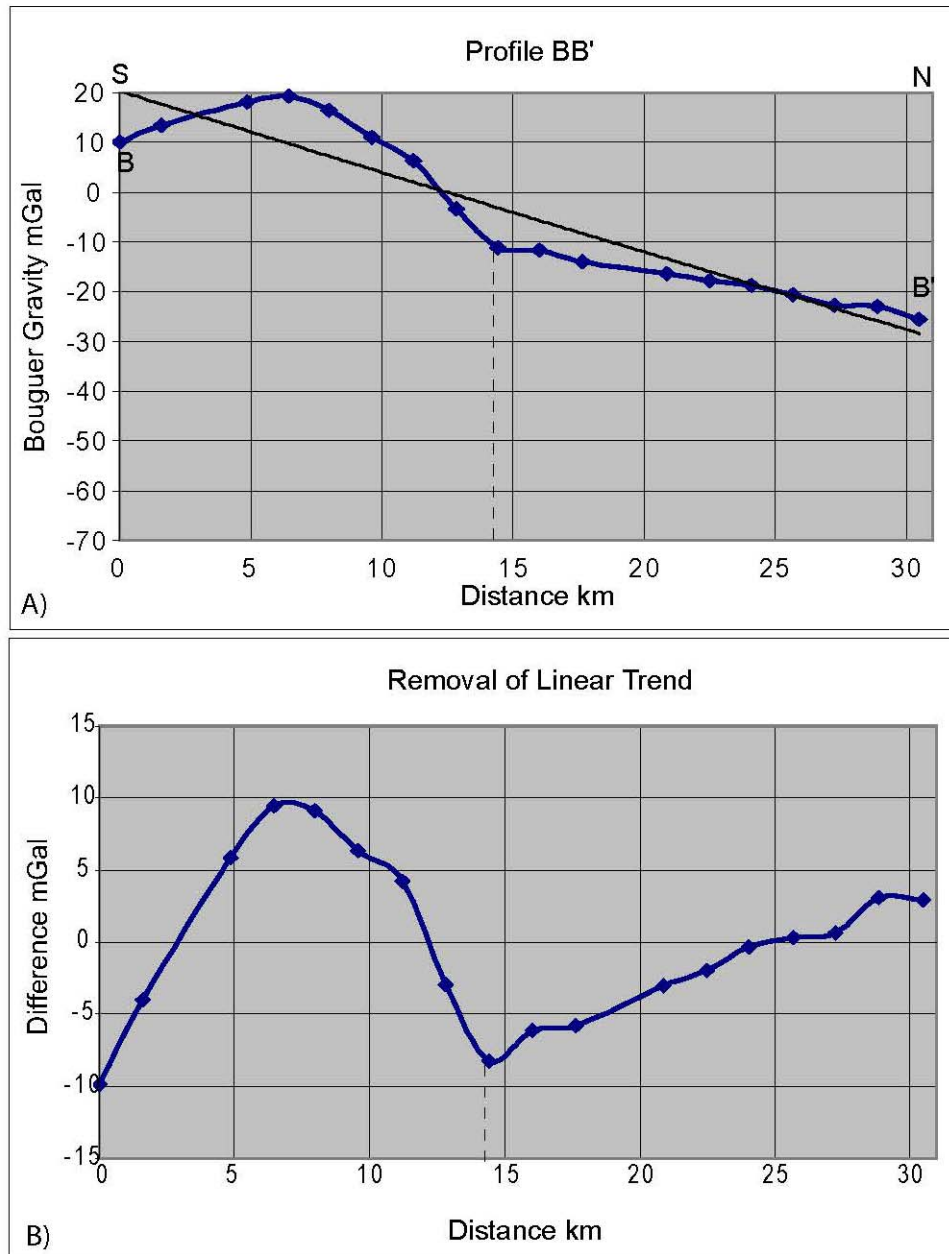


Figure III.11: (A) Ground gravity profile BB' beyond the northwestern end of the Meers fault scarp. The profile shows a little change at 14 km where the fault extension intersects the profile. (B) The removal of linear trend shows clearer change in gravity signal.

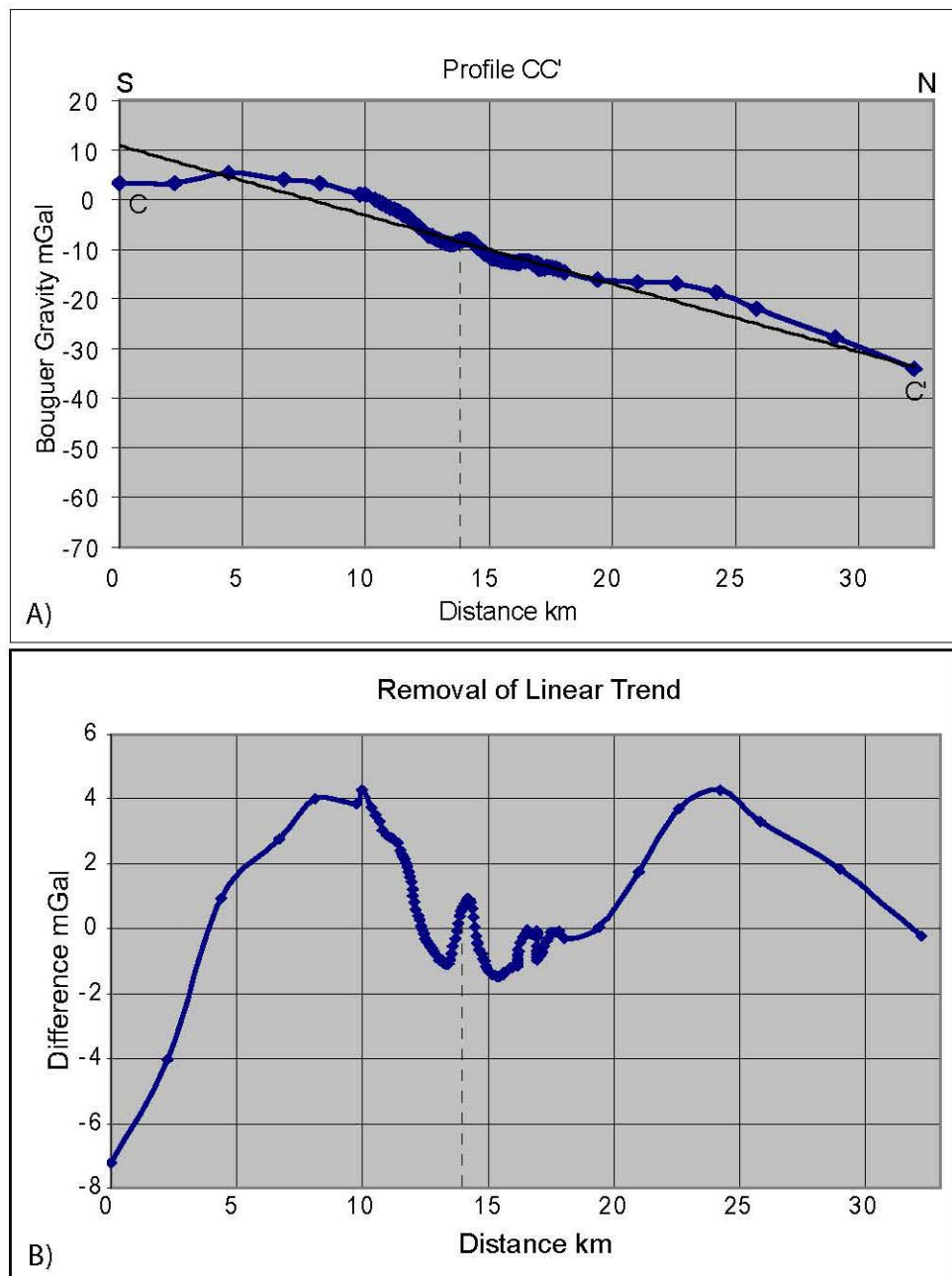


Figure III.12: (A) Ground gravity profile CC' beyond the northwestern end of the Meers fault scarp showing clear change in gravity expression at a distance of approximately 14 km. (B) The removal of the linear trend shows a clearer signal.

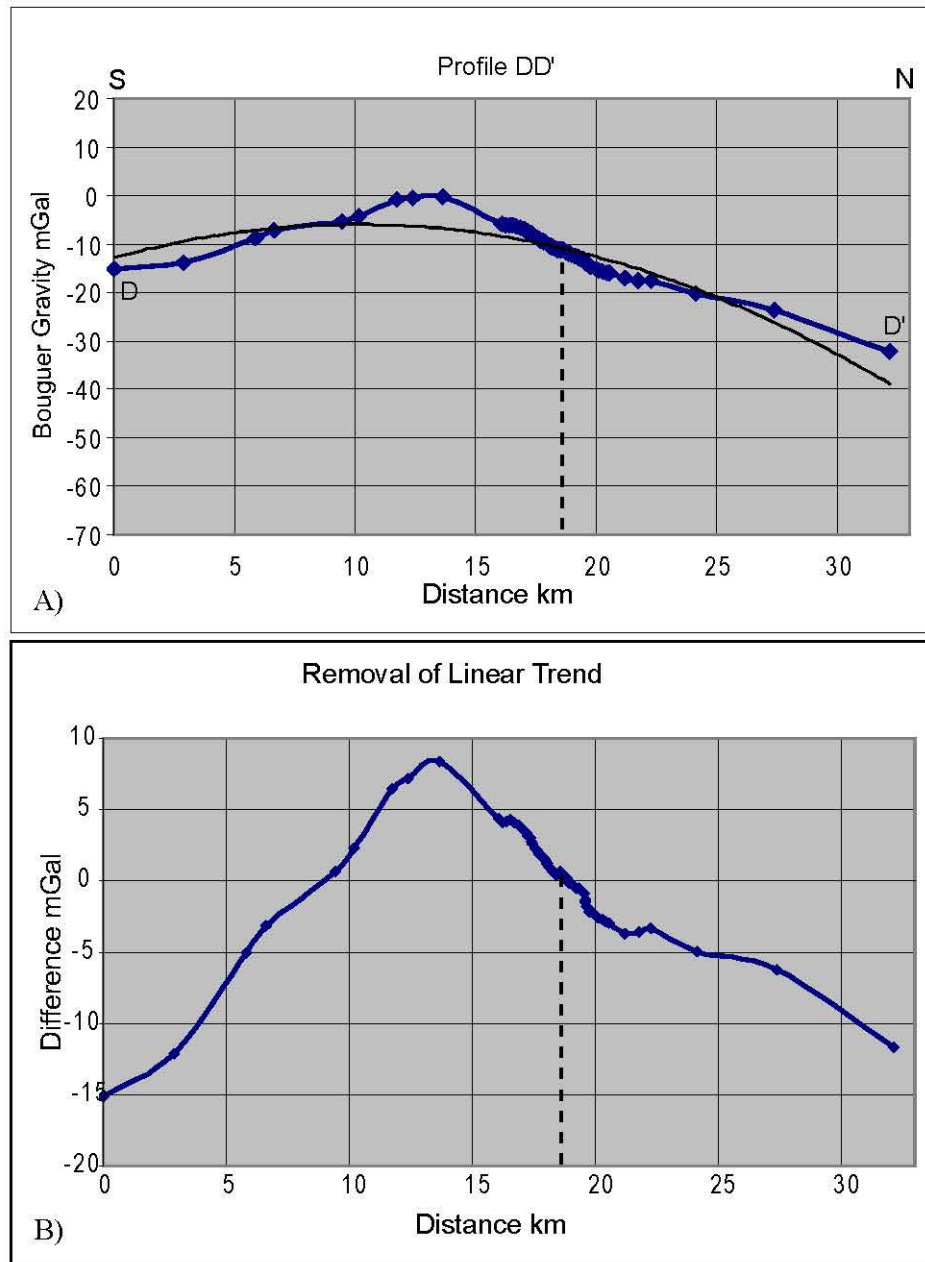


Figure III.13: (A) Ground gravity profile DD' that intersects the Meers fault scarp at a distance of approximately 18 km. The gravity expression shows little pumb where the Meers fault scarp intersects the profile. (B) The removal of the linear trend shows a clearer signal.

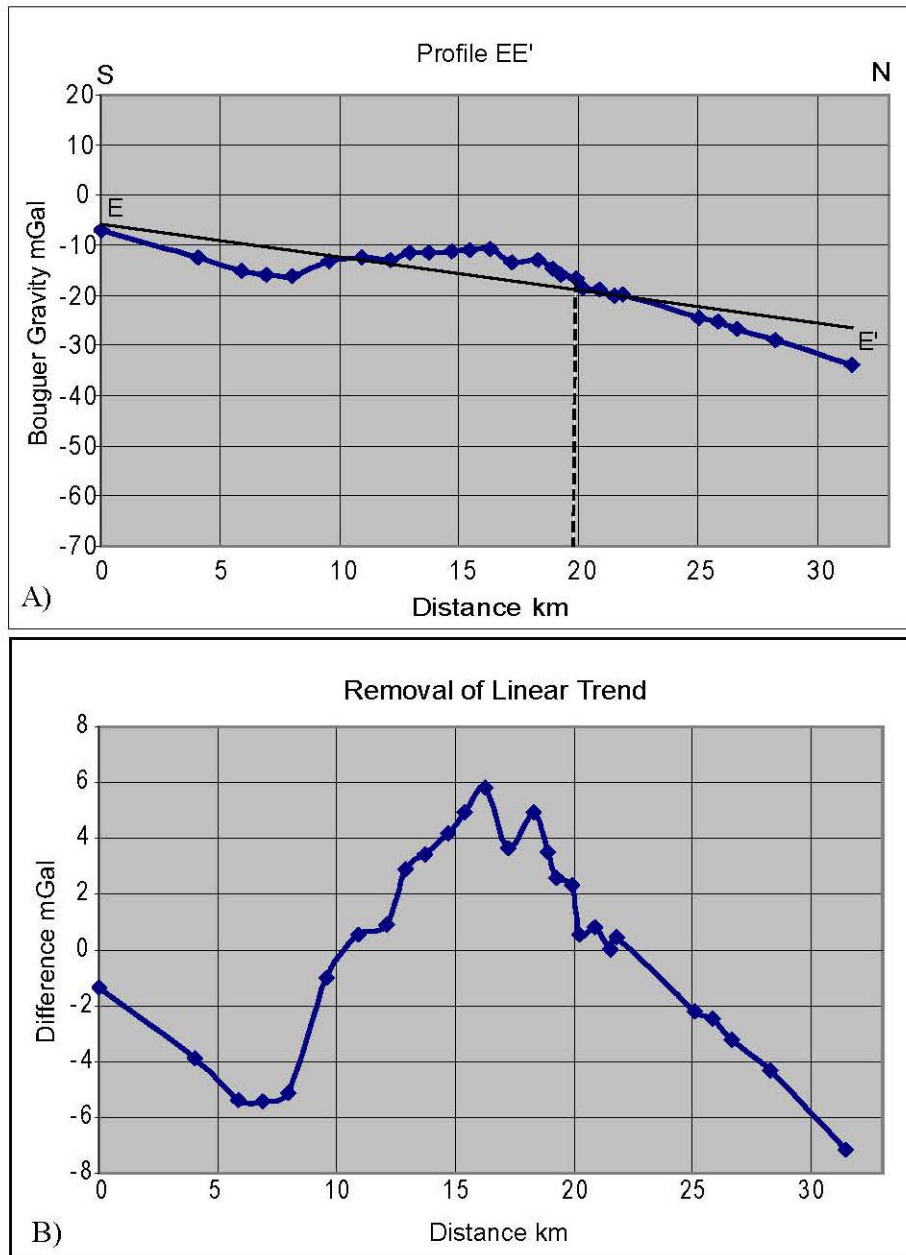


Figure III.14: (A) Ground gravity profile EE' across the Meers fault scarp. The profile intersects the fault scarp at a distance of approximately 20 km. (B) The removal of the linear trend. Neither the profile nor the removal of the linear trend show a signal.

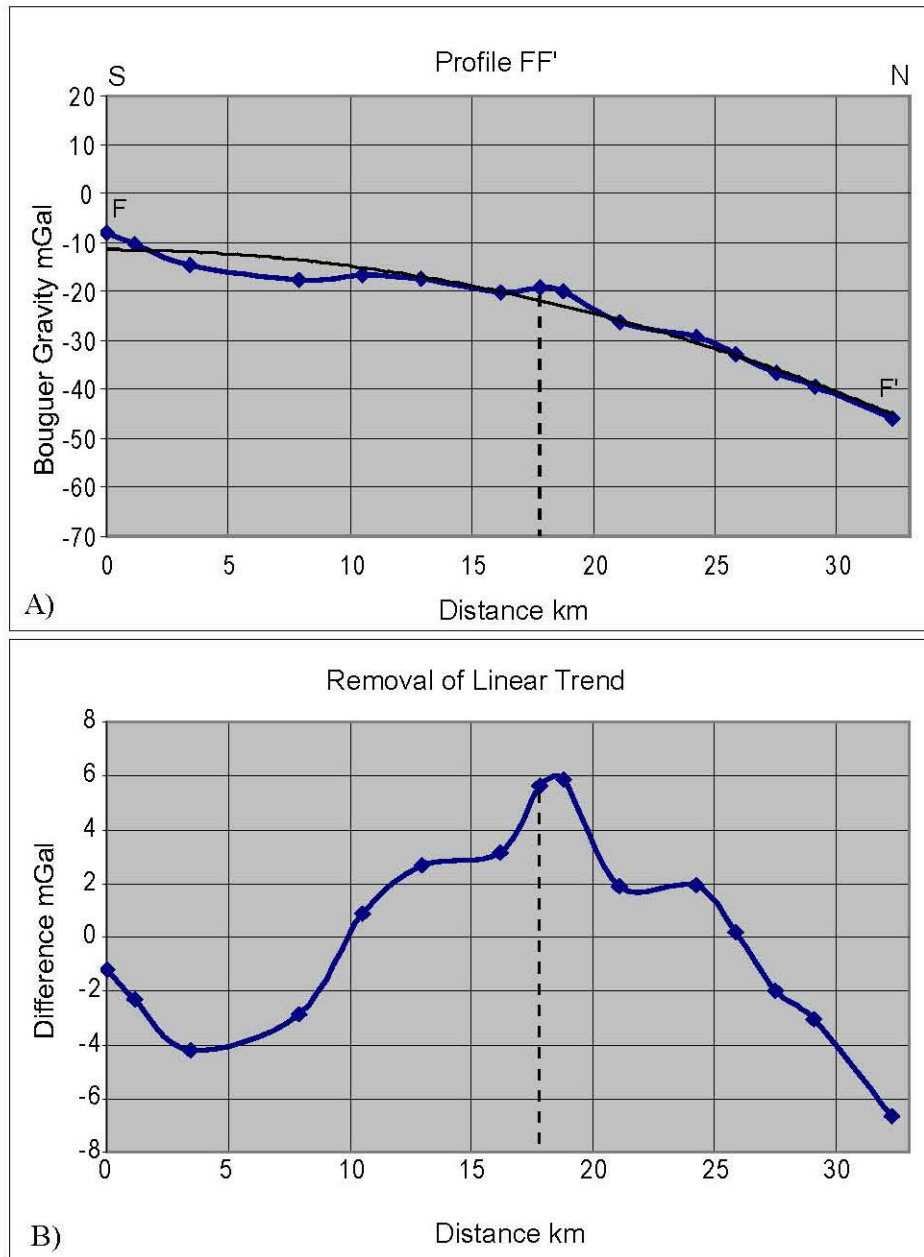


Figure III.15: (A) Ground gravity profile FF' that intersects the southeastern end of the Meers fault scarp at a distance of approximately 18 km. The gravity expression shows only a little change where the Meers fault scarp intersects the profile. (B) The removal of the linear trend shows a clearer signal

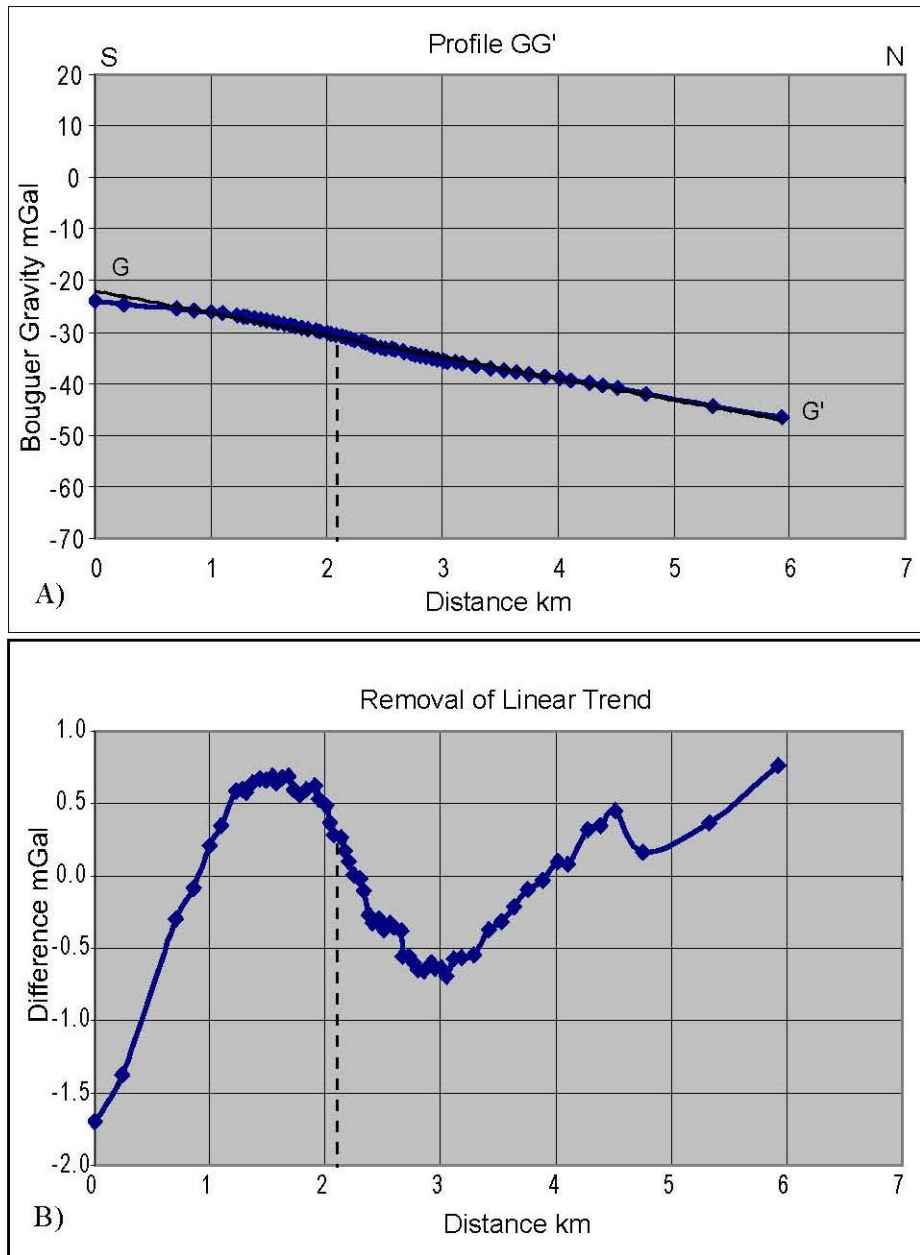


Figure III.16: (A) Ground gravity profile GG' located beyond the southeastern end of the Meers fault scarp. The profile does not show any gravity signature for the fault. (B) The removal of linear trend shows a very little change at a distance of 2.17 km where the possible fault extension intersects the profile.

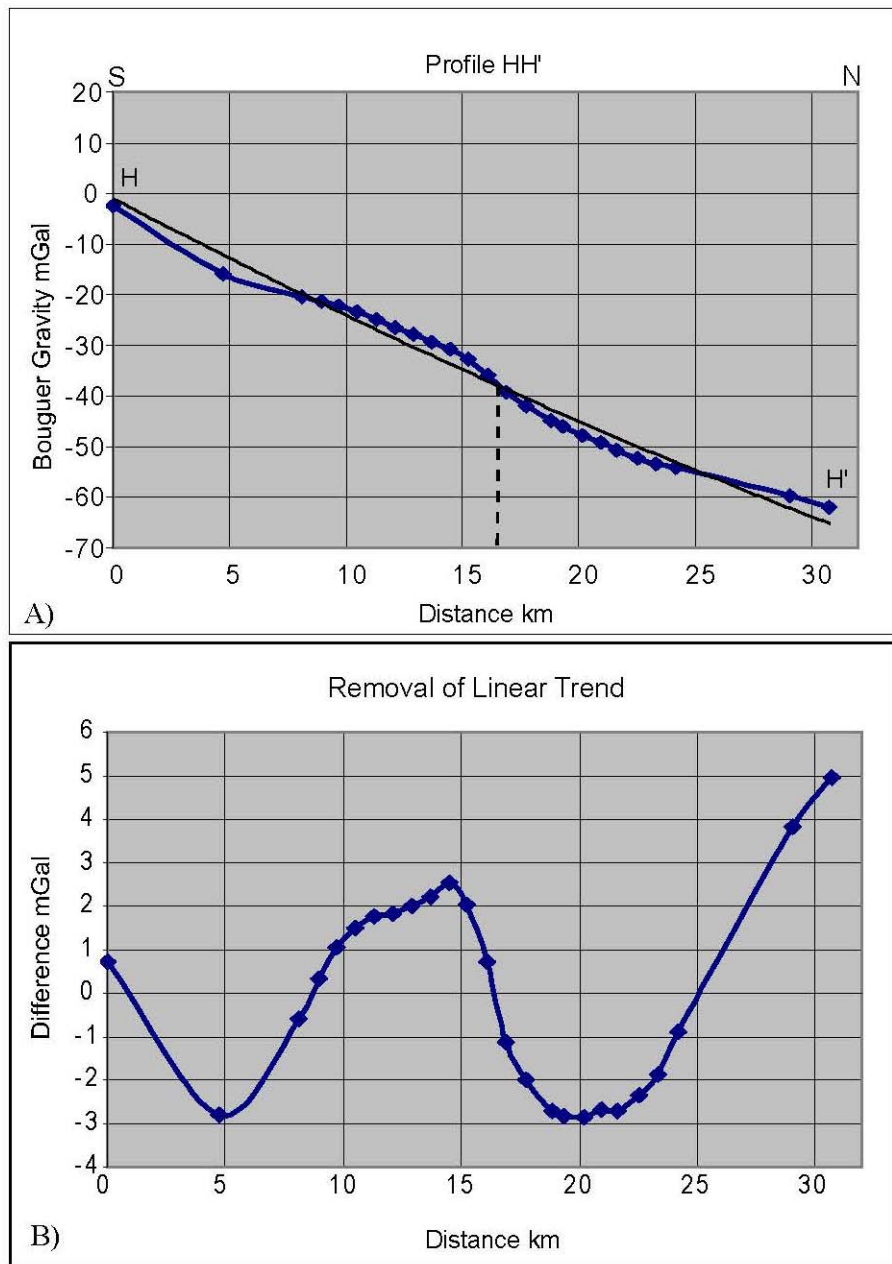


Figure III.17: (A) Ground gravity profile HH' located beyond the southeastern end of the Meers fault scarp. The gravity profile shows a little change at distance of 16-17 km where the fault extension intersects the profile intersects the profile.

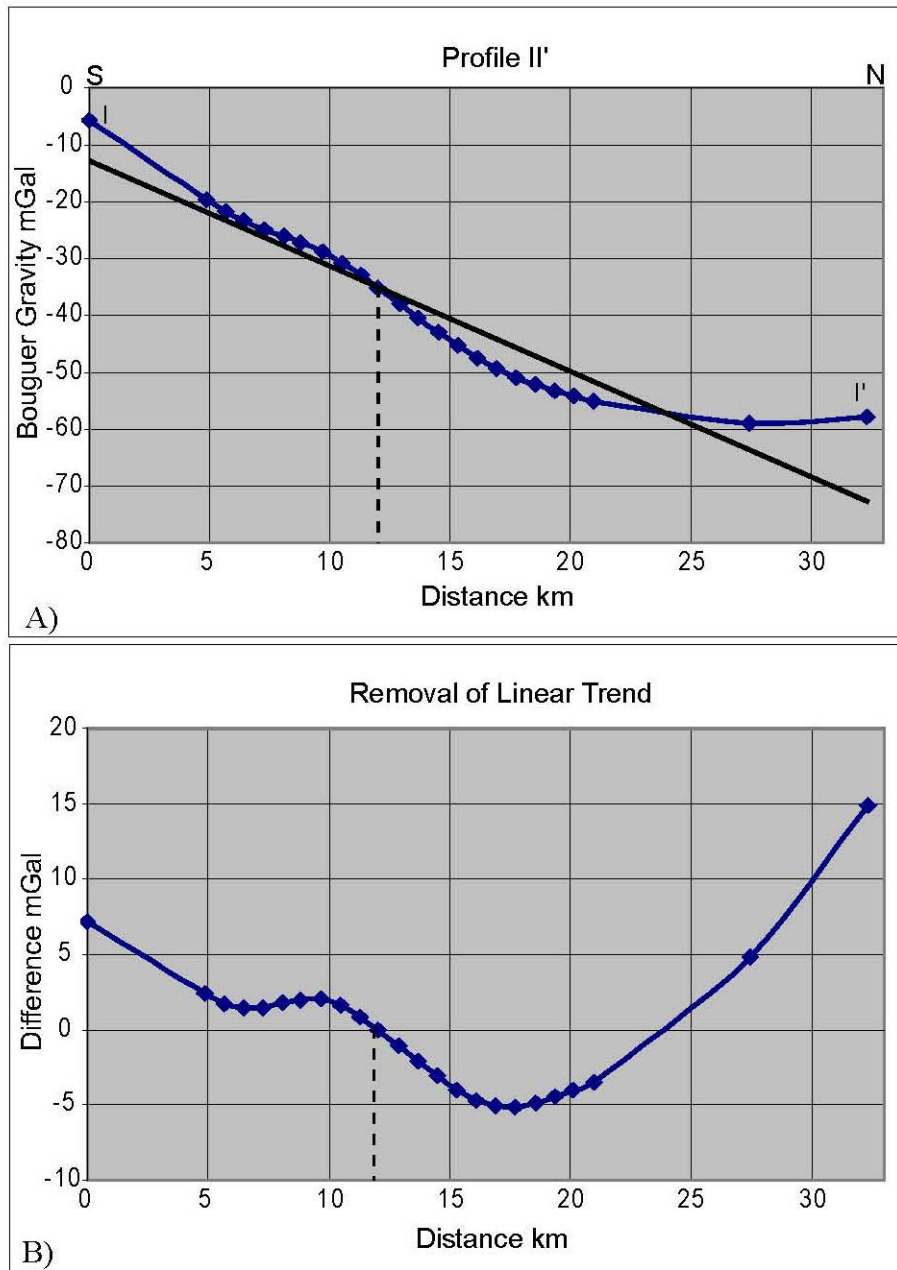


Figure III.18: (A) Ground gravity profile II' located beyond the southeastern end of the Meers fault scarp. The gravity profile shows little gravity change.

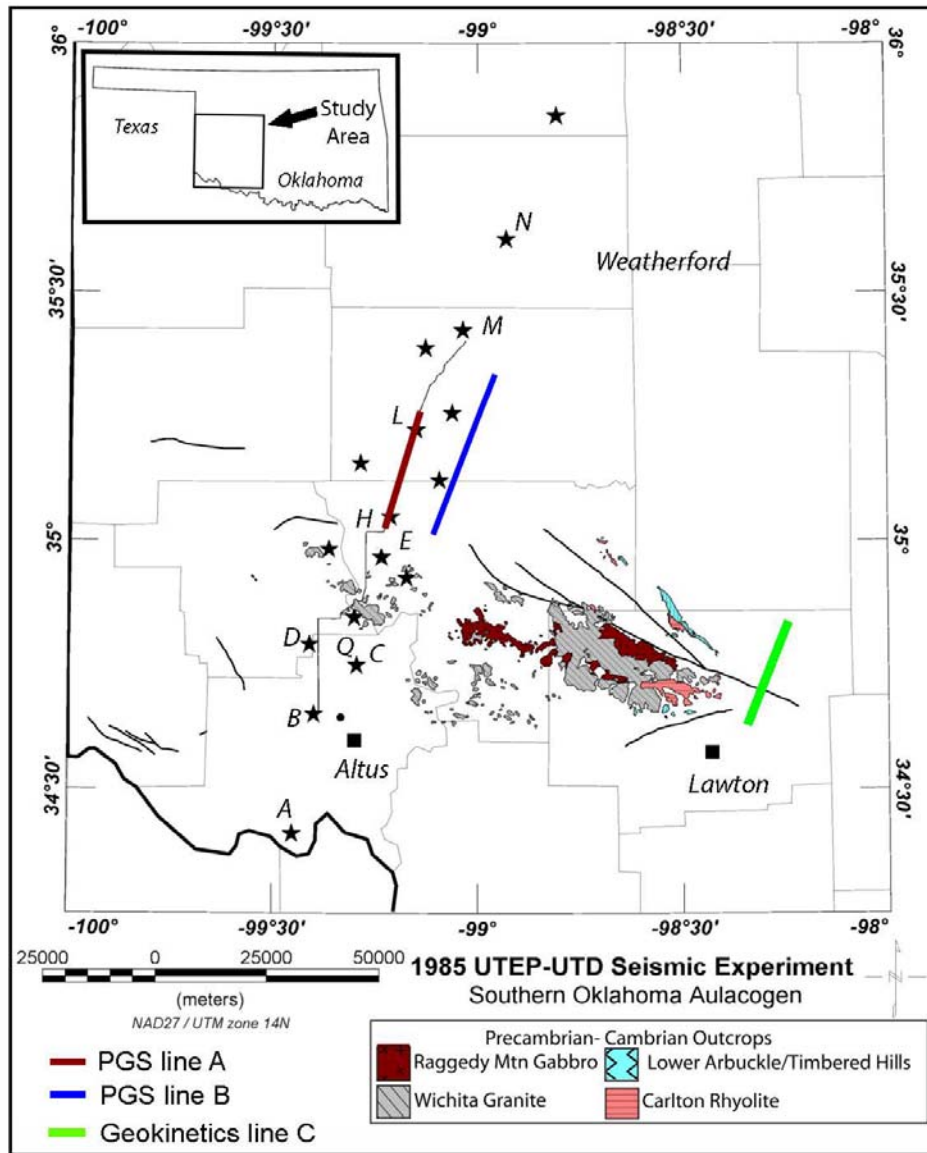


Figure III.19: Index map showing the locations of three seismic reflection lines. Seismic lines A, B are provided by Petroleum Geo-Services (PGS) and line C is provided by Geokinetics.

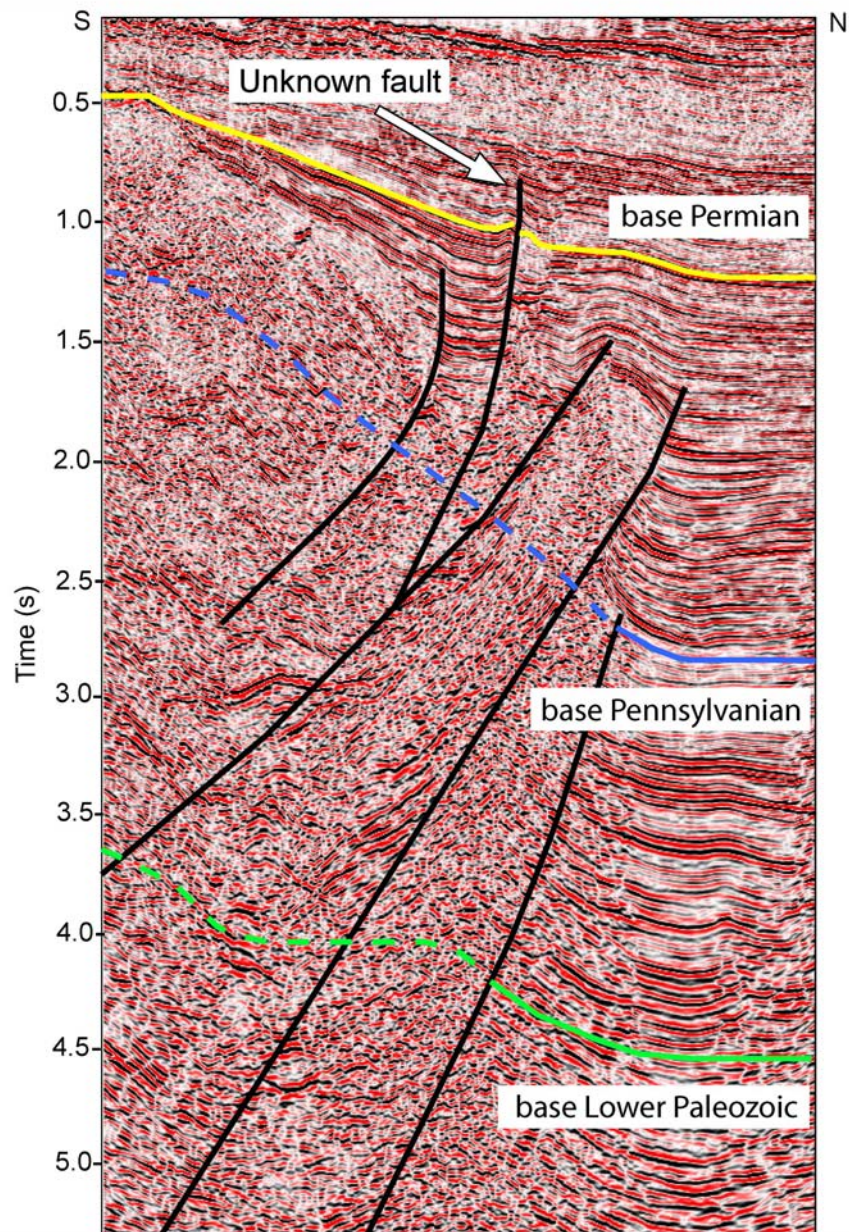


Figure III.20: Seismic reflection line A with an approximately 27 km long. The line shows a number of interpreted high-angle reverse faults. The white arrow points to unknown fault which has been activated in Late Paleozoic tectonism, from Rondot, 2009.

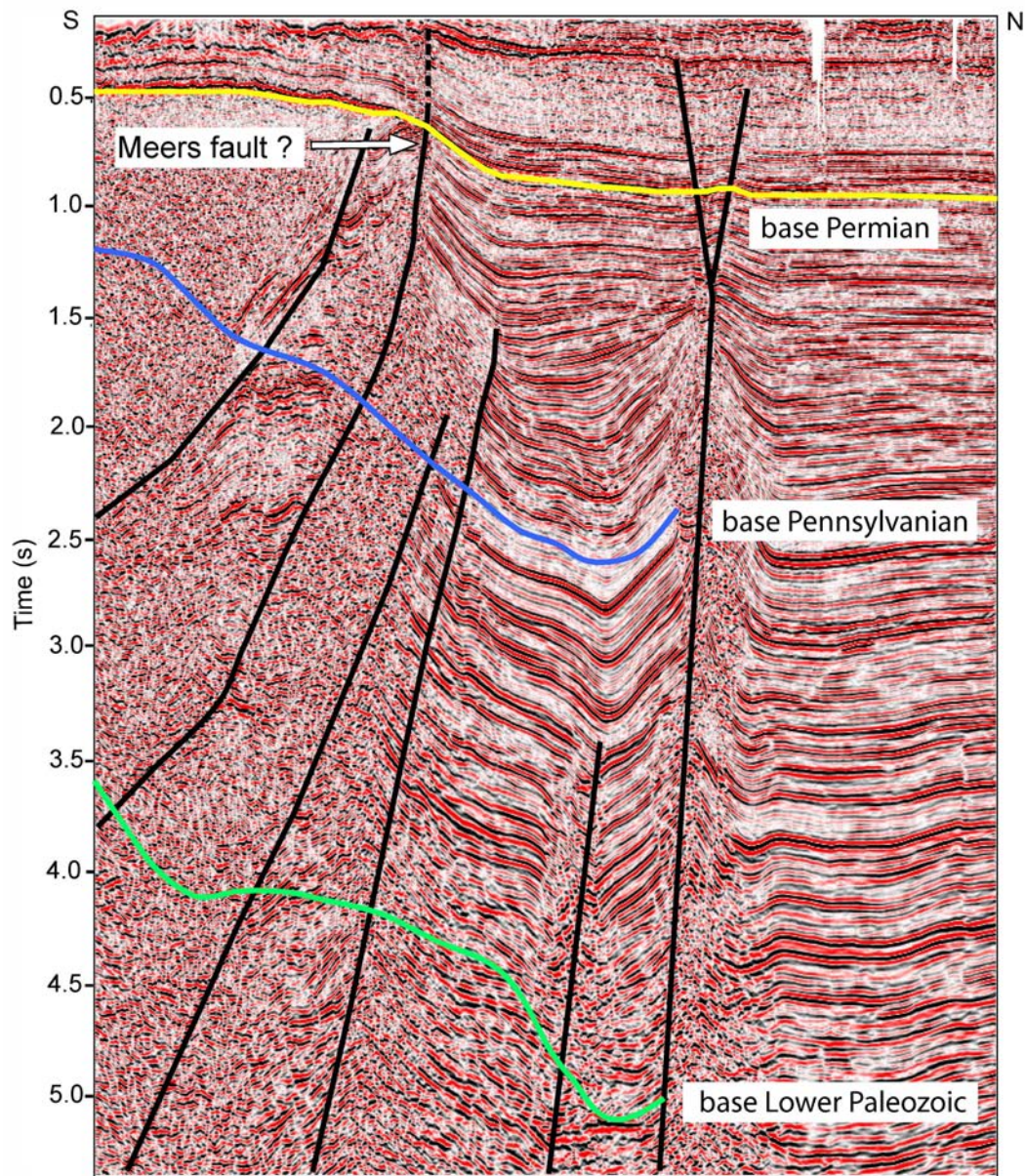


Figure III.21: Seismic reflection line B with an approximately 38 km long. I interpreted the Meers fault to be the one that extends to the surface (white arrow), from Rondot, 2009.

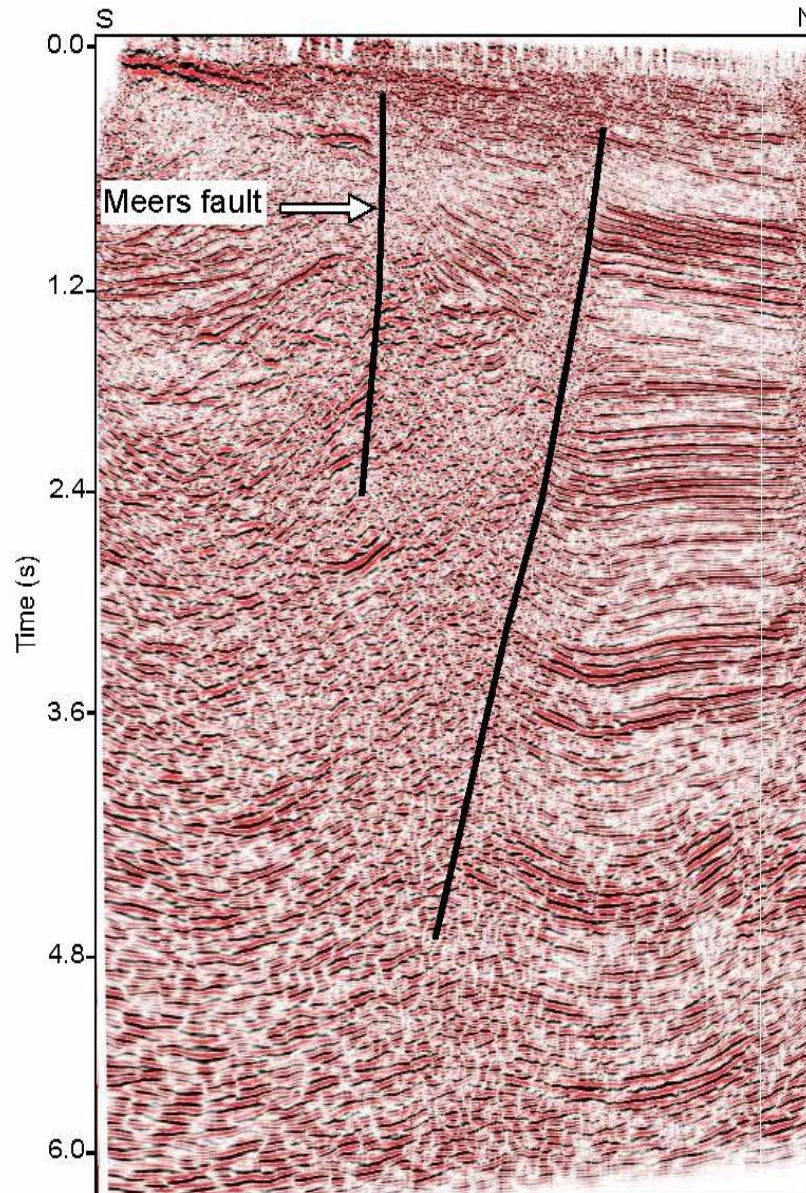


Figure III. 22: Seismic reflection line C beyond the southeastern end of the Meers fault scarp with 24 km long. The Meers fault is the one to the south (white arrow).



Figure III. 23: The Consortium for Continental Reflection Profiling (COCORP) seismic line 2-2A. The line shows the interpretation of the Mountain View (station No. 900) and Meers faults (Station No. 750). Deep reflections from Anadarko basin are shown by arrows, from Brewer et al., 1983.

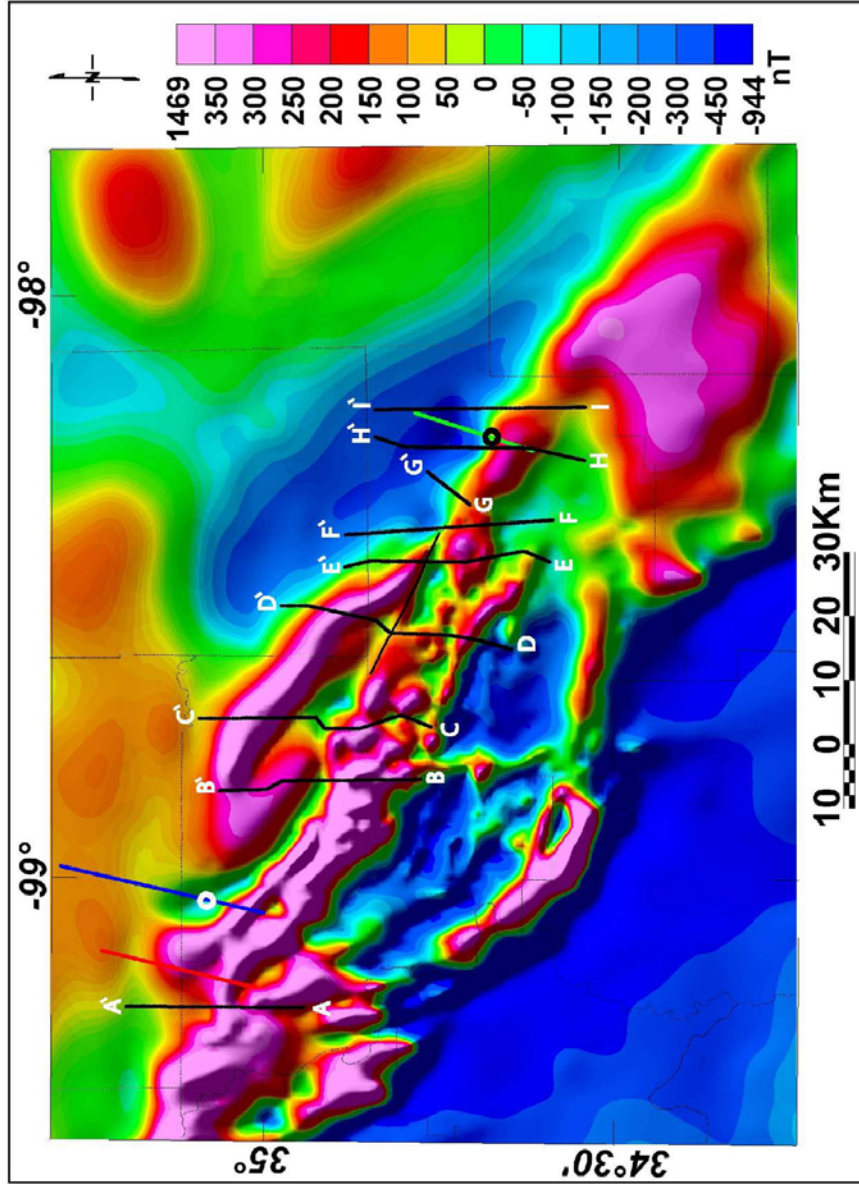


Figure III. 24: The RTP map showing the Meers fault scarp, and the locations of the ground gravity profiles and seismic reflection lines A (red), B (blue) and C (green). The white and black circles show and support the possible interpreted fault trace in seismic lines B and C.

REFERENCES

- Brewer, J. A., 1982, Study of southern Oklahoma aulacogen, using COCORP deep seismic-reflection profiles, *in* Gilbert, M. C., and Donovan, R. N., (eds.), *Geology of the eastern Wichita Mountains, southwestern Oklahoma: The University of Oklahoma at Norman, Oklahoma Geological Survey Guidebook 21*, p. 31-39.
- Brewer, J. A., Good, R., Oliver, J. E., Brown, L. D., and Kaufman, S., 1983, COCORP profiling across the southern Oklahoma aulacogen: Overthrusting of the Wichita Mountains and compression within the Anadarko basin: *Geology*, v. 11, p. 109-114.
- Burke, W. H., Otto, J. B., and Denison, R. E., 1969, Potassium-argon dating of basaltic rocks: *Journal of Geophysical Research*, v. 74, p. 1082-1086.
- Cetin, H., 1991, The northwest extension of the Meers fault in southwestern Oklahoma: Master's thesis, College Station, Texas, Texas A&M University, 68 p.
- Cetin, H., 1997, How did the Meers fault scarp form? Paleoearthquake or aseismic creep? A soil mechanical perspective: *Engineering Geology*, v. 47, p. 289-310.
- Cetin, H., 1998, Near-surface folding along an active fault: seismic or aseismic? *Tectonophysics*, v. 292, p. 279-291.
- Crone, A. J., and Luza, K. V., 1990, Style and timing of Holocene surface faulting on the Meers fault, southwestern Oklahoma: *Geological Society of America Bulletin*, v. 102, p. 1-17.
- Donovan, R. N., 1986, Geology of the Slick Hills, *in* Donovan, R. N., (ed.), *The Slick Hills of southwestern Oklahoma-Fragments of an aulacogen?: Oklahoma Geological Survey Guidebook 24*, p. 1-12.
- Donovan, R. N., Gilbert, M. C., Luza, K. V., Marchini, D., and Sanderson, D., 1983, Possible Quaternary movement on the Meers fault, southwestern Oklahoma: *Oklahoma Geology Notes*, v. 43, p. 124-133.

- Donovan, R. N., Marchini, W. R. D., McConnell, D. A., Beauchamp, W., and Sanderson, D. J., 1989, Structural imprint on the Slick Hills, southern Oklahoma, in Johnson, K. S., (ed.), Anadarko Basin Symposium, 1988: Oklahoma Geological Survey Circular 90, p. 78-84.
- Gilbert, M. C., 1982, Geologic setting of the eastern Wichita Mountains with a brief discussion of unresolved problems, in Gilbert, M. C., and Donovan, R. N., (eds.), Geology of the Eastern Wichita Mountains, southwestern Oklahoma: Oklahoma Geological Survey Guidebook 21, p. 1-30.
- Ham, W. E., Denison, R. E., and Merritt, C. A., 1964, Basement rocks and structural evolution of southern Oklahoma- A summary: American Association of Petroleum Geologists Bulletin, v. 49, p. 927-934.
- Ham W. E., and Wilson, J. L., 1967, Paleozoic epeirogeny and orogeny in the central United States, American Journal of Science, v. 265, p. 332-407.
- Harlton, B. H., 1951, Faults in the sedimentary part of the Wichita Mountains of Oklahoma: American Association of Petroleum Geologists Bulletin, v. 35, p. 988-999.
- Harlton, B. H., 1963, Frontal Wichita fault system of southwestern Oklahoma: American Association of Petroleum Geologists Bulletin, v. 47, p. 1552-1580.
- Hinze, W. J., Aiken, C., Brozena, J., Coakley, B., Dater, D., Flanagan, G., Forsberg, R., Hildenbrand, T., Keller, G. R., Keller, Kucks, R., Li, X., Mainville, A., Morin, R., Pilkington, M., Plouff, D., Ravat, D., Roman, D. Urrutia-Fucugauchi, J., Véronneau, M., Webring, M., and Winester, D., (2005), New standards for reducing gravity data: The North American gravity database: *GEOPHYSICS*, v. 70, p. 325-332.
- Holom, D. I., and Oldow, J. S., 2007, Gravity reduction spreadsheet to calculate the Bouguer anomaly using standardized methods and constants: The Geological Society of America, Geosphere, v. 3, p. 86-90.
- Johnson, K. S., 1989, Geologic evolution of the Anadarko basin, in Johnson, K. S., (ed.), Anadarko Basin Symposium, 1988: Oklahoma Geological Survey Circular 90, p.3-12.

- Jones-Cecil, M., 1995, Structural controls of Holocene reactivation of the Meers fault, southwestern Oklahoma, from magnetic studies: *Geological Society of America Bulletin*, v. 107, p. 98-112.
- Jones-Cecil, M., and Crone, A. J., 1989, Constraints on the Anadarko basin–Wichita uplift boundary interpreted from aeromagnetic data, *in* Johnson, K. S., (ed.), *Anadarko Basin Symposium, 1988: Oklahoma Geological Survey Circular 90*, p. 228-232.
- Jones-Cecil, M., Donovan, N. R., Bradley, L. A., 1995, Structural Framework of the Meers fault and Slick Hills Area, Southwestern Oklahoma, Based on Magnetic Data, *in* Johnson, K. S. (ed.), *Structural styles in the southern Midcontinent, 1992 symposium: Oklahoma Geological Survey Circular 97*, p. 187-207.
- Keller, G. R., Lidiak, E. G., Hinze, W. J., and Braile, L. W., 1983, The role of rifting in the tectonic development of the midcontinent, USA: *Tectonophysics*, v. 94, p. 391-412.
- Keller, G. R., T. G. Hildenbrand, R. Kucks, M. Webring, Allen Briesacher, Kristine Rujawitz, A. M. Hittelman, Dan Roman, Dan Winester, R. Aldouri, Roberto Torres, W. J. Hinze, Ann Gates, and John Seeley, 2006, A community effort to construct a gravity database for the United States and an associated web portal, *in*, Sinha, A. K. (ed.), *Geoinformatics: Data to Knowledge: Geological Society of America, Special Paper 397*, p. 21-34.
- Keller, G. R. and R. A. Stephenson, 2007, The Southern Oklahoma and Dniepr-Donets aulacogens: a comparative analysis, *in* Hatcher, R. D., Jr., Carlson, M. P., McBride, J. H., and Martínez Catalán, J. R. (eds.), *The 4D Framework of Continental Crust: Geological Society of America, Memoir 200*, p. 127-143.
- Kelson, K. I., and Swan, F. H., 1990, Paleoseismic history of the Meers fault, southwestern Oklahoma, and implications for evaluations of earthquake hazards in the central and eastern United States, *in* Weiss, A. W., *compiler*, *Proceedings, Seventeenth Water Reactor Safety Information Meeting, U.S. Nuclear Regulatory Commission NUREG/CP-0105, Volume 2: Washington, D.C., U.S. Nuclear Regulatory Commission*, p. 341-365.
- Lahti, I., and Karinen, T., 2010, Tilt derivative multiscale edges of magnetic data: The Leading Edge, v. 29, p. 24-29.

- Lemiscki, P. J., and Brown, L. D., 1988, Variable crustal structure of strike-slip fault zones as observed on deep seismic reflection profiles: Geological Society of America Bulletin, v. 100, p. 665-676.
- Luza, K. V., 1989, Neotectonics and seismicity of the Anadarko basin, in Johnson, K. S., (ed.), Anadarko Basin Symposium, 1988: Oklahoma Geological Survey Circular 90, p. 121-132.
- Madole, R. F., 1988, Stratigraphic evidence of Holocene faulting in the mid-continent: The Meers fault, southwestern Oklahoma. Geological Society of America Bulletin, v. 100, p. 392-401.
- McConnell, D. A., 1989a, Determination of offset across the northern margin of the Wichita uplift, southeast Oklahoma: Geological Society of America Bulletin, v. 101, p. 1317-1332.
- McConnell, D. A., 1989b, Constraints on magnitude and sense of slip across the northern margin of the Wichita uplift, southwest Oklahoma, *in* Johnson, K. S., (ed.), Anadarko basin symposium 1988, Oklahoma Geological Survey Circular 90, p. 85-96.
- McConnell, D. A., and Gilbert, M. C., 1990, Cambrian extensional tectonics and magmatism within the Southern Oklahoma aulacogen: Tectonophysics, v. 174, p. 147-157.
- Miller, R. D., Steeples, D. W., and Myers, P. B., 1990, Shallow seismic reflection across the Meers fault, Oklahoma: Geological Society of America Bulletin, v. 102, p. 18-25.
- Miller, H. G., and Singh, V., 1994, Potential field tilt-a new concept for location of potential field sources: Journal of Applied Geophysics, v. 32, p. 213-217.
- Nabighian, M. N., Grauch, V. J. S., Hansen, R. O., LaFehr, T. R., Li Y., Peirce, J. W., Phillips, J. D., and Ruder, M. E., 2005, The historical development of the magnetic method in exploration: Geophysics, 75th Anniversary, v. 70, p. 33ND-61ND.

- Purucker, M., 1986, Interpretation of an aeromagnetic survey along the Wichita Frontal fault zone, *in* Gilbert, M. C., (ed.), *Petrology of the Cambrian Wichita Mountains Igneous Suite: Oklahoma Geological Survey Guidebook 23*, p. 129–136.
- Ramelli, A. R., and Slemmons, D. B., 1986, Neotectonic activity of the Meers fault, *in* Donovan, R. N., (ed.), *The Slick Hills of southwestern Oklahoma-Fragments of an aulacogen?: Oklahoma Geological Survey Guidebook 24*, p. 45–54.
- Ramelli, A. R., Slemmons, D. B., and Brocoum, S. J., 1987, The Meers fault: Tectonic activity in southwestern Oklahoma, U.S. Nuclear Regulatory Commission, NUREG/CR-4852: Washington, D.C., U.S. Nuclear Regulatory Commission, 25 p.
- Robbins, S. L., Jones-Cecil, M., and Keller, G. R., 1989, Regional gravity of the Anadarko basin area and a more detailed look at the Wichita Frontal fault zone, *in* Johnson, K. S., (ed.) *Anadarko Basin Symposium, 1988: Oklahoma Geological Survey Circular 90*, p. 225–227.
- Robbins, S. L., and Keller, G. R., 1992, Complete Bouguer and isostatic residual gravity maps of the Anadarko basin, Wichita Mountains, and surrounding areas, Oklahoma, Kansas, Texas, and Colorado: U.S. Geological Survey Bulletin 1866-G, 11 p.
- Rondot, A. N., 2009, An integrated geophysical analysis of crustal structure in the Wichita Uplift region of southern Oklahoma: Master thesis, University of Oklahoma, 107 p.
- Slemmons, D. B., Ramelli, A. R., and Brocom, S. j., 1985, Earthquake potential of the Meers fault, Oklahoma: Seismological Society of America, Eastern section, *Earthquake Notes*, v. 55, p. 1.
- Stanley, T. M., Miller, G. W., and Standridge, and G. R., 2005, Geologic map of Lawton 30' X 60' quadrangle, Caddo, Comanche, Grady, Kiowa, Stephens, and Tillman Counties, Oklahoma: Norman, Oklahoma, Oklahoma Geological Survey Scale 1: 100 000, one sheet.

Vidrine, D. M., and Fernandez, L. A., 1986, Geochemistry and petrology of the Cold Springs Breccia, Wichita Mountains, Oklahoma, *in* Gilbert, M. C., (ed.,) *Petrology of the Cambrian Wichita Mountains Igneous Suite: Oklahoma Geological Survey Guidebook 23*, p. 86-106.

Viele, G. W. and Thomas, W. A., 1989, Tectonic synthesis of the Ouachita orogenic belt, *in* Hatcher, R. D., Jr., Thomas, W. A., and Viele, G. W. (eds.), *The Appalachian-Ouachita Orogen in the United States: Geological Society of America, The Geology of North America*, v. F-2, p. 695-728.

CONCLUSIONS

The current study demonstrates the power of the integration of diverse geophysical datasets with geology to investigate tectonic and structural processes responsible for the geological evolution of tectonic features in different tectonic settings. In the western Arkoma basin, the interpretation of 3-D seismic data reveals a zone of intense deformation or crustal weakness, which may represent tectonic inversion of the Early Cambrian rifting extensional structures as Late Paleozoic compressional ones. The magnetic edge detector techniques and Euler's method reveals fault trends that clearly correlate with those interpreted from seismic data. The interpretation of the gravity data of the Llano uplift area suggests that the Llano uplift originated as independent terrane with physical and geological properties that differ distinctly from its surrounding. The high gravity anomalies of the Llano uplift are related to shallow buried metaigneous rocks in the uppermost crust as well as underplating of mafic magma below the crust, whereas the high magnetic anomalies are related to the surface exposures of the metamorphic rocks. The integration of the gravity, magnetic and seismic data reveal a complex Late Paleozoic deformation in the Frontal Wichita Fault Zone that separates the Wichita uplift and the Anadarko basin. This fault zone separates rocks that have more variations in their magnetic properties than densities. Based on the magnetic expression, the fault can be extended in the subsurface in both northwest and southeast indicating that the fault has a total length of 95 km.